Seismic Performance of Steel Framed Water Tower Structures

by
Vianney Ntibaziyaremye

Thesis presented in fulfilment of the requirements for the degree of Master of Engineering in the Faculty of Civil Engineering at Stellenbosch University

Supervisor: Dr JAvB Strasheim

December 2016

Stellenbosch University https://scholar.sun.ac.za

Declaration

By submitting this thesis electronically, I declare that the entirety of the work contained therein is my own, original work, that I am the sole author thereof (save to the extent explicitly otherwise stated), that reproduction and publication thereof by Stellenbosch University will not infringe any third party rights and that I have not previously in its entirety or in part submitted it for obtaining any qualification.

December 2016

Copyright © 2016 Stellenbosch University

All rights reserved

Stellenbosch University https://scholar.sun.ac.za

Abstract

From the year 1620 until June, 2008, more than 27000 earthquakes of magnitude ranging from 0.2 to 6.3 have been recorded by the South African National Seismological Database (SANSD). The most affected regions are Cape Town, Ceres, Koffiefontein, Lesotho and the Witwatersrand Basin. The historical record showed that the earthquake with the longest time duration was felt in South Africa on 4 December 1809. It caused small damages to buildings in Cape Town and caused liquefaction and cracks in the soil in the region of Blauwberg. However, the 29 September 1969 earthquake was the strongest and the most damaging in South African earthquake history. It was felt across Western Cape as far as Ceres, Tulbagh and Wolseley. It was of magnitude 6.3 on the Richter scale. Many building structures were seriously damaged, a few people were killed and others were injured. Old and poorly constructed buildings were completely destroyed. The total cost of the damaged infrastructure was estimated at U.S. $24million. Given this history, South African is classified as being at risk of moderate intensity earthquakes.

The first version of seismic design code was released in 1980. It was updated in 1989 and 2010, but the updated code does not include all factors influencing the seismic response of the structures (e.g. soil foundation interaction). In addition, structures like dams, water towers, bridges, silos, pipelines, masts and chimneys were not covered. The new code limited its consideration to building structures. The concern is to know whether old structures or newer structures which are not covered by the new seismic designed code will be susceptible to damage by the seismic intensity assigned to the region of their location. Therefore, a methodology for seismic performance assessment of steel framed structures was presented from various publications and was applied to a typical water tower located in a high risk seismic zone of South Africa. The Winelands Engen 1-Stop water tower met the above criteria and was checked for its susceptibility to a seismic event. The results showed that the Engen 1-Stop water tower is vulnerable to the seismic risk attributed to its location. The seismic demand on the tower far exceeds its seismic capacity, which causes concern over whether the Engen 1-Stop water tower was designed to meet any seismic hazard.

Stellenbosch University https://scholar.sun.ac.za

Opsomming

Vanaf die jaar 1620 tot en met Junie 2008, het die Suid-Arikaanse Nasionale Seismologiese Databasis (SANSD) meer as 27000 aardbewings, wat tussen 0.2 en 6.3 op die Richter skaal meet, opgeneem. Kaapstad, Ceres, Koiffiefontein, Lesotho en die Witwatersrand Kom is onder meer die areas wat die meeste geteister word deur aardbewings. Historiese opnames toon dat die langste aardbewing in Suid-Afrika plaasgevind het op 04 Desember 1809. Daar was minimale skade aangerig aan geboue in die Kaapstad-omgewing, alhoewel vervloeiing en klein krake waargeneem was op die grond in die Blauwberg-area. Inteendeel het die sterkste aardbewing, wat die meeste verwoesting gesaai het, plaasgevind op 29 September 1969. Dié aardbewing het 6.3 gemeet op die Richter skaal en was gevoel regoor die Wes-Kaap provinsie. Die aardbewing was veral gevoel in areas soos Ceres, Tulbagh en Wolseley. Die aardbewing het gelei tot die ernstige skade aan geboue, lewensverlies en die besering van tale mense. As gevolg van die sterkte van die aardbewing het tale ou geboue, sowel as die wat nie ontwerp is vir aardbewings nie, ineengestort. Die beraamde skade as gevolg van die aardbewing was ongeveer U.S. $24 miljoen. Suid-Afrika word geklassifiseer as ‘n area met ‘n risiko van middelmatige intensiteit aardbewings.

Die eerste weergawe van die seismiese ontwerp kode was gepubliseer in 1980. Hersiene weergawes is beskikbaar gestel in 1989 en 2010, maar die nuutste weergawes sluit nie alle faktore met betrekking tot die invloed van seismiese reaksie van strukture soos byvoorbeeld die grond-fondasie interaksie in nie. Strukture soos damme, watertorings, brûe, silos, pyplyne, maste en skoorstene word ook nie gedek deur die nuutste kodes nie. Die ontwerpstappe en riglyne van die nuutste weergawe is beperk tot die ontwerp van geboue. Die vraag ontstaan dan of die ouer sowel as toekomstige nuwe strukture wat nie ingesluit is onder die nuwe ontwerp kode nie, nie dalk vatbaar is vir skade wat nie onder die nuwe seismiese intensiteit waaronder dit ge geklassifiseer word nie. Verskeie publikasies is geraadpleeg om ‘n metode vir die bepaal van die seismiese gedrag van staalraam strukture daar te stel. Hierna was die informasie gebruik en toegepas op ‘n watertoring in ‘n area met n hoë seismiese risiko in Suid-Afrika. Die Engen 1-Stop watertoring, geleë in die Wynland, is gekies vir die studie aangesien dit aan die vereiste kriteria voldoen het en is gebruik om die vatbaarheid daarvan te bepaal in die geval van seismiese gebeure. Die resultate het getoon dat die Engen 1-Stop water toring kwesbaar vir die seismiese risiko wat daaraan toegewys is aan die area waar dit is. Die studie het gevind dat die seismiese aanvraag op die toring

Stellenbosch University https://scholar.sun.ac.za

veel meer is as die seismiese kapasiteit waarvoor dit ontwerp is. Die vraag kan dus gestel word of die Engen 1-Stop onder bespreking ontwerp is vir enige seismiese gebeure en die gepaardgaande strukturele impak daarop.

Stellenbosch University https://scholar.sun.ac.za

Acknowledgements

I would like to express my sincere gratitude to the people and institutions below for contributing to the successful completion of my master's studies.

- My supervisor Dr JAvB Strasheim for being actively involved in every stage of this dissertation. His generous wise advice and guidance have contributed to the accuracy of this dissertation.
- Dr Trevor Neville Haas for his role in identifying the research topic.
- The lab manager Mr Stephan Zeranka. His technical assistance during laboratory testing is acknowledged.
- Laboratory and workshop personnel Mr. Charlton Ramat, Mr. Peter Cupido, Mr. Johan Van der Merwe and Mr. Deon Viljoen. Their assistance in different ways is highly appreciated.
- My classmates, particularly B. Le Roux, A. Bauer, A. Vital, L. Oliver and E. Nuraan. Their friendships and academic discussions are priceless. They made me feel at home in South Africa. To them, deeply, thank you. I owe very much to them.
- My family for their love, prayers and support throughout my life.
- The government of Rwanda for funding the first two years of my studies.
- Institute of Structural Engineering (ISE) at Stellenbosch University for funding the extension of my studies. Special thanks to Prof. Billy Boshoff; the ISE staff and head of Structural Engineering Division. I am really speechless at his wise advice, suggestions, and advocacy on different problems I faced on the route to this achievement. May God bless him.
- Rwanda High Commission in South Africa for administrative assistance.
- Stellenbosch University, particularly the entire staff of the civil engineering department and the engineering librarians. The realization of this work is a result of your combined efforts in one way or another.

"Glory to God."

Stellenbosch University https://scholar.sun.ac.za

To

Niyomungeri A.

Irankunda B.

Stellenbosch University https://scholar.sun.ac.za

Table of contents

Stellenbosch University https://scholar.sun.ac.za

Stellenbosch University https://scholar.sun.ac.za

Stellenbosch University https://scholar.sun.ac.za

Stellenbosch University https://scholar.sun.ac.za

List of figures

Stellenbosch University https://scholar.sun.ac.za

Stellenbosch University https://scholar.sun.ac.za

Stellenbosch University https://scholar.sun.ac.za

Stellenbosch University https://scholar.sun.ac.za

List of tables

Stellenbosch University https://scholar.sun.ac.za

List of symbols

$(K_j)_B$, $(K_{jj})_B$	modified static stiffnesses K_j and K_{jj} for bedrock effect
$(K_j)_E$, $(K_{jj})_E$	modified static stiffnesses K_j and K_{jj} for embedment effect
$[C]$	damping matrix of MDOF
$[M]$	mass matrix of MDOF
$\{1\}$	influence vector
$\{F\}$	storey force vector of MDOF
$\{U\}$	relative displacement vector of MDOF
$\{\phi\}$	mode shape of MDOF
μ	ductility factor
a	half width of the footprint dimension of the rectangular foundation
A_1, A_2	areas
a_1, a_2	dimensionless coefficients dependent on the translation and rotation radius of the foundation, and effective height h of the structure
A_f	area of the foundation
a_g	maximum ground acceleration
a_o	dimensionless frequency parameter
$\tilde{a}_o$	adjusted dimensionless frequency parameter
a_{pi}	initial performance acceleration of ESDOF in CSM
a_{pl}	plastic acceleration of MDOF
a_y	yield acceleration of SDOF in CSM
a_o^r	reduced dimensionless frequency parameter
b	half length of the footprint dimension of the rectangular foundation
B, L	half width and length of a rectangular foundation
b_e	effective dimension of the foundation
C^*	damping of ESDOF
C_2	modification factor representing the increased displacement due to second-order effects
C_c	convective period factor
C_i	dimensionless coefficient for impulse period

Stellenbosch University https://scholar.sun.ac.za

C_i	modification factor relating the expected maximum inelastic displacement to the displacement calculated from linear elastic response
c_j	dashpot coefficient modifier for the degree of freedom j
C_o	modification factor relating spectral displacement to equivalent SDOF to the top/roof displacement of MDOF
C_s	seismic coefficient calculated based on fundamental natural period T of fixed base condition of the structure
c_z^i	soil dashpot intensity
$\overline{C}_s$	seismic coefficient of the flexibly supported structure calculated based on effective/fundamental natural period $\widetilde{T}$ of the flexibly supported structure
$\overline{C}_j$	dashpot value for the degree of freedom j
dA	attributed area to one spring and dashpot of the foundation
D_j	maximum displacement for mode j
D_{jy}	yield deformation for the j^{th} mode of the inelastic SDOF
d_{pi}	initial performance displacement of ESDOF for CSM
d_{pl}	plastic displacement of MDOF
d_s	depth of the stratum or bedrock
d_y	yield displacement of SDOF in CSM
$\widetilde{D}$	rigidity of the foundation base
e	foundation depth
E	Young's modulus of the steel
E_d	energy dissipated by damping
E_S	Young's modulus of the soil
E_{so}	maximum strain energy
E_t	Young's modulus of the tank material
F	force
f	frequency corresponding to the dominant response of the structure, mostly taken as fundamentals frequency of the flexibly supported structure
F^*	storey force of ESDOF
f_e	frequency/dominant frequency of excitation

Stellenbosch University https://scholar.sun.ac.za

F_i	horizontal load applied at i^{th} level
F_{sjy}	force of the equivalent SDOF for mode j
$\tilde{f}$	fundamental/effective natural frequency of the flexibly supported structure
F_y^*	yield storey force of ESDOF
g	gravitational acceleration
G	shear modulus of the soil at large strain level
G_o	shear modulus of the soil at small strain level
H	overall depth of the water in the tank
h	height/effective height of the structure from the base to the centroid of the inertia forces
h_c	height of the convective mass
h_f	height of the mass m_f
h_i	height of the impulse mass, unless otherwise stated
H_t	total height of the structure
$H_u(\omega)$	transfer function amplitude
$h_i^{'}$, $h_c^{'}$	height of the impulse and convective masses for moment calculation
I_{yy}	moment of inertia of the foundation about y-axis
j	index which represents the degree of freedom, translation or rotation; unless otherwise stated
K	lateral static stiffness of the structure supported on undeformable ground level
K^*	elastic stiffness of ESDOF
K_c	spring for the convective mass
K_e	effective stiffness of MDOF
K_f	rotation and translation dynamic stiffness of the foundation
K_i	spring assigned to the impulse mass
K_i	initial stiffness of MDOF
k_j	dynamic stiffness modifier for the degree of freedom j
K_j, $\overline{K}_j$	static and dynamic stiffnesses of the foundation for translation in the j-direction
Kj_j, $\overline{K}_{jj}$	static and dynamic stiffnesses of the foundation for rotation about the j-axis

Stellenbosch University https://scholar.sun.ac.za

K_s	hardening stiffness of MDOF
k_z^i	soil spring intensity
l	length of the steel frame element
$m(t)$	exciting dynamic moment
M^*	mass of ESDOF
M, m	total mass of the superstructure
m_c	convective mass
m_f	mass of the steel frame
m_f	mass representing the flexibility of the tank walls
m_i	impulse mass
m_i	storey mass at i^{th} floor
m_l	total mass of the water contained in the tank
m_{rb}	mass of the roof and the base of the tank
m_s	mass of the empty tank and one third of the mass of the steel frame
m_w	mass of the tank walls
M_j^*	effective mass of the mode j
PF_1	modal participation factor in CSM
r	radius of the water tank
R_μ	strength reduction factor
R_e	foundation length ratio
r_f	radius of the foundation
r_g	radius of gyration
R_j	maximum modal response for mode j
r_j	translation radius of the foundation in the j-direction
r_{jj}	rotation radius of the foundation about the j-axis
R_{kj}, R_{cj}	stiffness and dashpot modifier for rocking effect about j-axis
R_{MPA}	total seismic demand
S	spacing of the columns of the tower
S_a	acceleration response of inelastic ESDOF
S_{ae}	pseudo-acceleration ordinate obtained from response spectrum

Stellenbosch University https://scholar.sun.ac.za

S_{ay}	yield acceleration obtained from capacity spectrum
S_d	displacement response of inelastic ESDOF
S_{de}	elastic displacement ordinate obtained from response spectrum
S_{ds}	design spectral acceleration at short periods
S_e	elastic design acceleration
$S_e(T_{con})$	convective spectral acceleration
$S_e(T_{imp})$	impulse spectral acceleration
S_g	free field ground motion
S_j	distribution of lateral force for mode *j*
t	equivalent uniform thickness of the tank
T_c	characteristic period of the ground motion i.e. transition period where constant acceleration comes to constant velocity
T_{con}	natural period of convective mass
T_e	effective period of MDOF
T_{eq}	elastic fundamental period of ESDOF
T_i	initial fundamental period of MDOF
T_{imp}, T_{con}	natural periods of the impulse and convective masses
T_n,/T	fundamental natural period of the rigidly supported structure
T_r	tension capacity of the bolt
T_u	ultimate tension force which could be applied to the bolt
$\tilde{T}$	fundamental /effective natural period of the flexibly supported structure
$\frac{\tilde{T}}{T}$	period lengthening ratio due to SSI
$\left(\frac{\tilde{T}}{T}\right)_{\text{mod}}$	modified period lengthening ratio $\frac{\tilde{T}}{T}$
u	top/roof displacement of MDOF
$u(t)$	top lateral displacement of SDOF structure
u^*	reference displacement of ESDOF
u_{FIM}	foundation input motion
u_g	time history ground displacement
u_m	maximum peak displacement of an inelastic system

Stellenbosch University https://scholar.sun.ac.za

u_t	target top/roof displacement of MDOF
u_{tj}	maximum displacement of MDOF
u_{tjy}	j^{th} mode top/roof displacement of MDOF
u_y	yield displacement of MDOF
$\ddot{u}_g$	ground acceleration
$\{\ddot{U}\}$	relative acceleration vector of MDOF
$\{\dot{U}\}$	relative velocity vector of MDOF
$\dot{u}^*$	reference velocity of ESDOF
$\ddot{u}^*$	reference acceleration of ESDOF
u_y^*	yield displacement of ESDOF
V	seismic base shear force calculated based on fixed base condition of the structure
V_b	base shear force of MDOF
V_{bjy}	base shear force of MDOF for mode j
V_r	shear capacity of the bolt
V_s	shear wave velocity
$V_{s,r}$	reduced shear waves velocity
V_u	ultimate shear force which could be applied to the bolt
V_y	yield base shear force of MDOF
$\widetilde{V}$	base shear force of the flexibly supported structure
W_i	portion of the total gravity load of the structure at level i
$\overline{W}$	effective seismic weight of the structure
ω	natural frequency
$y(t)$	exciting dynamic load
α	strain hardening ratio
α_j	dynamic stiffness and radiation damping modifier for the degree of freedom j
α_m	modal mass coefficient
α_v	incidence angle of the seismic waves
β	damping ratio of the structure supported on a ground level that can't be deformed
β_{eq}	equivalent damping coefficient of inelastic ESDOF

Stellenbosch University https://scholar.sun.ac.za

β_f	translation and rotation damping ratio of the foundation, hysteretic damping of the soil and radiation damping of foundation both included
$\beta_{f,j}$	damping ratio of the foundation (respectively, soil and foundation damping) for the degree of freedom j
$\beta_{f,r}$	translation and rotation radiation damping of the foundation
$\beta_{fr,j}$	radiation damping of the foundation for the degree of freedom j
β_o	hysteretic damping of ESDOF
β_s	hysteretic damping of the soil
$\tilde{\beta}$	damping/effective damping ratio of the flexibly supported structure
γ_1	Rayleigh stiffness damping coefficient
γ_I	importance factor of the structure
γ_o	Rayleigh mass damping coefficient
Δ	top lateral displacement of the superstructure
Δ_v	induced vertical displacement of the foundation
ΔV	reduction in base shear force V due to SSI
Δ_ϕ	induced rotation angle of the foundation
η	damping correction factor
η_j	static stiffness or modified static stiffness (for embedment effect and or bedrock effect) for the j mode of vibration
κ	ground motion incoherence parameter
ν	Poisson's ratio of the steel
ν_s	Poisson's ratio of the soil
π	PI, ratio of a circle perimeter to its diameter
ρ	mass density of the steel
ρ_s	soil density
ρ_w	mass density of the water
σ	wave parameter
σ_{ax}	allowable axial stress in the frame elements
σ_u	ultimate tensile strength
σ_y	yield stress
Φ	relative rigidity of the foundation

Stellenbosch University https://scholar.sun.ac.za

ϕ_{i1}	fundamental mode displacement magnitude at the i^{th} level of the structure
ϕ_{ij}	mode shape vector of i^{th} floor for mode j
ϕ_j	mode shape of vibration for mode j
ϕ_n	magnitude of mode shape at roof level of MDOF
ϕ_{nj}	j^{th} mode top shape value
ψ	velocity ratio

Stellenbosch University https://scholar.sun.ac.za

List of acronyms

2D	Two-Dimension
3D	Three-Dimension
ASCE	American Society of Civil Engineers
ATC	Applied Technology Council
BSSC	Building Seismic Safety Council
CDA	Code Design Approach
CSM	Capacity Spectrum Method
DCM	Displacement Coefficient Method
EC	Eurocode
EMDOF	Equivalent Multi-Degree of Freedom
EN	European Standard
ESDOF	Equivalent Single Degree of Freedom
FEMA	Federal Emergency Management Agency
FEM	Finite Element Method
LVDTs	Linear Variable Displacement Transducers
MDOF	Multi-Degree of Freedom
MPA	Modal Pushover Analysis
MVM	Modified Veletsos Method
NEHRP	National Earthquake Hazards Reduction Program
NLDA	Nonlinear Dynamic Analysis/Approach
PEER	Pacific Earthquake Engineering Research
PGA	Peak Ground Acceleration
POA	Pushover Analysis/Approach
SAISC	Southern African Institute of Steel Construction
SANS	South African National Standards
SDOF	Single Degree of Freedom
SRSS	Square Root Sum of Squares
SSI	Soil Structure Interaction
ADRS	Acceleration Displacement Response Spectrum

Stellenbosch University https://scholar.sun.ac.za

Chapter 1
Introduction

1.1 Background to the research question

A water tower is a vertical structural system supporting a water tank. The tank is situated on top at a height specified for sufficient water pressure, with the purpose of storing and distributing water. The stored water can be used for various purposes, including chemical manufacturing, farming, firefighting, industrial raw water treatment, irrigation services and the distribution of potable water. These structures have the advantage, *inter alia*, of supplying water at the desired pressure and can keep water from freezing during cold weather due to the filling up and emptying out movements of the water inside of the tank. In addition, the stored water in the tower can also help to supply peak demand as well as provide backup when supply is interrupted.

Water towers operate in cycles: the water tank is filled with water by a pumping system, generally during night-time, and the water is frequently supplied to the consumer during the daytime. The standard height of a water tower specified in the literature is 40 meters, but, as mentioned, it varies depending on the desired output water pressure. The materials used for the construction of water towers depend on various parameters such as shape, site limitations and aesthetics, but steel and concrete (or prestressed concrete) are mostly used.

Water towers have been constructed since ancient times. In the middle of the 19th century, it was even mandatory in America for a building of more than six storeys to have a rooftop water tower. During this period, water towers improved significantly. Presently, the country with the largest number of water towers is India. These towers are required to cope with widespread power outages.

In South Africa, water towers have been used intensively in water supply since 1990. As a result, accessibility to potable water has increased from 66% to 79% in a period of twenty years from 1990 to 2010. However, due to lack of maintenance, some water towers are susceptible to failure; adequate rehabilitation measures are thus required. With regard to the structural performance and reliability requirements, it was found that water towers are vulnerable to seismic excitation due to their low ductility (Birtharia & Jain, 2015). Nevertheless, despite the vulnerability of water towers, the seismic code of South Africa does not cover seismic design and evaluation of the water towers.

Stellenbosch University https://scholar.sun.ac.za

This study is therefore concerned with presenting a methodology for seismic performance assessment of steel framed water towers. The reviewed methodology was applied to a typical water tower located in a high seismic risk zone in South Africa. Based on the seismic risk map of South Africa (available from SANS 10160-4: 2011), the Engen Winelands 1-Stop water tower was selected for the purpose of this study.

1.2 Problem statement

In the past, the seismic design of a water tower was done by considering the total weight of the water reacting as a mass rigidly attached to the centre of gravity of the tank. Later, this method was proven to result in underestimation of the water pressure on the tank walls as well as overestimation of the base shear force and base moment when the structure is exposed to seismic action (Gaikwad & Mangulkar, 2013; Algreane, Osman, Karim & Kasa, 2011). This approach, as referred to in the literature, is based on the concepts of "static structural analysis".

Following the catastrophic failure of water tanks during an earthquake in Chile in 1960, research was conducted to assess the realistic seismic behaviour of water contained in the tanks (e.g. Housner, 1963). Consequently, a more accurate approach based on dynamic analysis techniques used for structures was developed, namely "dynamic analysis". It has been shown that under seismic action, the mass of the water contained in a tank with a freeboard can be modelled as two parts namely an impulse mass and a convective mass. The impulse mass represents the portion of the mass of water which reacts dynamically, as if is rigidly attached to the tank, and thus translates in unison with the tank. The convective mass represents the top part of the water that sloshes as the tank is excited by the dynamic load at the base. The latter is known as "sloshing effect'' and, apart from static pressure induced by water, it induces an additional dynamic pressure which results in a higher water pressure than that obtained from static analysis. This approach has been proven to provide a smaller base shear force and base moment than the static analysis approach. This leads to a more economical design for the structure.

Moreover, the introduction of soil structure/foundation interaction modelling into the seismic design procedures (displacement based procedure) showed that seismic soil structure interaction (SSI) analysis had been wrongly implemented into design codes and standards because SSI procedures available from the design codes and standards give reduced internal design forces

Stellenbosch University https://scholar.sun.ac.za

compared to the fixed base condition of the structure (refer to 2.3.3). The reason for this was that SSI analysis procedures adopted into the design codes and standards did not consider excessive lateral displacement induced by soil flexibility, which was found to result in increased internal forces. Later on, improved SSI analysis methods were developed which are now available (e.g. non-linear time history and displacement based analysis). Thus, a methodology including all of the above developments is need.

1.3 Research objectives

The main objective of this research is to review and present from the literature a numerical method for seismic performance assessment of steel framed water towers with consideration of the effect of soil foundation interaction as well as the sloshing effect of contained water, and to apply it to a typical existing water tower. More specifically, this research seeks to assess the seismic state of the Engen Winelands 1-Stop water tower, with consideration of the local yield and buckling of the frame elements (bracings and columns) as well as the global stability of the tower (i.e. overturning capacity). The global stability was checked at the column base, specifically the connection between the bottom column and the foundation (refer to 4.3.2). The local yield and buckling of both bracings and columns were taken into account at the stage of defining the section properties as well as analysis configurations i.e. defining and consideration of nonlinearity of material and geometry into analysis process (refer to 4.2.1.1 and 4.2.2.1).

1.4 Scope and limitation

The research will be applied to a case study for the evaluation of an existing water tower, namely, the steel water tower located at the Engen Winelands 1-Stop in South Africa. Furthermore, the research is limited in considering only a few of the relevant factors influencing the seismic response of the mentioned structure. Only the dynamic behaviour (convective and impulse responses) of the water in the tower and the soil flexibility will be considered. Various other parameters which might also contribute to the failure of the structure, such as wind load, blast load, etc., however, were not included. The structure was checked to consider: (i)local section yielding, (ii)local section buckling, and (iii) global structure stability.

Stellenbosch University https://scholar.sun.ac.za

1.5 Assumptions

The research was oriented towards its application to the analysis and evaluation of an existing structure, therefore, a reduction in overall strength of the structure could occur due to the deterioration (e.g. rusting) of materials as well as various other external and internal (e.g. fatigue) parameters. During the analysis process, all parameters which could result in reduced strength relative to the same newly built structure were ignored. Moreover, the walls of the water tank, the connection of the frame elements (bracings) to the vertical columns, as well as the connection of the tank to the top of the steel frame were assumed to be designed well enough to withstand any resultant applied force.

1.6 Overview of research conducted

The research conducted for this thesis is documented in six chapters:

Chapter 1: Introduction

In the first chapter, the objectives and scope of the research, background to the research question, and the assumptions used in analysis are discussed.

Chapter 2: Literature Review

Firstly, a summary on the dynamic modelling of water tanks is presented in chapter two. Secondly, a review of the effects of soil structure interaction (SSI) on the seismic response of structures and the implementation of SSI into seismic design code is discussed. Lastly, different methods of seismic performance assessment of structures are presented.

Chapter 3: Methodology

The methodology for assessing the structural performance of a steel frame water tower is discussed. All of the information which is necessary to achieve the main objective of assessing the seismic performance of a typical water tower is presented. This includes the size of the structural components and the mechanical properties of the materials used to build the water tower, the seismic and soil characteristics of the site where the water tower was built and the overall size of the tower. Moreover, a step-by-step methodology for assessing the performance of the water tower is described. Lastly, the allowable maximum stress in the lattice steel frame members is defined.

Stellenbosch University https://scholar.sun.ac.za

Chapter 4: Analysis and testing of the structure

This chapter contains two different parts. The first part presents the analysis of the test structure using laboratory procedures, code design procedures and numerical procedures. Based on these results, the design parameters (e.g. damping factor) for numerical analysis of the water tower under assessment are presented.

The second part of this chapter consists of the seismic assessment of the previously mentioned structure. Its seismic capacity obtained from modal pushover analysis, and its seismic demand obtained from code design analysis and nonlinear dynamic analysis are presented. In addition, this chapter also contains the requirements for maintaining the global stability of the water tower under assessment.

Chapter 5: Summary and discussion of results

In chapter 5, a summary of all the results obtained from chapter 4 is presented. The discussions on seismic capacity and seismic demand of the investigated water tower are included. The effect of the soil flexibility on the seismic response of the mentioned tower is also discussed.

Chapter 6: Conclusions and Recommendations

In the last chapter a general conclusion is drawn from the results discussed in chapter 5, providing recommendations for further research.

Stellenbosch University https://scholar.sun.ac.za

Chapter 2
Literature Review

2.1 Introduction

Water towers are widely known as elevated water storage tanks with the main objectives of safely maintaining and supplying water to the consumers with sufficient pressure. They should be big enough to satisfy the daily demand of the community, stable, durable and capable of maintaining the chemical properties of the stored water. Many water towers have a height of about 40 meters; however, the specified minimum size of water towers is a height of 6 meters and a diameter of 4 meters. Water towers can be categorised based on construction materials, e.g. steel, concrete or composite water towers.

The seismic collapse of a water system has led to catastrophic losses of property and human lives since it causes a lack of water for firefighting and consumption (Chen, 2010). The failure of water reticulation system that carried water from the San Andreas Lake to San Francisco during the San Francisco earthquake in 1906 is the case referred to most in literature This earthquake destroyed San Francisco city due to a lack of water for firefighting. Hosseinzadeh (2008) and Mehrpouya (2012), indicate that the seismic collapse of water tanks can result from: (i) damage to the roof of the tank due to sloshing of the contained liquid, (ii) elephant foot buckling of the shell of the tank due to excess axial force and overturning (see Figure 2.1), (iii) sliding of the tank due to excessive stress in the base anchors, (iv) differential settlement of the foundation which can cause global instability of the tank system, and (v) uplifting of the tank which can damage the pipes connected to it.

Some of the aforementioned failure modes can be taken into account at the analysis stage, e.g. settlement of the foundation and sloshing of the contained liquid; others such as elephant foot buckling and failure of the base anchors can be dealt with at the design stage. In section 2.2 of this chapter different approaches on dynamic analysis of water tanks with consideration of sloshing effects of the contained water are presented. Section 2.3 discusses a review of the analysis of the structure with consideration of the flexibility of the soil. The last section, section 2.4, contains the different methods of seismic assessment of the structure.

Stellenbosch University https://scholar.sun.ac.za

Figure 2.1: Illustrative example of elephant foot buckling of the tank wall at the base (Moghaddam & Sangi, 2011)

2.2 Dynamic modelling of water tanks

The failure of elevated water tanks during the earthquake in Chile mentioned in the section on the problem statement inspired many researchers to investigate the seismic behaviour of the liquid containers. Housner (1957) and (1963) can be considered as the first of these studies. Before this, the liquid storage tanks were considered to behave dynamically as one single degree of freedom with a completely filled tank as a critical condition. In practice water storage tanks are seldom kept fully filled; this approach thus ignored sloshing effect of incompletely filled tanks and it overestimated the response of the system (Gaikwad & Mangulkar, 2013). At present, alternative models which take the effects of sloshing into account are available and have even been adapted in different design codes (e.g. Priestley *et al.*, 1986; EN 1998-4, 2006). According to Jaiswal, Rai and Jain (2007), current models are categorised into two groups: rigid tank models (Housner, 1963; Veletsos & Yang, 1977; Veletsos, 1984) and flexible tank models (Veletsos, 1984; Haroun & Housner, 1981). Each group is described as follows:

Rigid tank models

In 1963 Housner developed the first double mass model for dynamic analysis of liquid storage tanks (Housner, 1963). He conducted his study by considering three different cases: an empty tank, a filled tank with free board and a completely filled tank. The study showed that an empty or completely filled tank, behaves as single mass undergoing the one single acceleration. Conversely, in the case of a filled tank with free-board, the hydrodynamic pressures caused by seismic excitation are split into two parts: impulse pressure and convective pressure. Impulse pressure represents the pressure induced by the bottom portion of liquid mass which behaves as rigidly

Stellenbosch University https://scholar.sun.ac.za

fixed to bottom of the container and it undergoes the same acceleration as the liquid container. Convective pressure on the other hand is the pressure induced by the top portion of the liquid mass which oscillates at the free surface of the liquid. In Housner's model (Figure 2.2) both impulse pressure and convective pressure are replaced by the equivalent masses: the impulse mass and convective mass. The impulse mass is labelled m_i and the convective mass m_c in Figure 2.2. The impulse mass is rigidly attached to the tank wall at the same height as the horizontal equivalent hydrodynamic force and the added equivalent convective mass is connected to the tank wall with springs which allows it to oscillate in the same manner as the water which it represents in the model. Housner assumed a rigid wall tank and his study presented expressions for masses, mass heights and springs in the required calculations. Wozniak and Mitchell (1978) generalized Housner's model to short and slender tanks.

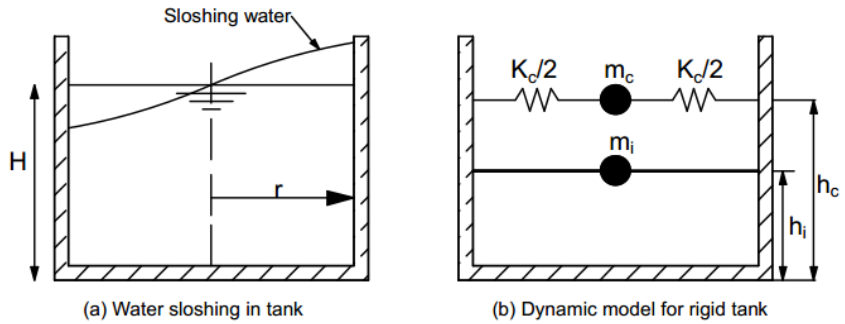

Figure 2.2: Housner's dynamic model (Housner, 1963)

Veletsos and Yang (1977) used a different approach than Housner in investigating dynamic behaviour of rigid tanks and they also derived a double mass model for the analysis of tanks with rigid walls. They assessed the effects of wall flexibility on the magnitude and distribution of the hydrodynamic pressures and the corresponding base shear force. To analyse dynamic behaviour of a flexible wall tank, they considered a completely filled tank and they used Flügge shell theory in combination with a Ritz-type energy procedure as well as the natural modes of vibration of a uniform cantilever beam. The results showed that Housner's (1963) approach is more accurate than Veletsos and Yang's (1977) approach and it was found that the wall flexibility increases the impulse pressure. Veletsos's (1984) model for a rigid walls tank is an improved version of that presented in Veletsos and Yang (1977).

Stellenbosch University https://scholar.sun.ac.za

Flexible tank models

Based on the same approach of Veletsos and Yang (1977), Haroun and Housner (1981) presented a triple mass model for a tank with flexible walls (see Figure 2.3) with the third mass, m_f, replacing the effect of wall flexibility to compute the response of the system. This triple mass model has been adapted by Veletsos (1984) and has been simplified to a two mass model by Malhotra, Wenk and Wieland (2000) (see section 3.2.1).

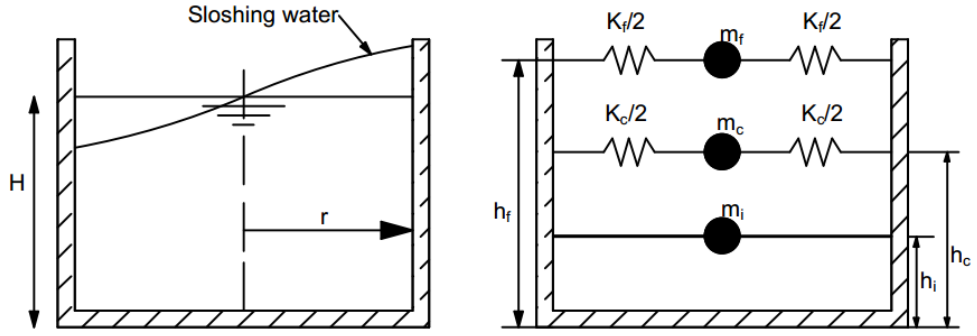

Figure 2.3: Mechanical model for flexible tank walls (Housner, 1963)

2.3 Seismic analysis with consideration of Soil Structure Interaction (SSI)

2.3.1 Introduction

In Civil engineering structures can be analysed and designed under the assumption that they are restrained at the foundation base against translation, rotation and settlement. When structures are excited by dynamic loadings (e.g. earthquake excitation) they normally transfer the shear force and bending moment at the base of the structure leading to the equilibrium condition of which requires the inertia force generated at the top mass of the structure (see Figure 2.4).

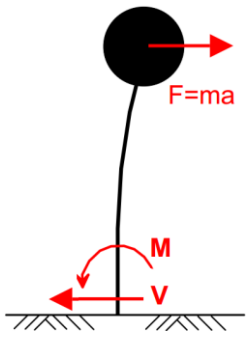

Figure 2.4: Force transfer to the base of structure (adapted from Stewart, 2004)

Stellenbosch University https://scholar.sun.ac.za

If the soil structure is not stiff enough to provide assumed base conditions, there would be horizontal translation and rotation at the base of the foundation which will result in additional displacement of the super-structure.

In displacement based analysis (e.g. P- Δ analysis) the additional displacement due to the flexible nature of the foundation increases the internal forces in the constituent sections/elements of the structure. Thus, if a structure is supported on a very flexible medium and is designed under an assumption of fixed base condition, it might be vulnerable to seismic excitation.

An example of the relevant modelling features required to model the real behaviour of the soil at a given site, is outlined here. Figure 2.5 shows two concrete structures with flexible beams and a shear wall supported by two different types of soil. The left structure is rigidly supported, whereas the structure on the right is flexibly supported. If these two structures are excited by the same intensity of dynamic load, the shear wall of the left structure will sustain the resultant forces. If yield happens, the shear wall will crack before it transfers the forces to the frame elements. In the case of the structure on the right side, the flexibility of the soil will not allow the shear wall to withstand resultant forces-it will rotate and induce cracks into the beams and it will act as a force transfer mechanism. Thus, if a structural engineer has provided the shear wall to withstand dynamic loadings, it will not act as such for the case of a flexible foundation and the structural behaviour shown on the right of Figure 2.5 will be observed.

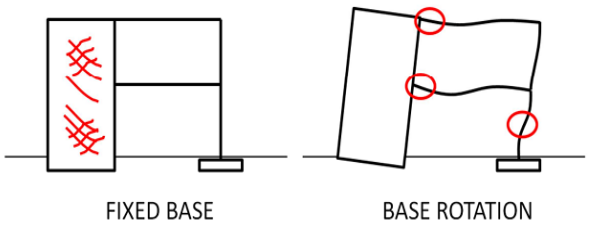

Figure 2.5: Failure example due to soil flexibility (adapted from Kotronis, Tamagnini & Grange, 2013)

Stellenbosch University https://scholar.sun.ac.za

2.3.2 Research done on Soil Structure Interaction

A Soil Structure Interaction analysis (SSI) investigates the response of the structure to the free field ground motion by incorporating the mechanical properties of the soil underlying and surrounding the foundation base. In other words, SSI analysis assesses the response of the structure with all system components combined together (i.e. soil, foundation and superstructure). Based on Veletsos and Prasad (1989:935) free field ground motion here denotes *"the motion which would be induced at the foundation soil interface if no structure were present".*

Incorporation of soil properties in the analysis (i.e. SSI analysis) of structures has been found to modify the response of the structure analysed under an assumption of fixed base condition in three ways: inertia interaction, kinematic interaction and foundation flexibility. Each modification to the response has been studied separately and has been referred to by its cause e.g. inertia interaction effects, kinematic interaction effects or foundation flexibility effects. These three response modification effects can be summarised as follows:

Inertial interaction effects

The inertial interaction effects refer to the change in natural frequency and damping coefficient of the structure resulting from displacement and rotation of the foundation at the soil foundation interface. The afore-mentioned displacement and rotation occur due to the forces transferred to the base of the structure from inertia force generated by the concentrated mass at the top of the structure and are proportional to the flexibility of the soil. The more flexible the soil the more it displaces and rotates.

The soil radiation damping effect is caused by the radiated energy at the foundation base from foundation movements (Figure 2.6) while hysteretic damping is caused by the cyclic stress strain behaviour of the soil. The intensity (energy) of the incoming seismic wave is reduced by the energy radiated in the damping process, whereas hysteretic damping refers to the dissipation of energy released by an earthquake through its propagation into the soil medium. Thus both hysteretic damping and damping caused by energy radiation act as source of seismic energy dissipation which affects the overall response of the system.

Stellenbosch University https://scholar.sun.ac.za

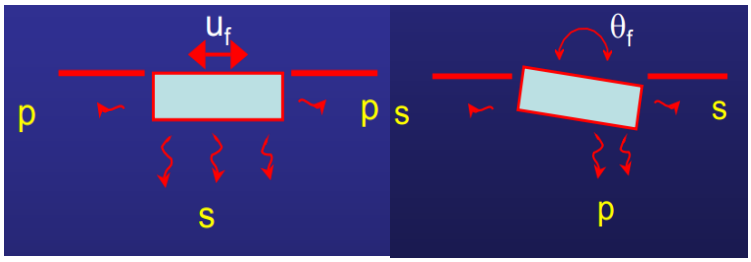

Figure 2.6: Radiation of energy at foundation base (adapted from Stewart, 2004)

The change in the fundamental period of structure is due to the reduced stiffness caused by the added rotational of the foundation which increases total displacement of superstructure and lengthens the fundamental period of the system (Figure 2.7). Since all those changes are related to inertia force they are referred to as *"inertial interaction effects*".

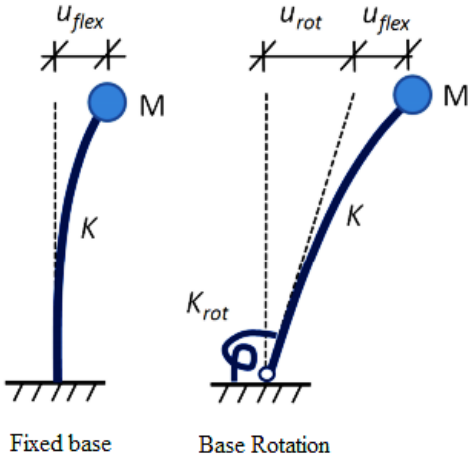

Figure 2.7: Total displacement of flexibly supported SDOF (adapted from Kotronis *et al.*, 2013)

Kinematic interaction effects

Kinematic interaction effects represent the change in response of the structure if the structure is analysed with consideration of free field motion as input motion, and with consideration of ground motion recorded at presence of the structure as input motion. The change in response depends on different parameters such as relative displacement of foundation to free field motion, foundation embedment, geometry of foundation, the incident angle of seismic waves.

Foundation deformation effects

Referring to Figure 2.6, if the foundation base is not stiff enough to behave as a rigid element with reference to the surrounding soil medium, it might also result in additional deformation of the

Stellenbosch University https://scholar.sun.ac.za

foundation which contributes again to the overall behaviour of the system. Thus the difference in response of the rigid base relative to the flexible base is referred to as "*foundation deformation effects*". For use in simplified engineering models this problem can be avoided by providing a stiff foundation relative to the surrounding material.

2.3.2.1 Review of soil structure inertia interaction effects

The first publication on foundation response to dynamic loading was written in 1936 by Eric Reissner. Reissner (1936) studied dynamic response of the circular foundation supported at the surface by elastic half space excited by vertical harmonic load generated by two rotating masses. He developed an equation of vertical displacement at the centre of the foundation as well as an equation of amplitude of motion. Reissner assumed a uniform distribution of pressure underneath the footing. His work was based on that of Lamb who published a paper titled "*On the Propagation of Tremors over the Surface of an Elastic Solid*" in 1904. Lamb (1904) studied the stress-strain-displacement of elastic half space medium excited by vertical dynamic point load applied at the surface of the medium, and he also extended Maxwell's law of static reciprocity to dynamic reciprocity. Lamb's work is referred to in literature as the "dynamic Boussinesq problem" because it is an extension of the "classical Boussinesq's problem" to dynamic loading. Reissner integrated Lamb's solution over a circular area (Richart, Hall & Woods, 1970:194). However, in some literature Reissner is referred to as the father of soil structure interaction (Kotronis *et al.*, 2013: 5).

Since Reissner's (1936) paper, a lot of research has been published on the topic of foundation vibration, but with different assumptions of stress distribution underneath the footing (parabolic, uniform or rigid base stress distribution; see Figure 2.8). It is not possible to review all of these studies here, but a complete overview is available in Richart, Hall and Woods (1970:192-243).

Figure 2.8:Effective pressure(modified from Richart *et al.* 1970)

Bycroft's 1956 paper, however, can be regarded as the most rational and realistic in regard to dynamic analysis of foundations (Bycroft, 1956; Parmelee, 1967). He discussed the dynamic

Stellenbosch University https://scholar.sun.ac.za

behaviour of harmonically loaded rigid circular foundation fixedly supported at the surface of an elastic half space as well as an elastic stratum (elastic layer). Bycroft developed displacement equations for the foundation for both vertical and horizontal translations as well as rotation about its centre. He assumed uniform pressure distribution underneath the foundation base, his displacement equations were based on a weighted average of the displacements and he ignored the change of soil properties during vibration.

Parmelee (1967) used of Bycroft's (1956) results in his work for developing displacement equations for the base mass (horizontal translation and rotation) and the top mass (horizontal translation) of a single degree of freedom structure with a fixed base condition. He also established a dynamic model for the SSI analysis of a building system subjected to horizontal periodic loading at the foundation base. In that model the soil damping values were ignored and the soil stiffness was calculated based on static values. It must also be noted that the developed equations for the foundation base do not take into account the effects of the inertia of the base mass.

Using his model, he examined the response of twelve buildings of different heights (5, 10, 15 and 20 storeys) and the results corresponded with his analytical expressions. The results showed that the flexibility of soil increases the response of the structural system and the fundamental mode of the system was found to be the only mode largely influenced by the stiffness of the soil, while other fundamental natural frequencies were found to change slightly with a change in soil stiffness. Additionally, Parmelee(1967) showed that as the supporting medium becomes more flexible as the resonant frequency of the system decreased to a value which is less than the natural frequency of the building in its fixed base condition.

Veletsos and Wei (1971) firstly reviewed previous research. In these studies the response of foundation was computed either assuming the parabolic, uniform or rigid base stress distribution of the contact pressure at soil-foundation interface (refer to Figure 2.8) or using the theory of elasticity which gives rise to mixed boundary conditions (Shah, 1968). The latter method was introduced after Parmelee's (1967) paper and it is known in literature as the “complete mixed boundary value problem” because of the difficulty associated with solving the set of analytical equations.

Stellenbosch University https://scholar.sun.ac.za

Moreover, in their previous studies there was also no provision for both foundation rotation induced by horizontal force and the lateral displacement of the foundation induced by overturning moment (this is referred to in the literature as "coupling effects"). In other words, the displacement equations have been established in the direction of the exciting forces only.

Secondly Veletsos and Wei (1971) also studied a steady state response of a massless rigid circular disk supported on the surface of an elastic half space, excited by both a harmonic horizontal load and a harmonic overturning moment. They developed displacement equation for the disk, equations for the stress distribution underneath the disk and established an equivalent analogical model for SSI analysis (see Figure 2.9). During the development of all the mentioned equations both the rotation amplitude induced by horizontal force and the lateral displacement induced by overturning moment were considered and each force effect was evaluated independently. In other words, the response of horizontal force was evaluated by considering zero normal contact stress and the response of overturning moment was provided by assuming zero horizontal contact stress. It is also essential to recognise that the soil medium which was on the sides of the disc was considered as stress free. Moreover, the rotation amplitude induced by horizontal force and the lateral displacement induced by overturning moment, *i.e. "coupling effects",* were not taken into consideration in the damping and stiffness equations (equation 2.1 to 2.4) of Veletsos and Wei's model presented in Figure 2.9 (see page 41). All these assumptions used by these researchers are referred to in literature as the "relaxed mixed boundary value problem".

According to Bielak (1971) for the complete mixed boundary value problem all the components of displacements underneath the footing have to be provided whereas in the relaxed mixed boundary value problem, at least one component of surface stress is zero.

The writers (Veletsos & Wei, 1971) compared their solutions with those of previous researchers and both results were in good agreement with low range of frequency of vibration (their previous results were limited to low frequency of vibration applications). Veletsos and Wei's (1971) solutions appeared to be the most realistic SSI analysis results because they were in good agreement with the previous results and they extended to high frequency of oscillation.

Stellenbosch University https://scholar.sun.ac.za

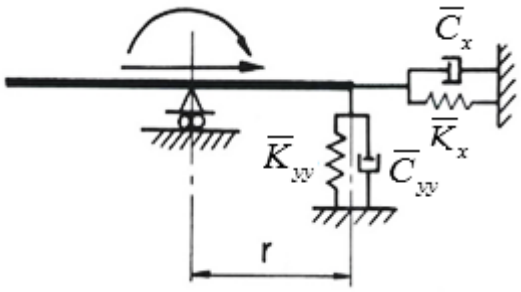

Figure 2.9: Simplified analogical model of SSI analysis (Veletsos & Wei, 1971)

This afore-mentioned model was aimed to simplify the problem of SSI analysis by modifying the fixity of the base condition of the structure in order to include soil properties of underlying materials in the analysis as a function of soil reactions (stiffness and damping of soil). As shown in the figure above, this model is limited to the surface supported rigid foundation dynamically loaded by overturning moment and horizontal force. The equations of the model derived by Veletsos and Wei (1971) are as follows:

$$\overline{K}_x = k_x K_x \tag{2.1}$$

$$\overline{K}_{yy} = k_{yy} K_{yy} \tag{2.2}$$

$$\overline{C}_x = \eta_x \frac{K_x r_f}{V_s} \tag{2.3}$$

$$\overline{C}_{yy} = \eta_{yy} \frac{K_{yy} r_f}{V_s} \tag{2.4}$$

$$K_x = \frac{8}{2-\nu_s} G r_f \tag{2.5}$$

$$K_{yy} = \frac{8}{3(1-\nu_s)} G r_f^3 \tag{2.6}$$

$$V_s = \sqrt{G_o / \rho_s} \tag{2.7}$$

Where $\overline{K}_x$ and $\overline{K}_{yy}$ are dynamic translation and rocking stiffnesses of the foundation, K_x and K_{yy} are static translation and rocking stiffnesses of the foundation, r_f is the radius of the foundation, ν_s is the Poisson's ratio of soil, G_o is the shear modulus of the soil, $\overline{C}_x$ and $\overline{C}_\theta$ are the translation

Stellenbosch University https://scholar.sun.ac.za

and rocking damping/dashpot coefficients of the foundation, ρ_s is the mass density of the half space, k_x, k_{yy}, η_x and η_{yy} are dimensionless parameters which are a function of the dimensionless frequency parameter a_o given by:

$$a_o = \omega r_f / V_s \tag{2.8}$$

k_x, k_{yy}, η_x and η_{yy} values are given in the referenced article.

Jennings and Bielak (1973) used impedance functions (i.e. the force-displacement relationship of the soil) from Bielak (1971) in their study of the steady state and earthquake response of a single and multi-storey building. The impedance functions used were developed based on the principle of the relaxed mixed boundary value problem. The foundation in both cases was a circular plate of negligible thickness and non-zero mass perfectly bonded to the surface of elastic half-space. Equations for horizontal translation of the floor masses, base mass and rotation of the system in the plane of motion were developed. The authors also developed equations for the natural frequency and damping coefficient of the equivalent fixed base system. In this study the effects of base mass and rotational mass moment of inertia of the floors to the response of the system were evaluated and the results showed the same observations as that of Parmelee (1967). It was also shown that the base mass and rotational mass moment of inertia of the floors change the response of the system slightly; e.g. for a single storey, if the base mass is increased to two times the floor mass this leads to a reduction of 2.5% of resonance frequency. The authors did not explicitly define the range of system parameters which might increase or decrease the effective damping of the system for either a damped or un-damped structure; however, it was shown that the soil interaction can increase or decrease the effective damping of the system depending on system parameters. Moreover, the results of Jennings & Bielak showed that SSI analysis of a multi-storey structure might be applied only for the first mode of vibration of a system; the contribution of higher vibration modes to SSI is deemed negligible.

Veletsos and Meek (1974) used Veletsos and Wei's (1971) model in their study of the main parameters which must be considered in SSI analysis. Both the translational base mass and rotational mass moment of superstructure were ignored and three horizontal base excitations were examined: harmonic excitation, actual earthquake record and pulse excitations. The authors also

Stellenbosch University https://scholar.sun.ac.za

simplified the problem of SSI by developing an equivalent single degree of freedom model for a typical superstructure design and displacement calculation which is varied for all possible types of excitations (see Figure 2.10). The frequency of excitation for transient loads was taken as the dominant frequency, but the authors presented an alternative method of its calculation and both concepts were found in good agreement.

Three main key parameters were found to control the response of the system: the wave parameter σ ; the value h/r_f and the ratio f_e/f.

$$\sigma = V_s / fh \tag{2.9}$$

Here h is the height of the structure from base to the centroid of the inertia forces, f is the fundamental natural frequency of the structure fixed at the base, and f_e is the dominant frequency of excitation. The changes in response of the structure increase with increasing values of h/r or decreasing values of σ . The frequency ratio f_e/f defines if the structure is low-frequency, medium frequency or high frequency. In a system with a wave parameter (σ) greater than 20, the effects of soil flexibility to the response of structure were found insignificant i.e. the system behaves as fixed based structure.

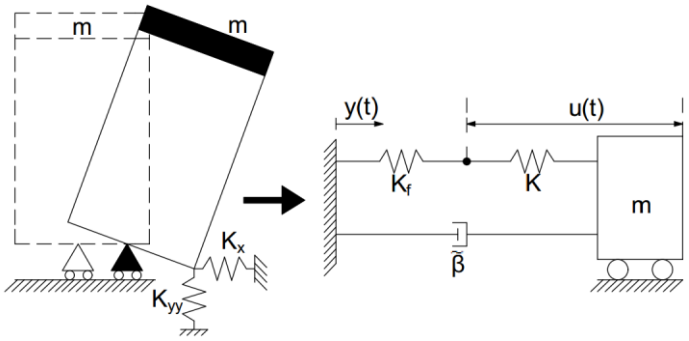

Figure 2.10: Single degree of freedom replacement oscillator (adapted from Veletsos & Meek, 1974)

The effective natural period ($\tilde{T}$) and effective damping coefficient ($\tilde{\beta}$) of the above replacement oscillator are:

$$\frac{\tilde{T}}{T} = \sqrt{\left(1 + \frac{K}{\bar{K}_x} + \frac{K}{\bar{K}_{yy}} \frac{h^2}{r_f^2}\right)} \tag{2.10}$$

Stellenbosch University https://scholar.sun.ac.za

$$\tilde{\beta} = \left(\frac{\tilde{T}}{T}\right)^{-3} \left(\beta + \beta_{fr}\right) \tag{2.11}$$

Here K, β and T are the static stiffness, damping coefficient and fundamental period of the structure fixed at the base. Additional parameters are as previously defined. The foundation damping coefficient β_{fr} represents the damping portion of the radiated energy resulting from the translation and rocking of the foundation. The dynamic stiffness of $\overline{K}_x$ and $\overline{K}_{yy}$, of the foundation are frequency dependent and are evaluated based on the effective natural frequency $\tilde{f}$ of the replacement oscillator. As the latter frequency is unknown at first, an iterative approach is required to determine this frequency. These replacement oscillator equations complied well with the differently formulated equations presented by Jennings and Bielak (1973) in which the base mass and rotational mass moment of the superstructure were ignored. Small inaccuracies in the effective system damping computed using the equations were noted for low values of h/r. The Veletsos and Meek's (1974) equation was found to be more accurate.

The dynamic behaviour of the foundations supported at the surface of a dissipative medium were first discussed by Kobori *et al.* (1971) and subsequently by Veletsos and Verbic (1973). The latter paper contains valuable information on SSI analysis, e.g. modelling of the elastic half space and machine foundations. Kobori *et al* (1971) studied the harmonic vibration (vertical, horizontal and rotational vibrations) of a rectangular plate supported at the surface of a viscoelastic half space by using an assumed pressure distribution at the soil foundation interface. Conversely, Veletsos and Verbic's (1973) research is based on the combination of the relaxed and complete mixed boundary value problems. They studied the translations (vertical and horizontal) and rotation of the steady state response of harmonically loaded rigid massless and rigid mass foundations supported at the surface of a viscoelastic half space.

Veletsos and Verbic made use of impedance functions they used in their prior research of Verbic & Veletsos (1972). These functions are based on a complete mixed boundary value problem for vertical vibration and a relaxed mixed boundary value problem for both rocking and horizontal translation with exclusion of coupling effects. Veletsos and Verbic (1973) expanded these functions of stiffness and damping coefficients representing the response of the supporting

Stellenbosch University https://scholar.sun.ac.za

medium for both translations and rotation of foundations (for a massless foundation as well as foundation with mass). Lastly, they developed a simple model of half space modelling representing both viscoelastic and elastic half space media. Their results showed that the viscoelasticity effects of the medium decrease its natural frequency and increase its damping capacity. The damping effect is greater than that which might be obtained using an elastic medium and natural frequency is lower. However, a decrease in the damping value has been observed for low frequency of excitation. It was realized that more results in the range of frequencies where the damping value might decrease are required.

Bielak (1975) investigated earthquake response of a linear single story building of rigid cylindrical foundation embedded into a viscoelastic half space medium. The author provided equations for both natural frequency and damping ratio of an equivalent structure analysed in its fixed base condition. The results showed that the embedment of the foundation increased the natural frequency and damping ratio of the system, but the effective damping of the system may be less or greater than that of the fixed structure depending on the system parameters.

Veletsos and Nair (1975) investigated dynamic behaviour of single degree of freedom structures supported at the surface of a linear viscoelastic half space. The investigated structures were assumed as linear with viscous damping. The considered loads were horizontal harmonic free field and earthquake excitations. In modelling the supporting medium two models were considered separately: the standard Voigt model and the constant hysteretic model. In the former model the specific energy loss factor is proportional to the exciting frequency whereas in the constant hysteretic model the specific energy loss factor is independent of the exciting frequency. The researchers presented a simplified single degree of freedom oscillator for SSI analysis of the structure supported at the surface of a soil medium which exhibits hysteretic damping behaviour (see Figure 2.11).

Veletsos and Nair (1975) presented the method of combining two different models for viscoelastic media (i.e. the Voigt model and the hysteretic model) and they suggested the applicability of the oscillator to the Voigt model analysis for practical purposes. Restraining actions of the linear viscoelastic half space have been represented by the values of linear springs and viscous dampers (see Veletsos & Verbic, 1973). The results showed that hysteretic action in soil structure decreases

Stellenbosch University https://scholar.sun.ac.za

the deformation amplitude of the system in the medium as well as the high frequency range and increases it in the low frequency range. The low frequency range is defined as the range of frequencies in which the peak response of the structure is controlled by the pseudo acceleration. For the medium frequency range, the response of the structure is governed by the strain energy absorbed by the system i.e. the pseudo velocity controls the structure response whereas the high frequency range corresponds to the constant peak displacement of the structure, and therefore, the pseudo displacement of the system controls the response. The length of each range is variable depending on the ground motion. The method for determining frequency ranges for a typical ground motion is illustrated in Veletsos and Vann (1971). For the discussion of frequency ranges in this paragraph the term "frequency" refers to the natural frequency of the structure with a fixed base.

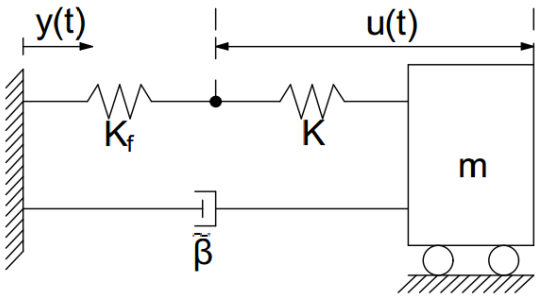

Figure 2.11: Replacement oscillator of hysteretic soil structure analysis (Veletsos & Nair 1975).

The effective natural frequency, $\tilde{f}$ and effective damping factor $\tilde{\beta}$ of the replacement oscillator are given as:

$$\frac{\tilde{T}}{T} = \sqrt{1 + \frac{K}{\bar{K}_x} + \frac{Kh^2}{\bar{K}_{yy}}} \tag{2.12}$$

$$\tilde{\beta} = \beta_f + \left(\frac{\tilde{T}}{T}\right)^{-3} \beta \tag{2.13}$$

The foundation dynamic stiffnesses, $\bar{K}_x$ and $\bar{K}_{yy}$, as well as the foundation damping factor, β_f are frequency dependent and are evaluated based on the effective natural frequency $\tilde{f}$ of the replacement oscillator which is initially unknown. In this case either the iteration method can be used for solving the equations, starting with the natural frequency of the fixed base structure f

Stellenbosch University https://scholar.sun.ac.za

as effective natural frequency of the replacement oscillator or a graphic method as presented by Veletsos (1977) can be used. These equations are different from those presented by Veletsos and Meek (1974) in that the foundation damping factor β_f includes both hysteretic damping of the soil and radiation damping of the foundation. The above equations of Veletsos and Nair (1975) are of a particular case in which the effects of the foundation mass on the response of the system are not considered. See Veletsos and Nair (1975) for the same equations with consideration of the foundation mass.

Bielak (1976) extended modal superposition of classical modes damping to non-classical modes damping. Consequently, he developed equations for the effective frequency and damping ratio of the structure in its fixed base condition as well as for both horizontal translation and rotational equations of the foundation mass and superstructure. Bielak considered a linear multi-storey structure with a circular rigid mass foundation perfectly bonded to the surface of a viscoelastic half space and free to rotate and translate in the horizontal direction. The foundation thickness was taken as negligible and the contribution of foundation stiffness to the overall stiffness of the system was taken as constant and evaluated at the fundamental natural frequency of the system whereas that of the damping ratio was evaluated as frequency dependent for the corresponding system mode.

Luco (1980) studied the effect of inertia interaction on the response of the multi-degree of freedom structures by considering a planar elastic structure with a rigid foundation supported at the surface of viscoelastic half space. The author ignored the mass of the foundation and the rotational inertia of the superstructure as well as the coupling effects of the foundation.
Luco developed displacement equations for both the foundation and superstructure in which the equivalent natural frequency and equivalent damping ratio of the structure in its fixed base condition were derived. The research concentrated on the fundamental mode of the system seeing that Parmelee (1967) and Jennings and Bielak (1973) proved that the other mode shapes are not influenced by soil flexibility. Luco's equations correlated well with those of Jennings and Bielak (1973) for the structure of one single degree of freedom. However, for the multi-storey structure, both displacement and rotation equations of the foundation did not correlate well.

Stellenbosch University https://scholar.sun.ac.za

Avilés and Pérez-Rocha (1996) discussed the different parameters necessary in embedded foundation analysis of SSI. Moreover, they developed simple analytical expressions for the effective frequency and damping coefficient calculation of single degree system embedded into a dissipative layered soil and excited by steady state harmonic loading. These analytical equations are based on the same concept as the equations developed by Veletsos and Meek (1974) and Veletsos and Nair (1975) – the only difference is the case studies considered.

As in various studies, the foundation base was taken as a circular plate and the base mass was assumed to respond in two different degrees of freedom: lateral translation and rocking. The researchers revealed that the linear and rotational inertia of foundation mass may be neglected for the structures of slenderness ratios in the range of $2 \le h/r_f \le 5$ and stiffness ratios of $\left(h\tilde{T}\right)/\left(d_s T\right) \le 2$ For foundations with sidewalls (see Figure 2.12), two severe cases were considered: sidewalls extending over the foundation depth and foundation without sidewalls. The sidewalls in contact with surrounding soil depth reduce the structural response, decrease the system period and increase the damping value of the system as the stratum depth increases. By contrast, for a foundation without sidewalls or with sidewalls not in contact with the surrounding soil, all of these parameters are inverted. Furthermore, it has also been shown that the equivalent period of vibration is not significantly affected by stratum depth, but damping capacity is affected significantly: it increases as stratum depth does. Thus, the damping capacity of a structure for a shallow stratum is smaller than that for a deep stratum.

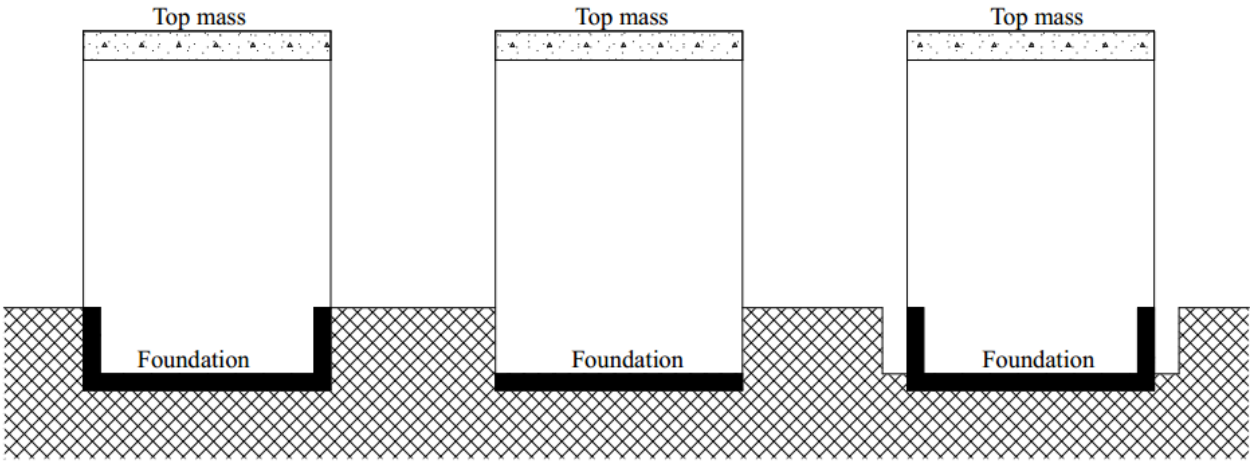

Figure 2.12: Illustrative example of the embedded foundations considered by Avilés and Pérez-Rocha (Avilés and Pérez-Rocha, 1996)

Stellenbosch University https://scholar.sun.ac.za

Summary:

A lot of scholarly work has been done on soil structure interaction, as can be gathered from Mason (2011) and Jones (2013). For this reason not all publications on this subject could be reviewed herein, but a complete review is available in, inter alia, Kausel (2010), Roesset (2013) and Lou *et al*. (2011). The papers reviewed here mostly focused on linear structures and some on material nonlinearity of the superstructure, e.g. Moghaddasi *et al.* (2012) and Avilés and Pérez-Rocha (2003) and (2005). They were treated as a group in this section seeing that they indicate that Soil Structure Interaction analysis (SSI) of structures with consideration of material nonlinearity of the superstructure reduces the seismic demand of the structure.

Based on all the mentioned references, the problem of inertia interaction has been made clear and understandable. Despite various approaches used for assessing this problem, the same observations have been revealed. The principal effects of inertia interaction are to increase fundamental period of the fixed base structure and to change (increase or decrease depending on system parameters) its corresponding damping coefficient. The subsequent fundamental natural period and damping coefficient were referred to equivalent fundamental natural period and damping coefficient. The total effect may increase or decrease maximum displacement of the structure depending on system parameters. These changes are observed for the fundamental mode and other modes are not practically affected. Moreover, different parameters which control inertia interaction were defined (Veletsos & Meek, 1974). The studies of Stewart, Fenves and Seed (1999) and Stewart, Seed and Fenves (1999) showed that for a system with $h/V_s T < 0.1$ inertia interaction effects are negligible.

In general, the solutions to the problem of inertia interaction has been provided by modifying the fundamental natural period and damping coefficient of the fixed base structure in order to make it easy to be implemented in seismic design codes utilizing spectrum analysis. Additional studies (e.g. Worku , 2014; Stewart *et al.* , 1999; Mylonakis & Gazetas, 2000) have demonstrated this concept as an economical method because it gives a reduced resultant seismic design force compared to that of the fixed based condition. On the other hand, Mylonakis *et al* (2006) and Mylonakis and Gazetas (2000) have demonstrated different cases where even if the resultant seismic design force may be reduced, it is not conservative due to additional horizontal displacement of the superstructure caused by the rotation of the foundation base which causes increased internal forces in secondary seismic elements. To account for that additional

Stellenbosch University https://scholar.sun.ac.za

displacement, Worku (2014) has recommended considering inertia interaction analysis in a displacement based method. An advantage of this recommendation has also been noted by Anastasopoulos *et al.* (2010) who mentioned different failure modes caused by inertia interaction. Based on the aforementioned, the displacement-based method can clearly be considered as the best method of inertia interaction analysis.

2.3.2.2 A review on kinematic interaction

In earthquake engineering, structures are generally analysed by assuming that all points of the structure foundation experience the same free field motion recorded at a "*control point*" as input motion of the foundation. This concept has also been adopted in many studies (e.g. Stewart *et al.*, 2003; Stewart *et al.*, 1999; Worku, 2014).

Obviously, this is not a realistic assumption because the soil profiles underneath the foundation may be different in mechanical properties which may change the amplitude of incident seismic waves. This assumption is only realistic for sets of coherent seismic waves propagating in the vertical direction (Veletsos & Prasad, 1989). The change of seismic wave amplitude due to propagation path is known in literature as "*the wave passage effect*".

Additional parameters are also available such as dissimilarity in mechanical properties of both soil medium and foundation which causes refraction and reflection of seismic waves back to the soil at the foundation soil interface, or the dispersion of seismic waves from different source locations which causes seismic waves to impact the soil foundation interface at different incident angles and instants in time (Figure 2.13). This is referred to as "*the ground motion incoherence effect*". However, when the structure is supported at the surface of the soil medium these phenomena of reflection and refraction do not occur (Kotronis *et al.*, 2013).

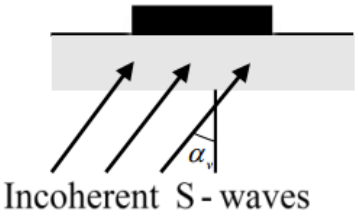

Figure 2.13: Illustrative example of seismic waves transmitted at inclined angle

Stellenbosch University https://scholar.sun.ac.za

Furthermore, the foundation embedment and foundation inertia force also contribute to the dissimilarity between the input motion and the free field motion because ground motion decreases with depth and inertia forces reduce the imposed ground motion.

In summary, all those parameters contributing to the change of free field motion are studied and grouped together in two categories i.e. base slab averaging effect and foundation embedment effect (ATC, 2005). The base slab motion averaging effect is defined as the difference in amplitude of the input motion and free field motion which may be caused by incident angle of seismic waves, non-uniformity of materials through the propagation path of the seismic waves as well as various other parameters. The foundation embedment effect represents the decrease in foundation input motion relative to free field motion due to reduction in amplitude of free field motion with depth as well as scattering of incident seismic waves at the foundation base level. Normally, base slab motion averaging introduces additional motion constituents such as torsion and rotation (Mylonakisa, Nikolaoub & Gazetas, 2006; Kim & Stewart, 2003), but the most important motion is translation (NEHRP Consultants Joint Venture, 2012).

Various authors (Elsabee & Morray, 1977; Day, 1978; Kausel *et al.*, 1978; Veletsos & Prasad, 1989; Mita & Luco, 1989a; Abrahamson *et al.*, 1991 ; Veletsos *et al.*, 1997; Kim, 2001; Kim & Stewart, 2003) have focused on the problem of kinematic interaction, generally by establishing the relationship between foundation input and free field motions, i.e. “transfer functions”. However, some authors studied the problem by developing analytical expressions (equations) for the effective natural period and damping coefficient of an equivalent single degree of freedom fixed at the base (e.g. Avilés & Pérez-Rocha, 1998; Avilés & Suárez, 2002; Kramer & Stewart, 2004; Mylonakisa *et al.*, 2006). The latter paper (Mylonakisa *et al.*, 2006) presents impedance functions of input and free field motions in the frequency domain whereas Kramer and Stewart (2004) published papers on the kinematic interaction, summarised them and developed a complete set of kinematic interaction analysis procedures. The procedures to analyse foundations are developed for the following foundation types:

i. Surface foundations

Figure 2.14 represents a simplified graphical method for the estimation of the transfer function displacement amplitude computed using a transfer function for circular and rectangular rigid

Stellenbosch University https://scholar.sun.ac.za

massless foundations supported at the surface of homogeneous elastic medium and excited by incoherent waves at an angle α_v to the vertical plane. The transfer function amplitude is a function of adjusted dimensionless frequency parameter $\tilde{a}_o$.

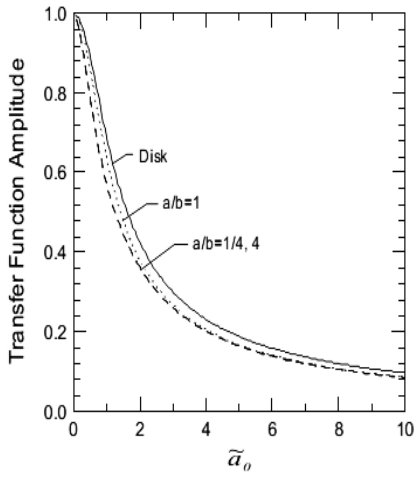

Figure 2.14: Transfer function amplitude or impedance function amplitude for vertically incident incoherent waves (from Kramer & Stewart, 2004)

In Figure 2.14, the curve labelled "disk" represents a rigid circular foundation whereas the parameters a and b represent one half of the smaller and greater footprint dimensions of a rectangular foundation (with b being taken perpendicular to the incidence direction of the seismic waves). The adjusted dimensionless frequency parameter $\tilde{a}_o$ is evaluated as:

$$\tilde{a}_o = a_o^r \sqrt{\kappa^2 + \sin^2 \alpha_v} \qquad \text{for a circular foundation} \tag{2.14}$$

$$\tilde{a}_o = \frac{\omega b_e}{2V_{s,r}} \sqrt{\kappa^2 + \sin^2 \alpha_v \left(\frac{b}{b_e}\right)^2} \qquad \text{for a rectangular foundation} \tag{2.15}$$

Where $a_o^r = \omega r_f / V_{s,r}$, $b_e = \sqrt{ab}$, foundation radius $r_f = \sqrt{A_f / \pi}$ (A_f = foundation area) and $V_{s,r}$ is the reduced shear wave velocity. The ground motion incoherence parameter κ was obtained from Kim and Stewart (2003) and is written as:

$$\kappa = 7.4 * 10^{-4} (V_s - 50) \quad [\text{m/s}] \tag{2.16}$$

Stellenbosch University https://scholar.sun.ac.za

Where V_s is defined as the radius, r_f , divided by the time taken by the shear wave to propagate from depth, r_f , to the ground surface. The depth is measured upwards from the base of the foundation. This approach is limited to the foundation with embedment ratios of e/r_f <0.5 (*e*=foundation depth).

Figure 2.14 is based on the work of Veletsos and Prasad (1989) and Veletsos *et al.* (1997) who presented impedance functions for both circular and rectangular rigid massless foundations supported at the surface of homogeneous elastic medium and subjected to incoherent shear waves propagating at an inclined angle α_v relative to the vertical plane. However, the relationship presented by Figure 2.14 can be alternatively derived from equation 2.17 (NEHRP Consultants Joint Venture, 2012).

$$H_u(\omega) = \frac{u_{FIM}}{S_g} = \frac{1}{\tilde{a}_o^2}\left\{1 - \exp(-2\tilde{a}_o^2)\left[I_o(\tilde{a}_o^2) + I_1(2\tilde{a}_o^2)\right]\right\} \tag{2.17}$$

Where $H_u(\omega)$ defines the transfer function amplitude, u_{FIM} -the foundation input motion, S_g –the free field ground motion, and the parameters I_o and I_1 are modified Bessel functions. Referencing to Watson (1995), the modified Bessel functions are given as:

$$\left(I_o(2\tilde{a}_o^2) + I_1(2\tilde{a}_o^2)\right) = \begin{cases} 1 + \tilde{a}_o^2 + \tilde{a}_o^4 + \dfrac{\tilde{a}_o^6}{2} + \dfrac{\tilde{a}_o^8}{4} + \dfrac{\tilde{a}_o^{10}}{12} & \text{for } \tilde{a}_o \le 1 \\ \exp(2\tilde{a}_o^2)\left[\dfrac{1}{\sqrt{\pi}\tilde{a}_o}\left(1 - \dfrac{1}{12\tilde{a}_o^{12}}\right)\right] & \text{for } \tilde{a}_o > 1 \end{cases} \tag{2.18}$$

ii. Embedded foundation

The procedures described here for reducing the foundation input motion relative to the free field motion are specifically due to a decrease in depth of ground motion and scattering (reflection and refraction) of incoming waves at foundation base, i.e. “the foundation embedment effect”. For an embedded foundation, the foundation embedment effect as well as the base slab motion averaging effect applies whereas for the surface foundation the base slab averaging effect is the only effect that applies (Kotronis *et al.*, 2013). In this case (embedded foundation) the resultant transfer

Stellenbosch University https://scholar.sun.ac.za

function is a product of both the two transfer functions calculated separately. The transfer function amplitude for an embedded foundation in horizontal translation is estimated as:

$$H_u(\omega) = \cos\left(\frac{e}{r} a_o\right) = \cos\left(\frac{e\omega}{V_s}\right) \geq 0.454 \qquad (2.19)$$

All parameters in this equation are as previously defined. It is essential to note that applicability of this equation is limited to embedment quotient $e/r_f = 1$.

The numerical solutions of Mylonakisa *et al.* (2006) are the same results as the ones discussed above (Kramer & Stewart, 2004) except that they are applicable in the frequency domain. Moreover, all mentioned procedures for kinematic interaction effects estimation are in agreement with the field (on site) results as well as the finite element results of Stewart and Tileylioglu (2007). These procedures were adopted by the Applied Technology Council (ATC 2005). Basically, the kinematic interaction is important for a structure with short fundamental periods (<0.5s), or with larger plan dimensions compared to the length of the dominant seismic waves or a structure with a deep foundation i.e. depth $\geq 10\, feet \approx 3m$ (ATC, 2005).

Application of transfer function

Studies on the seismic response spectrum analysis method (e.g. ATC 2005) have showed that the transfer function solutions are evaluated as discussed previously (equations 2.17 and 2.19), for vibration frequencies of 5Hz and higher, the solution at 5Hz can be used. In the case of free field ground motion given in time history format, calculation procedures are available from the mentioned references (e.g. ATC, 2005, Kramer & Stewart, 2004). These procedures make use of the Fourier transformation of the free field ground motion. Considering the solution to the problem of kinematic interaction which is available, and the studies mentioned in this section, which have revealed that neglecting kinematic interaction effects is conservative because it increases the seismic demand (Kramer & Stewart, 2004:4-34), the kinematic effect will be ignored in the next sections.

Stellenbosch University https://scholar.sun.ac.za

2.3.2.3 A review on foundation flexibility

There are few studies that report on the effects of foundation flexibility on the response of the structure, e.g. Iguchi and Luco (1982); Riggs and Waas (1985) and Liou and Huang (1994).

Iguchi and Luco (1982) developed impedance functions for a massless flexible circular foundation resting at the surface of dissipative medium supporting a rigid core fixed to the foundation (Figure 2.15). The foundation was allowed to rotate and translate in a vertical direction and the contact surface was taken as frictionless. The results showed that the flexibility of the foundation decreases the effective damping value and it might be lower than that of a rigid foundation. At low frequencies of excitation, the effective stiffness was found less than that of a rigid foundation, but for high frequencies of excitation the results showed the inverse results. Note that all the observations apply to both rotation and vertical translation.

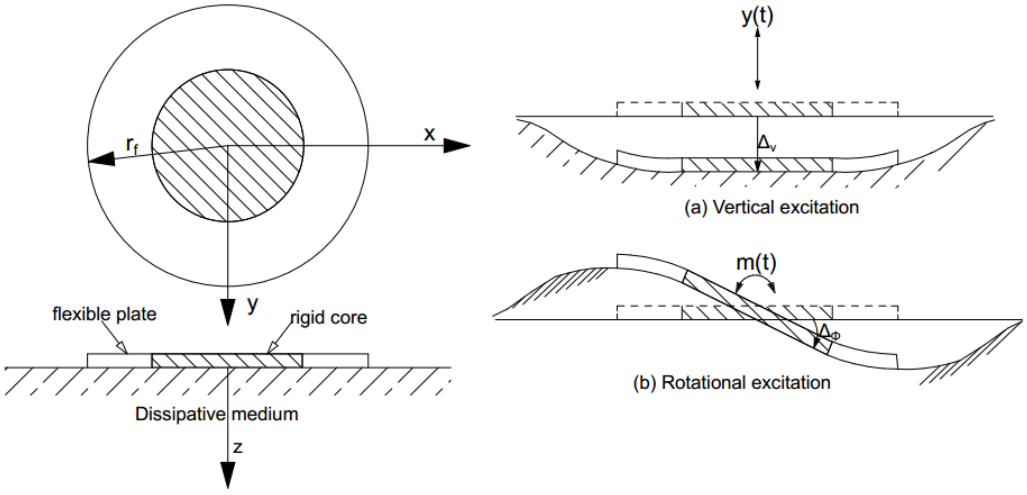

Figure 2.15: Model considered by Iguchi and Luco for investigation of foundation effect for the response of the structure (based on Iguchi & Luco, 1982)

Riggs and Waas (1985) studied the effect of foundation flexibility on the response of a cylindrical reactor building. They found that for a reactor building, the base foundation may be assumed to be rigid.

Liou and Huang (1994) investigated the effect of the foundation on the response of both a rigid plate supporting a rigid core and a rigid plate supporting a thin cylindrical wall resting on surface of a dissipative medium. The results showed that the foundation flexibility does not contribute to horizontal response of the foundation if the foundation is not very flexible. It was also found that

Stellenbosch University https://scholar.sun.ac.za

the mechanical properties of the supported structure influence the response of the system, i.e. the response of a rigid plate with a rigid core was different to that of a rigid plate with a thin cylindrical wall. Moreover, the authors showed that a foundation with parameter $\Phi \geq 10$ (see equation 2.20) can be considered as a rigid foundation and the contribution of the foundation to the horizontal response of the system needs to be considered for values of Phi (Φ) less than 0.01($\Phi < 0.01$). The values of Phi are computed as follows:

$$\Phi = \frac{\overline{D}}{G_o r_f^3} \tag{2.20}$$

Where G_0 is the shear modulus of elasticity of the soil at small strain level, $\overline{D}$ is the rigidity of the foundation base. Other parameters are as previously defined.

The criteria for defining a rigid foundation have also been discussed by Todorovska *et al*. (2001). They demonstrated that if the shear modulus of the foundation is less than 16 times that of the soil, then the foundation must be recognised as a flexible foundation. Currently, there is no numerical method of implementing the foundation effects into an analysis (Stewart & Tileylioglu, 2007), however, in various studies the assumption of a rigid foundation have been made (Arefi, 2008; Stewart *et al.*, 1999; Worku, 2014). Stewart & Tileylioglu (2007). NEHRP Consultants Joint Venture (2012) have integrated the effects of foundation into an analysis model by distributing the soil reactions (damping and stiffness values) along the sides and underneath the foundation. The concept of the distribution of the soil reactions along the sides and underneath the foundation developed by NEHRP Consultants Joint Venture (2012) is discussed in chapter three.

2.3.3 A review on standards and code provisions

2.3.3.1 Building codes and standards

SSI were implemented in various American design codes and standards many years ago. It was suggested by the Applied Technology Council in 1978 and it was implemented in National Earthquake Hazard Reduction Program (NEHRP) in 1986 (Veletsos, 1993). The latest versions of the applicable codes and standards are ASCE (2013); ASCE (2014); ASCE (2010); ATC (2005); BSSC (2004a) and BSSC (2004b). European standards do not mention soil flexibility (Arefi, 2008). However, in EN 1998-5: 2004 section 6 a number of structural configuration cases are listed

Stellenbosch University https://scholar.sun.ac.za

where SSI must be considered. The force based and displacement based approach to SSI are implemented in all the cited design codes and standards. For the displacement based approach nonlinear static analysis using pushover analysis is used while for the force based approach response spectrum analysis is used. Time history analysis is not mentioned in any of the above mentioned publications.

(i) Force based approach

The following design procedures of SSI were extracted from chapter 19 of ASCE (2010). For the purpose of this thesis the kinematic interaction effects are not factored and the symbols were modified slightly for the sake for uniformity with the symbols used here.

- **Equivalent lateral force procedures**

Base shear

The effect of SSI on the base shear force (V) is to reduce it by a factor ΔV as follows.

$$\tilde{V} = V - \Delta V \tag{2.21}$$

Where V is the base shear force calculated for a fixed base structure, and ΔV is the SSI reduction factor. The SSI reduction factor ΔV is calculated as follows:

$$\Delta V = \left[C_s - \tilde{C}_s \left(\frac{0.05}{\tilde{\beta}} \right)^{0.4} \right] \overline{W} \leq 0.3V \tag{2.22}$$

The term C_s is the seismic coefficient obtained from the design response spectrum as ordinate and with fundamental natural period of the fixed structure as abscissa. The term $\tilde{C}_s$ is also a seismic coefficient and is obtained in the same way as the first term except that the fundamental natural period of the fixed base structure is replaced by the effective fundamental natural period $\tilde{T}$ of the flexibly supported structure. $\overline{W}$ is the effective seismic weight of structure which is equal to either 70% of the structure weight or to 100% of it if the structure weight is concentrated at one single level. $\tilde{\beta}$ is the effective structural damping ratio of flexibly supported structure.

Stellenbosch University https://scholar.sun.ac.za

Estimation of the fundament effective period

The effective fundamental period is evaluated as follows.

$$\frac{\tilde{T}}{T} = \sqrt{1 + \frac{K}{\bar{K}_x} + \frac{K * h^2}{\bar{K}_{yy}}} \tag{2.23}$$

T is the fundamental period of the fixed base structure; K is the static stiffness of the structure in its fixed base condition, $\bar{K}_x$ is the dynamic lateral stiffness of the foundation calculated in the direction in which the structure is being analysed, $\bar{K}_{yy}$ is the dynamic rotational/ rocking stiffness of the foundation measured in the same direction as $\bar{K}_x$, and h is the effective height of the structure which is taken as 70% of the height of the structure. For a structure with mass concentrated at a single level, the effective height is taken as the height of that level. The static stiffness K of the structure is estimated using:

$$K = 4\pi^2 \left(\frac{\bar{W}}{gT^2} \right) \tag{2.24}$$

Where g is gravitational acceleration.

Estimation of the effective damping ratio

The effective damping ratio is calculated as follows

$$\tilde{\beta} = \beta_f + \frac{0.05}{\left(\frac{\tilde{T}}{T} \right)^3} \tag{2.25}$$

Where β_f is the foundation damping ratio, it is not evaluated directly from an analytical expression but is determined from a graph in which the period ratio is related to the foundation damping ratio β_f as a function of the structural aspect ratio h/r and the ratio $S_{DS}/2.5$ (refer to Figure 2.16). Here S_{DS} is the design spectral acceleration at short periods of the structural vibration i.e. S_{DS} is the ordinate of the design spectral acceleration associated to the constant acceleration.

Stellenbosch University https://scholar.sun.ac.za

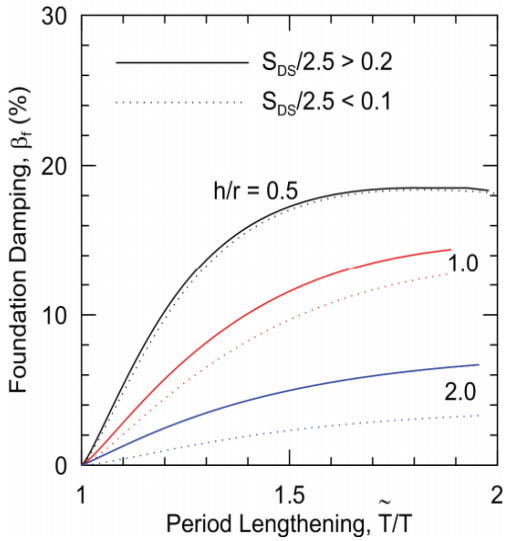

Figure 2.16: Foundation damping factor (adapted from ASCE, 2010)

The relationship of the graph of Figure 2.16 is based on the procedures of Veletsos and Nair (1975) and it includes both radiation damping of the foundation and hysteretic damping of the soil.

- **Modal analysis procedures**

The implementation of SSI in modal analysis is the same as in equivalent lateral force analysis, but a slight modification is made to the expression for the effective height (h). It is calculated as follows:

$$h = \frac{\sum_{i}^{n} W_i \phi_{i1} h_i}{\sum_{i=1}^{n} W_i \phi_{i1}} \tag{2.26}$$

Where W_i is portion of the total gravity load of the structure at level *i;* ϕ_{i1} is fundamental mode displacement amplitude at the i^{th} level of the structure and h_i is the height above the base up to level *i*.

In modal analysis, modification of the fundamental period and damping ratio of the structure in its fixed base condition is done seeing that SSI effects are allowed for in the fundamental mode of vibration only. It has been shown by various authors (e.g. Parmelee, 1967 ; Jennings & Bielak, 1973) that the fundamental mode of vibration is the only mode affected by soil structure effects.

Stellenbosch University https://scholar.sun.ac.za

Distribution of lateral forces

The reduced base shear is distributed over the height of the structure in the same way as it is done for base shear force evaluated under the fixed base condition.

(ii) Nonlinear static analysis using the displacement based approach

The displacement-based approach is a method by which lateral static forces that increase monotonically are applied over the height of a structure which has a flexible support at the foundation base until instability of the system is achieved. The flexibility of the foundation base is modelled by replacing the supporting soil with its corresponding static stiffnesses (Figure 2.17). A pushover curve representing the relationship between top displacement versus base shear force is obtained from this analysis. Based on this curve, the ductility demand μ of the structure including soil effects can be evaluated. After the ductility demand μ has been obtained, the effective fundamental period lengthening ratio $\tilde{T}/T$, calculated by equation 2.23, is modified as follows (ATC, 2005):

$$\left(\frac{\tilde{T}}{T}\right)_{\text{mod}} = \left\{1+\frac{1}{\mu}\left(\frac{\tilde{T}}{T}\right)^2 - 1\right\}^{0.5} \tag{2.27}$$

The corresponding damping coefficient $\tilde{\beta}$ of the system is calculated using

$$\tilde{\beta} = \beta_f + \frac{0.05}{\left(\frac{\tilde{T}}{T}\right)^3_{\text{mod}}} \tag{2.28}$$

and

$$\beta_f = a_1\left(\frac{\tilde{T}_{\text{mod}}}{T_{\text{mod}}} - 1\right) + a_2\left(\frac{\tilde{T}_{\text{mod}}}{T_{\text{mod}}} - 1\right)^2 \tag{2.29}$$

Where a_1 and a_2 are dimensionless coefficients dependent on the translation and rotation radius of the foundation as well as the effective height of the structure (ATC, 2005).

Stellenbosch University https://scholar.sun.ac.za

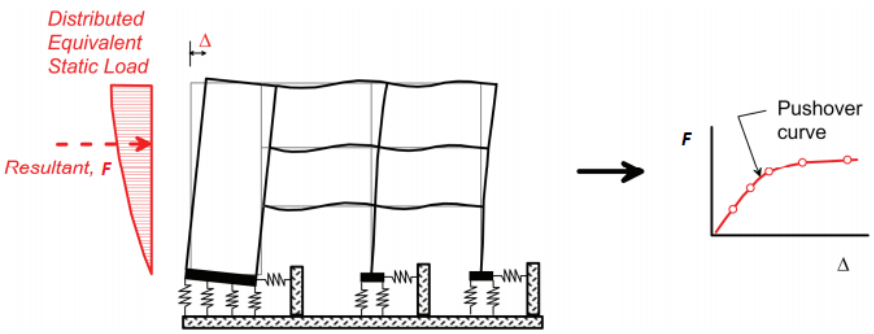

Figure 2.17: Illustrative example of displacement based approach for SSI (NEHRP Consultants Joint Venture, 2012)

2.3.3.2 Codes and standards for water storage tanks

The flexibility of the foundation soil supporting the water tank structure has a negligible effect on the convective component, but it does affect the impulse component (Veletsos & Tang, 1990). The impulse mode represents the response of the portion of the water which reacts as if attached to the tank and thus moves in unison with the tank as the tank responds to a given earthquake. The response of the portion of the water's surface which oscillates during a given earthquake is referred to as the convective mode. These mass components of the water contained in the tank were discussed in section 1.2. According to Jaiswal *et al.* (2007), a few Standards have paid attention to the effect of soil flexibility on the seismic response of water tanks (e.g. Priestley *et al.*, 1986; EN 1998-4: 2006). Generally, SSI is implemented in design codes of water storage tanks in the same way as in building codes (i.e. "*Force based approach"*, presented above). The only difference is that the period of the impulse mode and its corresponding damping value are modified (Veletsos, 1984) whereas that of the convective mode is kept unaffected.

2.4 Seismic performance assessment methods

Essentially, the seismic performance assessment of a structure requires two quantities i.e. seismic capacity and seismic demand. The seismic capacity shows the maximum ability of a structure to withstand seismic action whereas seismic demand represents the effects of an earthquake on the structure. If the seismic demand is lower than the seismic capacity an acceptable performance of the structure under the considered earthquake action can be ensured.

Stellenbosch University https://scholar.sun.ac.za

Two most accurate methods are available for estimating the above two quantities i.e. nonlinear time history analysis and nonlinear static (pushover) analysis (EC8, 2004). The former is the most accurate approach for assessing the seismic demand of a structure as it gives the response of the structure at each recorded time instant of the ground motion. However, this method is time consuming due to the inherent variability of the ground motion and various complications which can be encountered in modelling the structural system. Therefore, for a structure with a simple geometry, nonlinear pushover analysis is recommended as an alternative.

2.4.1 Nonlinear time history

The nonlinear dynamic analysis gives the response of the structure to a given seismic event through direct numerical integration of the governing dynamic equations of motion of the structure using the ground acceleration data as input. The accuracy of the results is determined by the modelling techniques used for the analysis as well as the choice of appropriate time-history data and the correct scaling of the time-history response spectra. Also of importance is that an appropriate number of time-history analyses be performed to obtain statically reliable results.

2.4.2 Nonlinear pushover approach

Pushover analysis (POA) is a technique by which a structure is subjected to monotonically increasing lateral load of defined shape until the target top displacement or structural failure is achieved. It is mostly used to investigate the maximum capacity (i.e. the maximum base shear force) of the existing structure or a newly designed structure (ATC-40, 1996). It gives the graphical representation of top displacement versus base shear force and compares it to the seismic demand. The latter relationship (i.e. base shear force versus top displacement) is widely known as "*the capacity curve*". POA is based on the principle that the response of the structure is controlled by the fundamental mode shape of the structure and remains constant during both elastic and non-elastic response. On the other hand, pushover analysis can be defined as a technique that simplifies the dynamic analysis of MDOF model to the equivalent SDOF model and afterwards relates the response of the equivalent SDOF to MDOF models (Figure 2.18).

Stellenbosch University https://scholar.sun.ac.za

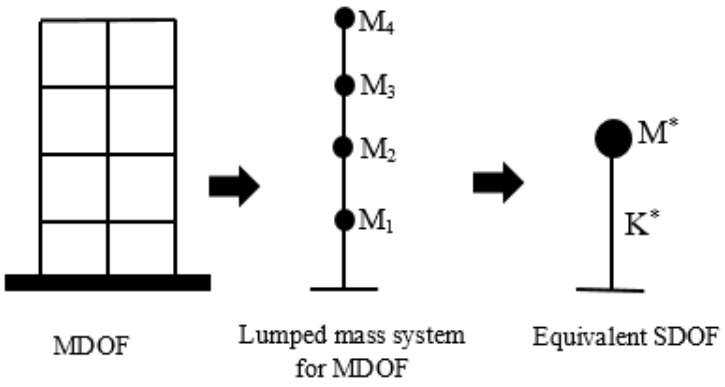

Figure 2.18: The basic concept of POA(adapted from Themelis, 2008)

2.4.2.1 Transformation of a MDOF system to a SDOF system

The dynamic response of a multi-degree of freedom (MDOF) system is governed by the differential, equation 2.30, where: $[M]$ is the mass matrix, $[C]$ is the damping matrix, $\{F\}$ is the storey force vector, $\ddot{u}_g$ is the ground acceleration, $\{\phi\}$ is the mode shape vector for the system, $\{U\}$ is the relative displacement vector (the dots define first and second derivatives), and $\{1\}$ is the influence factor. The latter is the displacements of the masses derived from a static application of unit ground displacement and it induces rigid body motion of the structural mass associated with the model.

$$[M]\{\ddot{U}\}+[C]\{\dot{U}\}+\{F\}=-[M]\{1\}\ddot{u}_g \tag{2.30}$$

The transformation of equation 2.30 to its equivalent single degree of freedom system has been illustrated by various authors (e.g. Fajfar, 2000; Themelis, 2008) and is written as

$$M^*\ddot{u}^*+C^*\dot{u}^*+F^*=-M^*\ddot{u}_g \tag{2.31}$$

and

$$M^*=\{\phi\}^T[M]\{1\} \tag{2.32}$$

$$C^*=\{\phi\}^T[C]\{\phi\}\frac{\{\phi\}^T[M]\{1\}}{\{\phi\}^T[M]\{\phi\}} \tag{2.33}$$

$$F^*=\{\phi\}^T\{F\} \tag{2.34}$$

$$u^*=\frac{\{\phi\}^T[M]\{\phi\}}{\{\phi\}^T[M]\{1\}}u_t \tag{2.35}$$

Stellenbosch University https://scholar.sun.ac.za

Where u^*, M^*, C^*, F^* are the top displacement, mass, damping, storey force of equivalent single degree of freedom, and u_t is the target top/roof displacement resulting from nonlinear static (pushover) analysis of a MDOF system. This is done by applying monotonically increasing horizontal lateral loads to the system.

The output of nonlinear static analysis of a MDOF system is the base shear force-top (roof) displacement relationship from which the properties of the equivalent SDOF can be derived by using equations 2.34 and 2.35 (see Figure 2.19):

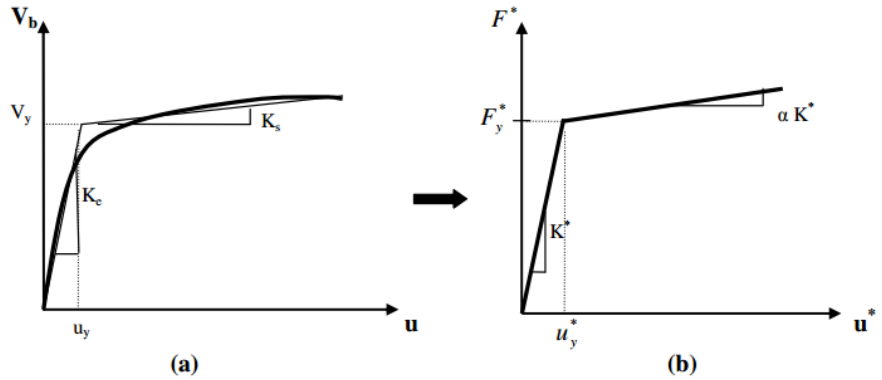

Figure 2.19: (a) Base shear force-top displacement relationship of MDOF; (b) bilinearised force-displacement relationship of equivalent SDOF (modified from Themelis, 2008)

Figure 2.19 (a) illustrates the base shear force (V_b) – top (roof) displacement (u) relationship of a nonlinear pushover analysis of a MDOF system. The curve is transformed into a bilinear curve of yield point (V_y,u_y) from which effective stiffness K_e and hardening or softening stiffness K_s are determined (see equations 2.36 and 2.37 below).

$$K_e = \frac{V_y}{u_y} \tag{2.36}$$

$$K_s = \alpha K_e \tag{2.37}$$

From the bilinear curve of the MDOF system (Figure 2.19 (a)), the force-displacement relationship curve of the equivalent SDOF system (Figure 2.19(b)) is derived by using equations 2.34 and 2.35. The strain - hardening ratio α is the same for both systems. From Figure 2.19(b), the properties of the equivalent SDOF system are defined by the expressions below:

Stellenbosch University https://scholar.sun.ac.za

$$T_{eq} = 2\pi\sqrt{\frac{M^*}{K^*}} \tag{2.38}$$

$$K^* = F_y^* / u_y^* \tag{2.39}$$

Where K^* and T_{eq} are the elastic stiffness and fundamental period of the equivalent SDOF respectively.

2.4.2.2 Horizontal load distribution

As mentioned previously, POA requires a certain number of horizontal increasing loads applied at the centre of the masses in order to produce increasing horizontal displacement of a structure from the elastic response phase to the inelastic phase and further. Various approaches to determine the required number of forces are available in literature (Themelis, 2008). For example, EC8 (2004) recommends at least two horizontal load patterns be applied at the centre of each mass. The lateral forces may either be of a uniform distribution or a structural mode shape distribution. For a uniform shape distribution, the lateral forces F_i are proportional to the corresponding masses whereas for the modal shape distribution, the forces F_i are proportional to the fundamental mode shape of the structure or other selected mode shape vectors.

(i) Uniform shape distribution

$$\{F_i\} \alpha \{W_i\}$$

(ii) Modal shape distribution

$$\{F_i\} \alpha \{\phi_{ij}\}$$

Where W_i is the weight at i floor and ϕ_{ij} is the normalised mode shape displacement of i floor of mode j.

Stellenbosch University https://scholar.sun.ac.za

2.4.2.3 A review of pushover analysis methods

Based on Themelis (2008), there are five main methods of pushover analysis:

1. Capacity spectrum method
2. Improved capacity spectrum method
3. N2 method
4. Displacement coefficient method
5. Modal pushover analysis

1. Capacity spectrum method (CSM)

CSM is a nonlinear static analysis method introduced by Freeman, Nicoletti and Tyrell (1975) and it has been adapted extensively in design codes. The description herein of this method is mainly based on information collected from ATC-40 (1996). It involves several steps which can be summarised as follows:

i. Nonlinear static (Pushover) Analysis of a MDOF System

The horizontal lateral loads of modal shape are distributed vertically on the system as described in section 2.4.2.2, and the POA is performed. Based on analysis, the base shear force-top (roof) displacement curve is derived (Figure 2.19(a)). This is widely known as capacity curve for the MDOF system.

ii. Derivation of equivalent SDOF

The capacity curve of MDOF (Figure 2.20) is bilinearised so that the area A_1 is equal to area A_2. From the bilinearised curve, the properties of the equivalent single degree of freedom system can be determined by using equations 2.38 and 2.39 as discussed in section 2.4.2.1.

Stellenbosch University https://scholar.sun.ac.za

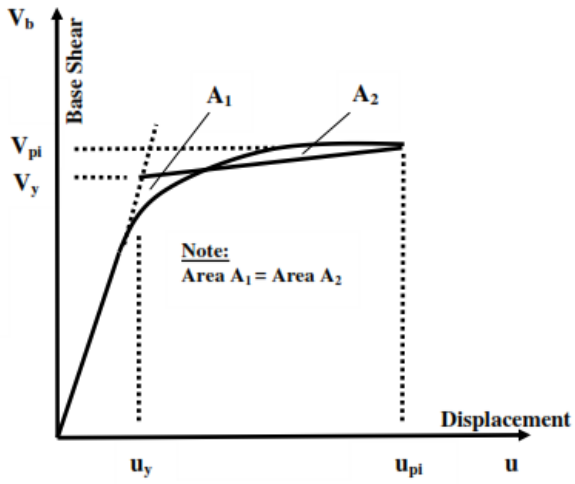

Figure 2.20: An illustrative example of capacity curve for a MDOF system (Themelis, 2008)

iii. Conversion of Capacity Curve to Capacity Spectrum

The capacity spectrum is a graphical representation of acceleration response S_a, versus displacement response S_d. It can also be defined as the graphical representation of the capacity curve in acceleration displacement response spectrum format (ADRS). It is derived from the capacity curve (Figure 2.19(a)) by using the expressions below:

$$S_a = \frac{V_b}{\alpha_m M} \tag{2.40}$$

$$S_d = \frac{u}{PF_1 \phi_{ij}} \tag{2.41}$$

Where M is the total mass of the system, ϕ_{ij} is the modal displacement amplitude at level i for mode j, PF_1 is the modal participation factor and α_m is the modal mass coefficient. Other parameters have been defined previously. The modal participation factor and modal mass coefficient are calculated from the following expressions:

$$PF_1 = \frac{\{\phi\}^T [M] \{1\}}{\{\phi\}^T [M] \{\phi\}} \tag{2.42}$$

Stellenbosch University https://scholar.sun.ac.za

$$\alpha_m = \frac{\left[\sum_{j=1}^{n} m_i \phi_{ij}\right]^2}{\sum_{i=1}^{n} m_i \sum_{j=1}^{n} m_i \phi_{ij}^2} \tag{2.43}$$

Where m_i is the mass at level i.

iv. The Elastic Demand Spectrum

The elastic demand spectrum is developed by performing a nonlinear dynamic analysis on various single degree of freedom structures of different periods. For each single degree of freedom of period *T*, a maximum acceleration, displacement, and velocity is obtained. The graphical representation of the obtained maximum acceleration S_a versus its corresponding fundamental period *T* for each single degree of freedom structure gives the elastic demand spectrum (Figure 2.21). The obtained elastic demand spectrum is transformed into acceleration-displacement (AD) format by means of equation 2.44.

$$S_a = \omega^2 S_d \tag{2.44}$$

Where ω is the fundamental natural frequency of the structure and S_a and S_d are the response spectrum acceleration and displacement respectively.

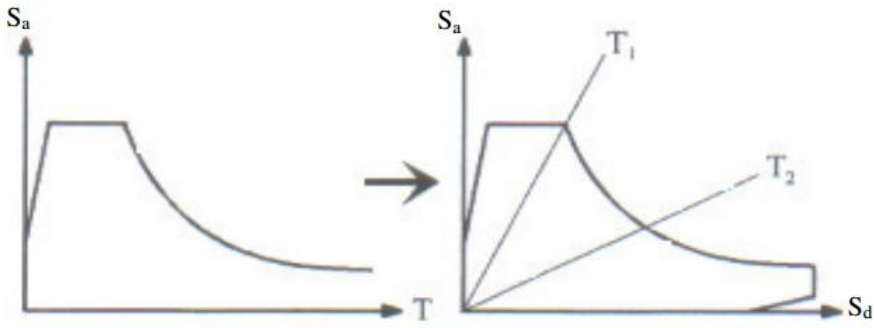

Figure 2.21: Conversion of elastic demand spectrum to ADRS (adapted from Themelis, 2008)

v. Combination of the Capacity Spectrum and Elastic Demand Spectrum

At this stage, the Capacity Spectrum and Elastic Demand Spectrum both in ADRS format are combined in one graph. From that graph, the initial performance point of the structure may be

Stellenbosch University https://scholar.sun.ac.za

estimated. The performance point defines the point at which the seismic demand is equal to the seismic capacity of the structure for a given earthquake. This point is estimated based on the principle of equal displacement, i.e. the inelastic displacement of the structure is equal to elastic displacement of the same structure which will take place if it remains perfectly elastic (ATC-40, 1996). It is obtained by drawing a line upwards of the same slope as the initial stiffness of the structure until it intersects Elastic Demand Spectrum; the vertical line passing through that intersection point is drawn. The intersection point of the vertical line and Capacity Spectrum represents the initial performance point (Figure 2.22).

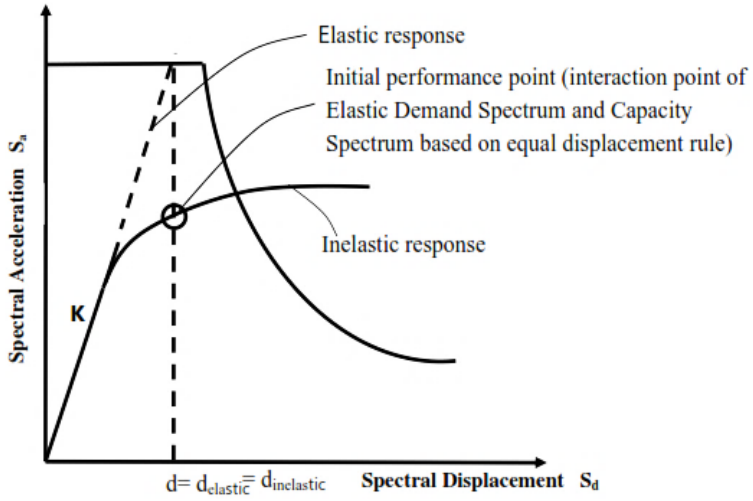

Figure 2.22: Estimation of initial performance point (modified from Themelis, 2008)

vi. Bilinearisation of the Capacity curve (ADRS format)

The Capacity Spectrum in ADRS format developed from step (iii) is bilinearised by chosing a yield point (a_y, d_y) such that area A1 is equal to A2 (Figure 2.23).

Stellenbosch University https://scholar.sun.ac.za

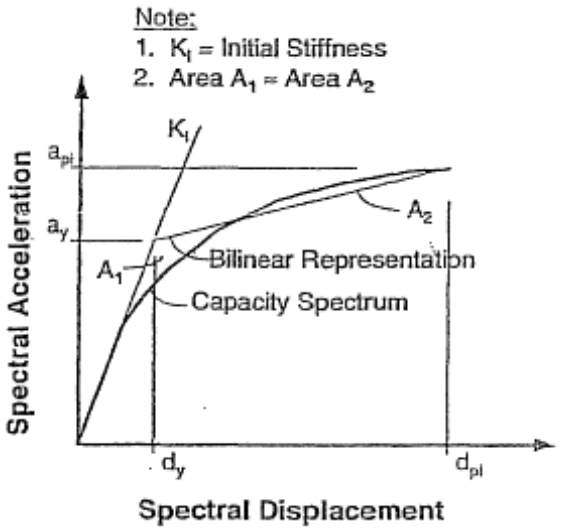

Figure 2.23: Bilinearised capacity spectrum in ADRS format (adapted from ATC, 1996)

vii. Estimation of the equivalent damping and Reduction factor for the Elastic Demand Spectrum

If seismic vibration action causes a structure to respond into its inelastic range an increase in the overall damping of the structure is found. This is over and above the inherent viscous damping which the structure exhibits. This results from energy loss due to structural movement (repetitive internal deformation and restoration of the original position of structural components) and is known as hysteretic damping. Therefore, the resultant equivalent damping is estimated as follows:

$$\beta_{eq} = \beta_o + 5\% \tag{2.45}$$

Where 5% represents viscous damping of the structure and β_o its corresponding hysteretic damping. Based on literature (Chopra, 2007), hysteretic damping could be estimated as follows:

$$\beta_o = \frac{1}{4\pi}\frac{E_d}{E_{So}} \tag{2.46}$$

Where E_d is energy dissipated by damping and E_{so} is the maximum strain energy absorbed by the structure. With reference to Figure 2.24, the equivalent viscous damping of the structure is estimated from the capacity spectrum as follows (ATC-40, 1996):

Stellenbosch University https://scholar.sun.ac.za

$$\beta_o = \frac{2}{\pi}\frac{a_y d_{pi} - d_y a_{pi}}{a_{pi} d_{pi}} \tag{2.47}$$

Therefore, equation (2.45) becomes:

$$\beta_{eq} = \frac{2}{\pi}\frac{a_y d_{pi} - d_y a_{pi}}{a_{pi} d_{pi}} + 5\% \tag{2.48}$$

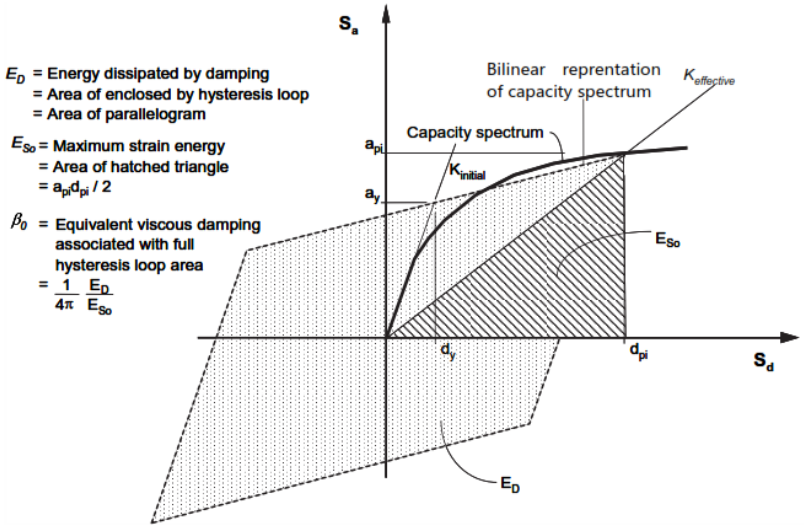

Figure 2.24: Estimation of hysteretic damping associated with structural movement (ATC-40, 1996)

At this point, the values of the resultant effective viscous damping calculated by means of equation 2.48 are obtained. The elastic demand spectrum reduction factor is then calculated with reference to literature (i.e. EC8, 2004; Newmark & Hall, 1982) and a new elastic demand spectrum (reduced demand spectrum) is derived.

viii. Estimation of the Performance Point

Single degree of freedom

With the elastic demand spectrum reduction factor calculated in the latter step, a new elastic demand spectrum is drawn up and combined in one graph with the capacity spectrum. From the combined graph (Figure 2.25) a new performance point is determined as previously discussed in step v. If the reduced elastic demand spectrum intersects the capacity curve within a tolerance limit of $\pm 5\%$ displacement of the initial performance point determined in step v, then the initially selected performance point would represent the performance point of the structure under

Stellenbosch University https://scholar.sun.ac.za

consideration (with the displacement d_{pi} representing the maximum displacement S_d of the applicable seismic demand). If the reduced elastic demand capacity does not intersect the capacity curve within the tolerable margin, the same process should be repeated starting from step iv.

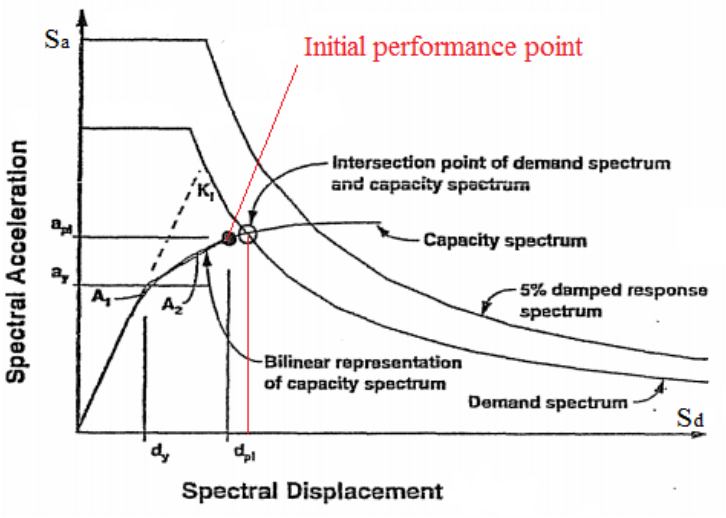

Figure 2.25: Determination of performance point (modified from ATC-40, 1996)

Multi Degree of Freedom (MDOF)

After the performance point is obtained using the steps outlined above, the resultant performance displacement is converted into the target displacement of the MDOF system by the following relation:

$$u_t = PF_1\phi_{ij}S_d \tag{2.49}$$

2. Improved capacity spectrum method (ICSM)

The capacity spectrum method introduced in 1970s was later improved by Chopra and Goel (2000) by introducing a ductility factor into the capacity demand. ICSM differs from CSM at the step of calculating the new/reduced capacity spectrum demand. Instead of adapting the capacity spectrum demand to the constant equivalent-damping ratio, the capacity spectrum demand using the constant damping ratio is replaced by the capacity demand spectrum using a constant ductility factors μ (Figure 2.26). All other calculation procedures are the same. The performance point is obtained at the point at which the capacity curve intersects the capacity demand spectrum of the associated

Stellenbosch University https://scholar.sun.ac.za

ductility factor. If the displacement value corresponding to the performance point does not fall within the margin of tolerance, the application of an iteration procedure such as for CSM will be required.

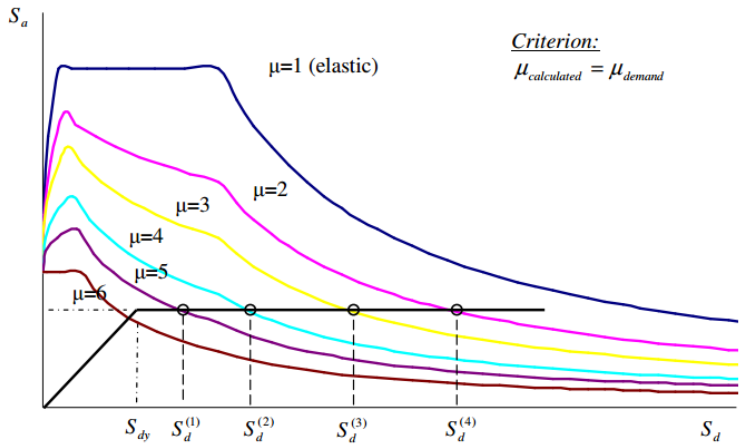

Figure 2.26: Illustrative example of capacity spectrum demand with various ductility factors

The ductility factor μ is related to hysteretic damping, β_o, and equivalent fundamental natural period by the following relationships (Chopra & Goel, 2000).

$$\beta_o = \frac{1}{4\pi}\frac{E_D}{E_{so}} = \frac{2}{\pi}\frac{(\mu-1)(1-\alpha)}{\mu(1+\alpha\mu-\alpha)} \tag{2.50}$$

$$T_{eq} = T\sqrt{\frac{\mu}{1+\alpha\mu-\alpha}} \tag{2.51}$$

Where μ is the ductility factor which is the ratio of maximum peak displacement of an inelastic system over yield displacement ($\mu = u_m / u_y$), α is the constant of proportionality between elastic stiffness and inelastic stiffness, and T is the fundamental natural period of an elastic system.

3. N2 method

The N2 method was introduced in 1988 as another alternative to CSM (Themelis, 2008). It does not require any iteration and the required quantities are computed directly. However, it mainly differs from CSM at the step where the performance point is calculated. At that step, the capacity

Stellenbosch University https://scholar.sun.ac.za

spectrum and demand spectrum should both be in Displacement-Acceleration format. The steps of the N2 method are as follows (Fajfar, 2000):

i. Pushover Analysis (POA)

The POA step is the same as that of the CSM.

ii. Determination of equivalent SDOF

This is also the same as that of the CSM.

iii. Conversion of capacity curve to capacity spectrum

The capacity curve is converted to capacity spectrum in ADRS format by means of following relationship:

$$S_a = \frac{V_b}{\Gamma_j M^*} \tag{2.52}$$

$$S_d = \frac{u}{\Gamma_j \phi_n} \tag{2.53}$$

Where V_b is the base shear force, $M^* = \sum m_i \phi_{ij}$ is effective mass of the structure, Γ_j is participation factor for vibration mode *j* and ϕ_n is the normalised displacement amplitude for the mode shape at the top of the structure. The above equations give the same results as equations 2.40 and 2.41.

iv. Determining the seismic demand and the demand spectrum in ADRS format

First, the elastic demand spectrum in ADRS format is estimated as for CSM, and then it is converted to an inelastic demand spectrum which is a function of the ductility factor μ by using the expressions below:

$$S_a = \frac{S_{ae}}{R_\mu} \tag{2.54}$$

$$S_d = \mu \frac{T^2}{4\pi^2} S_a \tag{2.55}$$

Stellenbosch University https://scholar.sun.ac.za

with

$$R_\mu = \begin{cases} (\mu - 1)\dfrac{T}{T_c} + 1 & T < T_c \\ \mu & T \geq T_c \end{cases} \tag{2.56}$$

Where μ is the ductility factor, i.e. the ratio between maximum displacement and yield displacement, R_μ is the reduction factor due to hysteretic damping, T is the fundamental period, and T_c is the characteristic period of the ground motion, where the acceleration response transitions between constant acceleration and constant velocity (see Figure 2.28).

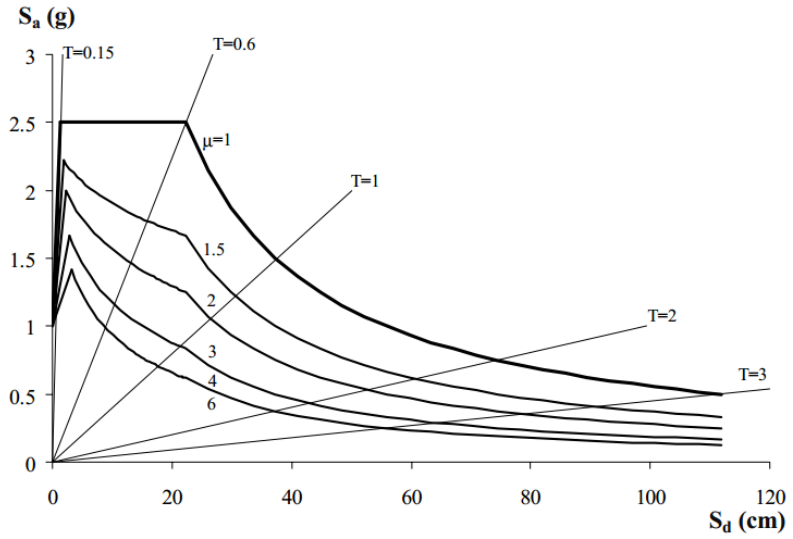

Figure 2.27: Illustrative example of demand spectrum of constant ductility factors in ADRS format (adapted from Fajfar, 2000)

Stellenbosch University https://scholar.sun.ac.za

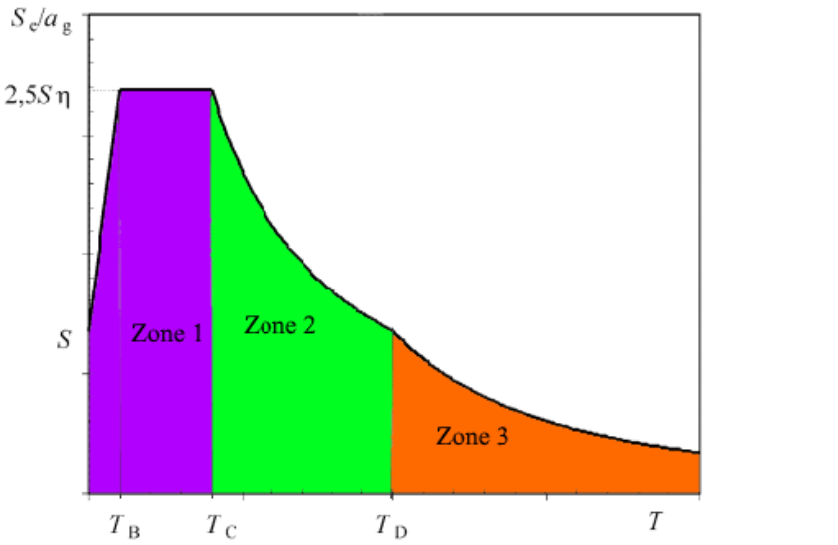

Zone 1: Low frequency range representing constant response acceleration
Zone 2: Medium frequency range representing constant response velocity
Zone 3: High frequency range representing constant response displacement

Figure 2.28: Illustrative example of response spectrum components (modified from EC8-1, 2004)

v. Seismic demand estimation of an equivalent SDOF system

Using the graph combining demand spectrum and capacity spectrum in ADRS format, the acceleration and displacement demand of an equivalent elastic system are derived by determining the intersection point of the radial axis with the elastic spectrum (Figure 2.29). The radial axis represents the elastic period T^* of equivalent SDOF system as defined by equation 2.38.

Stellenbosch University https://scholar.sun.ac.za

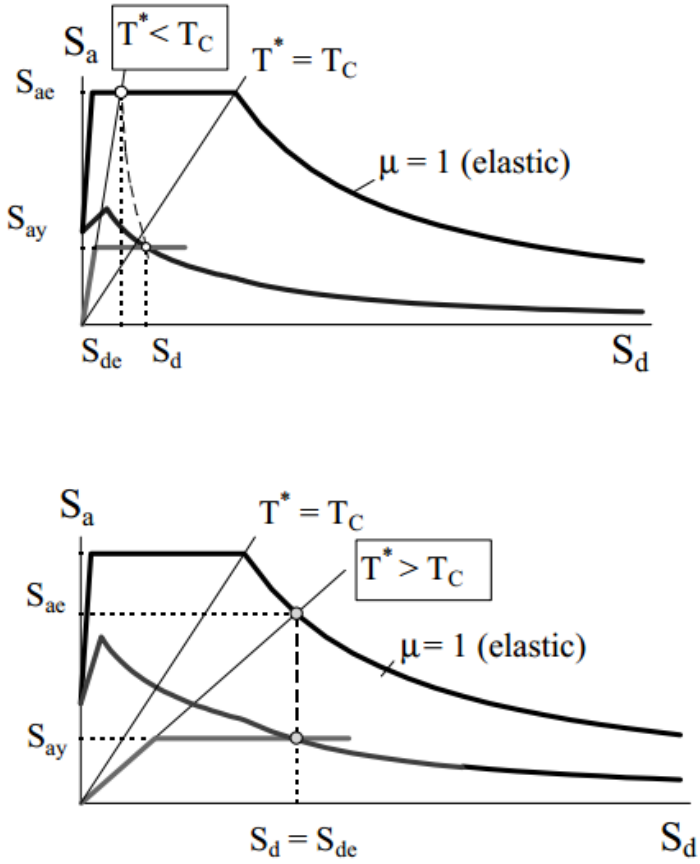

Figure 2.29: A graph combining the demand spectrum and the capacity spectrum in ADRS format (adapted from Fajfar, 2000)

The elastic acceleration demand S_{ae} and yield acceleration S_{ay} are also now obtained from the graph. The resultant hysteretic damping reduction factor R_μ is given by the following equation:

$$R_\mu = \frac{S_{ae}(T^*)}{S_{ay}} \tag{2.57}$$

The seismic inelastic displacement demand of the equivalent SDOF system is given by the following equation:

$$S_d = \begin{cases} \frac{S_{de}}{R_\mu}(R_\mu - 1)\frac{T_c}{T^*} + 1 & T^* < T_c \\ S_{de} & T^* \geq T_c \end{cases} \tag{2.58}$$

Stellenbosch University https://scholar.sun.ac.za

It can also be determined graphically as the intersection point of the demand capacity with the demand spectrum which corresponds to the ductility factor μ where μ is equal to:

$$\mu = \begin{cases} \left(R_\mu - 1\right)\frac{T_c}{T^*} + 1 & T^* < T_c \\ R_\mu & T^* \geq T_c \end{cases} \tag{2.59}$$

vi. Seismic demand of a MDOF system

The seismic inelastic demand S_d of the equivalent SDOF system is related to the inelastic demand u_t of a MDOF system as follows:

$$u_t = \Gamma_j S_d \tag{2.60}$$

4. Displacement Coefficient Method (DCM)

This method (DCM) differs mainly from the previously discussed POA methods in terms of the estimation of the displacement demand. It does not require the conversion of the capacity curve to the capacity spectrum. The maximum displacement demand is evaluated by means of a numerical equation. All the steps of this method, as extracted from ATC-40 (1996) can be summarised as:

i. Pushover Analysis (POA)

The POA step is the same as the one for the CSM.

ii. Bilinearisation of the capacity curve

The capacity curve obtained from the POA is bilinearised by means of trial and error such that the effective elastic stiffness K_e intersects the capacity curve at the point $0.6V_y$, where V_y is the intersection point between effective elastic stiffness K_e and effective post yield stiffness αK_e (Figure 2.30). A trial and error method is required to determine V_y because the value of V_y is not known at first. From the bilinearised curve, the effective fundamental period T_e is evaluated as follows:

Stellenbosch University https://scholar.sun.ac.za

$$T_e = T_i \sqrt{\frac{K_i}{K_e}} \tag{2.61}$$

Where T_i is the elastic fundamental period, K_i is the elastic stiffness and K_e is the effective elastic stiffness.

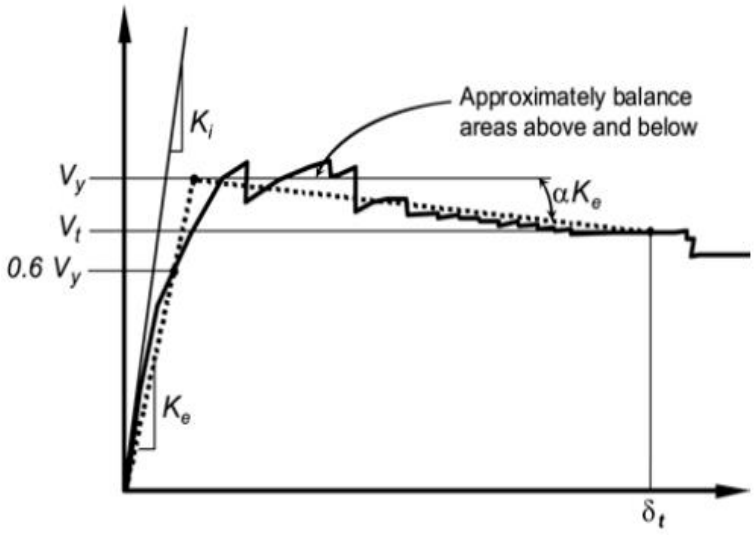

Figure 2.30: Bilinearisation of capacity curve (extracted from ASCE, 2000)

iii. Displacement demand evaluation

The analytical equation for displacement demand calculation is defined as follows.

$$\delta_t = C_0 C_1 C_2 C_3 S_a \frac{T_e^2}{4\pi^2} \tag{2.62}$$

where

C_0 is the modification factor to relate spectral displacement of the equivalent SDOF system to the top displacement of a MDOF;

C_1 is the modification factor relating the expected maximum inelastic displacement to the displacements calculated for linear elastic response;

C_2 is the modification factor representing the increased displacements due to second-order effects; and

Stellenbosch University https://scholar.sun.ac.za

S_a is the response spectrum acceleration corresponding to the effective fundamental period T_e.

Further details on numerical evaluation/ numerical values of the listed coefficients are available from ATC-40 (1996).

5. Modal Pushover Analysis (MPA)

The MPA method, developed by Chopra and Goel (2001), is based on the theory of structural dynamics. This pushover analysis entails applying an inertia force distributed over the height of the structure for each vibration mode of interest. The seismic demand is then computed using a combination of the resultant maximum displacement from each mode. It has been proven that seismic demand can be estimated well based on the combination of the first two or three modes. The steps of MPA are as follows:

i. Calculation of dynamic characteristics

The dynamic properties of the structure under consideration are evaluated from modal analysis. The fundamental periods T_n and mode shapes ϕ_j are obtained from the results for each mode of interest. For each mode j, the required lateral forces S_j for performing the pushover analysis are given by the following:

$$S_j = [M]\{\phi_j\} \tag{2.63}$$

Where $[M]$ is the mass matrix of the structure and ϕ_j is mode shape of mode j.

ii. Pushover analysis (POA)

The POA for the MPA method is the same as that of the CSM method, but for the MPA method the capacity curve (base force-top/roof displacement curve) should be established for each mode j of interest.

iii. Inelastic response of the equivalent SDOF system

During this step each capacity curve of the j^{th} mode of interest is then converted to force-displacement relationship by means of the following equations:

Stellenbosch University https://scholar.sun.ac.za

$$\frac{V_{bjy}}{M_j^*} = \frac{F_{sjy}}{L_j} \tag{2.64}$$

$$D_{jy} = \frac{u_{tjy}}{\Gamma_j \phi_{nj}} \tag{2.65}$$

Where M_j^* is the effective mass of the mode j;

V_{bjy} is the base shear force of the MDOF system for mode j;

F_{sjy} is the force of the equivalent SDOF system for mode j;

Γ_j is the participation factor for mode j;

D_{jy} is the yield deformation for the j^{th} mode inelastic SDOF;

L_j is the total mass for mode j;

u_{tjy} is the top displacement for the MDOF system for the j mode; and

ϕ_{nj} is the j^{th} mode top mode shape horizontal displacement value.

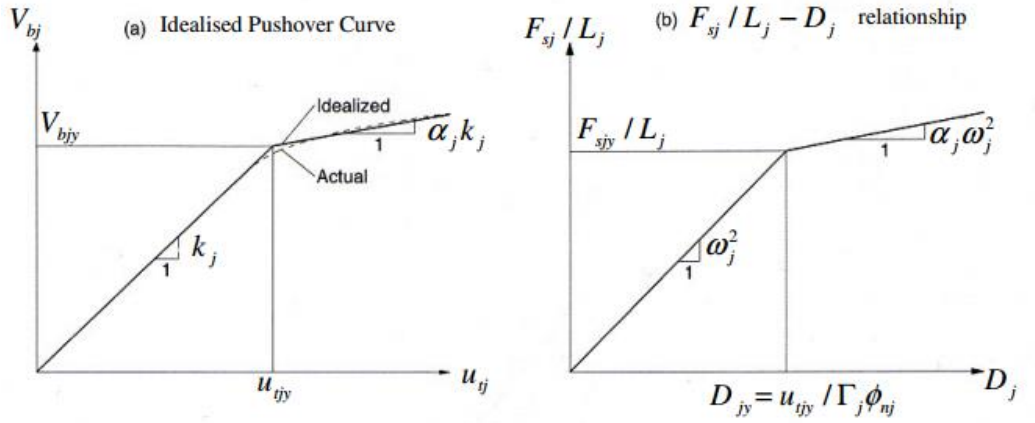

Figure 2.31: Dynamic characteristics of equivalent SDOF system obtained from capacity curve (extracted from Chopra & Goel, 2002)

iv. Determination of maximum displacement of the j^{th} mode of the equivalent inelastic SDOF system

For each selected mode j, the maximum displacement D_j of the equivalent SDOF system is obtained from a nonlinear dynamic analysis or the inelastic response spectrum or a design response spectrum.

Stellenbosch University https://scholar.sun.ac.za

v. Calculation of maximum displacement of MDOF

The maximum displacement D_j of the equivalent inelastic SDOF is related to the maximum displacement u_{tj} of the MDOF system by

$$u_{tj} = \Gamma_j \phi_{nj} D_j \tag{2.66}$$

vi. Total seismic response demand

The total seismic displacement demand R_{MPA} is obtained from the combination of the maximum modal responses R_j. For example, if the square root of the sum of squares (SRSS) rule is selected as combination rule, the total response demand will be given by

$$R_{MPA} = \left(\sum_{j=1}^{n} R_j^2 \right)^{1/2} \tag{2.67}$$

Where n represents the number of modes of interest.

Conclusion

As reported by Themelis (2008), extensive research has been conducted on pushover analysis methods to evaluate seismic response of structures. The latest studies conducted on the accuracy of different pushover procedures/methods have shown that Modal Pushover Analysis (MPA) is the most accurate method.

Stellenbosch University https://scholar.sun.ac.za

Chapter 3
Methodology

3.1 Introduction

The main objective of this research was to identify a methodology for assessing the structural performance of a steel frame water tower and apply this to evaluate whether the elevated steel water tank at the Engen Winelands 1-Stop in South Africa can withstand the seismic demand at its location. In this investigation the seismic demand of a typical elevated steel water tower supported by a steel frame was estimated from nonlinear dynamic analysis and the response spectrum approach prescribed by the Eurocode seismic design code. Afterwards, the results of both approaches (nonlinear dynamic and response spectrum) were compared to the seismic capacity estimated from Modal Pushover Analysis (MPA). Thereafter, the overall stability of the system was checked. During this analysis process, the structure was subjected to earthquake excitation corresponding to its site location as specified by the South African National Standard for the basis of structural design and actions for buildings and industrial structures /Part 4: Seismic actions and general requirements for buildings (SANS 10160-4:2011), and the finite element software package ABAQUS (SIMULIA, 2012) was used to perform the nonlinear dynamic analysis and MPA analyses.

The first step in the process was the analysis of the structure by considering it as perfectly fixed at the ground level. The second step was to analyse it by modifying its fixed base condition to flexible foundation by incorporating the flexibility of site soil at the foundation level. This was done by introducing dashpots and springs of equivalent soil properties as discussed in chapter two. For the purpose of checking the effects of soil flexibility to the general response of the system, the results of both foundation formulations were compared.

In order to validate the ABAQUS Finite Element Analysis (FEA), a steel frame structure was constructed and tested in the laboratory. This was done to ensure that suitable applicable analysis techniques were selected for the ABAQUS modelling of the structure. This chapter describes the numerical analysis methodology and parameters used to achieve the stated objective. A description of laboratory tests and results and the FEA analysis procedures and results are provided in Chapter 4.

Stellenbosch University https://scholar.sun.ac.za

3.2 Numerical method for structural performance assessment of a steel frame water tower

A numerical method for modelling a water tower structure and simulating its motion subject to a given earthquake is described here. The water tower model is built by replacing the mass of the water with equivalent impulsive and convective masses, and the flexibility of the soil is simulated with equivalent soil springs and dashpots. In the case where the flexibility of the soil is not taken into account the base of the model is fixed or pinned. This section describes the numerical analysis model with consideration of SSI as well as the methods used.

3.2.1 Dynamic modelling of water tank

With regard to the mechanical characteristics of the structure under investigation i.e. the case study of this research (refer to 3.4.1.3), the liquid - tank interaction is modelled as for a tank with flexible walls. For the case of a rigid container, Housner's (1963) modelling approach can be used.

With reference to section 2.2, Veletsos (1984) provided a model for a flexible wall tank which has been simplified by Malhotra *et al.* (2000). The latter simplified model is shown in Figure 3.1.

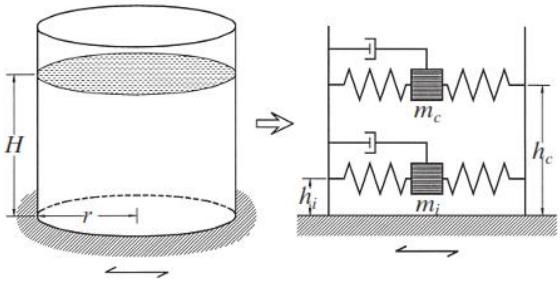

Figure 3.1: Dynamic model for flexible wall tank (adapted from Malhotra *et al.*, 2000)

The characteristics of the model are given in Table 3.1: H is the height of water, r is the tank radius, C_i is the dimensionless coefficient, C_c is the coefficient expressed in s/m$^{1/2}$, E_t is the modulus of elasticity of the tank material, ρ_w is the mass density of the water, t is the equivalent uniform thickness of the tank wall, h_i and h_c are the height of impulse mass m_i and convective mass m_c, and, $h_i^{'}$ and $h_c^{'}$ are the height of impulse and convective masses for moment calculation. The natural periods of the motion of the impulse and convective masses are given by:

Stellenbosch University https://scholar.sun.ac.za

$$T_{imp} = C_i \frac{H\sqrt{\rho_w}}{\sqrt{t/r} * \sqrt{E_t}} \tag{3.1}$$

$$T_{con} = C_c \sqrt{r} \tag{3.2}$$

All the parameters above were derived for a circular container. For other tank shapes, the values of *H* and *r* are evaluated from an equivalent circular tank (Algreane *et al.*, 2011).

Table 3.1: Values of impulse and convective modes for different sizes of water tanks

H/r	C_i	C_c[s/m$^{1/2}$]	m_i/m_l	m_c/m_l	h_i/H	h_c/H	h_i'/H	h_c'/H
0.3	9.28	2.09	0.176	0.824	0.400	0.521	2.640	3.414
0.5	7.74	1.74	0.300	0.700	0.400	0.543	1.460	1.517
0.7	6.97	1.60	0.414	0.586	0.401	0.571	1.009	1.011
1.0	6.36	1.52	0.548	0.452	0.419	0.616	0.721	0.785
1.5	6.06	1.48	0.686	0.314	0.439	0.690	0.555	0.734
2.0	6.21	1.48	0.763	0.237	0.448	0.751	0.500	0.764
2.5	6.56	1.48	0.810	0.190	0.452	0.794	0.480	0.796
3.0	7.03	1.48	0.842	0.158	0.453	0.825	0.472	0.825

3.2.2 Dynamic modelling of soil foundation interaction

Based on literature (Kotronis *et al.*, 2013; NEHRP Consultants Joint Venture, 2012) there are two approaches for SSI analysis i.e. the "*Direct method"* and "*Substructure method*. Each method is defined and described as follows:

A. Direct method

In direct approach the soil and structure are modelled and analysed together in one model (see Figure 3.2). The direct approach requires nonlinear soil structure interaction analysis which is not used often. The nonlinearity of the founding soil or the complexity of the foundation shape can lead to extensive computational effort.

Stellenbosch University https://scholar.sun.ac.za

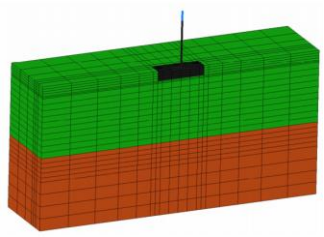

Figure 3.2: Direct approach for SSI modelling of bridge column supported on two different layers of soil (modified from Kotronis *et al.*, 2013)

B. Substructure approach

The substructure approach is a SSI analysis method which is based on the principle of superposition, but of, modification of the input seismic waves due to the presence of the foundation, calculation of the dynamic response of the soil-foundation subsystem not taking into account inertia effects of the superstructure and analysis of the above connected to a model of the superstructure (see Figure 3.3). This method assumes that the response of the soil is linear. Research has proven the suitability of this approach to models where a moderate nonlinear response of the soil applies (Mylonakis & Nikolaou, 1997).

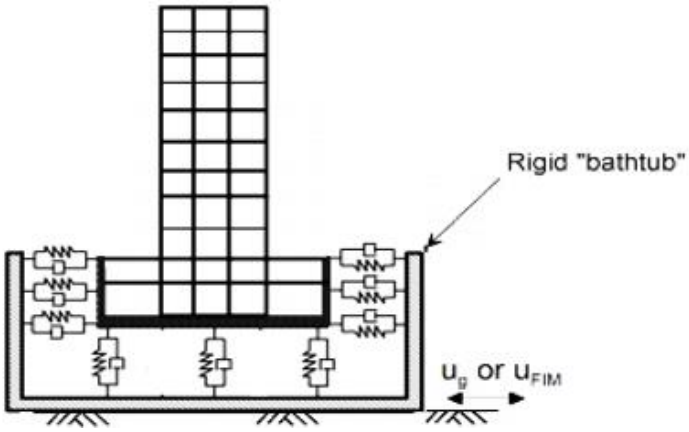

Figure 3.3: Substructure approach for SSI analysis (modified from PEER, 2010)

The substructure method involves four steps:

(i) assessment of the free field motion of the site and its corresponding soil properties;

(ii) determination of the relationship between the free field motion and the foundation input motion using transfer function amplitude to convert the free field motion into foundation input motion;

Stellenbosch University https://scholar.sun.ac.za

(iii) using the model stiffness and damping formulation to calculate the soil reactions and integration of them into the analysis model; and finally

(iv) a response analysis of the structure as loaded combined with the soil reactions using the foundation input motion as the exciting dynamic load.

- **Assessment of free field motion and soil properties of the site**

  At this stage the free field ground motion as well as the shear wave velocity of the soil under consideration is identified. The former represents the earthquake input motion at the specified point in absence of the structure and the foundation.

- **Identification of foundation input motion**

  As discussed previously in section 2.3.2, the structural foundation input motion differs from the free earthquake field ground motion due to a number of considerations. These include the following: relative displacement of foundation to free field motion coming from the inertia force of the foundation mass; foundation embedment; geometry of the foundation; and the incident angle of seismic waves. With reference to section 2.3.2.2, the calculation procedure of the foundation input motion has been discussed and it was concluded that analysing the structure using the free field ground motion is more conservative than analysing it with the foundation input motion. For the purposes of applying this numerical method to the case study of this research, the foundation input motion was taken to be the same as the free ground motion.

- **Calculation of soil reactions and their integration into analysis process**

  (a) Calculation of soil reactions

  Essentially, any research on soil structure interaction/soil foundation interaction is first based on elaboration of the soil reactions/impedance functions. As can be seen from section 2.3.2, a number of approaches have been developed to the study of SSI. Some researchers have concentrated solely on developing impedance functions, which shows the relationship between the application of a particular force to the soil and the resulting displacement (Dobry *et al.* ,1986; Gazetas & Tassoulas ,1987; Mita & Luco ,1989b; Gazetas, 1991; etc.), others have elaborated impedance functions and then used them in the study of different parameters contributing to the response of the system (e.g. Parmelee & Wronkiewicz, 1971; Novak & Sachs, 1973; Beredugo & Novak, 1972; etc.)

Stellenbosch University https://scholar.sun.ac.za

and some studied different parameters controlling the response of the structure by using impedance functions developed in other research e.g. Veletsos and Meek (1974).

Of this wide range of research on SSI, the soil reactions of Pais and Kausel (1988) are the most simplified and easily usable and that of Mylonakisa *et al.*(2006) are both the most recent and it is extended to different cases. Most available results of SSI can be critiqued on the basis that few have been validated by experimental results. The impedances functions developed by Veletsos and Wei (1971) and Veletsos and Verbic (1973), however, have been validated analytically and experimentally (ATC, 2005). These latter impedance functions are derived from a rigid circular foundation supported at the surface of elastic half space as well as a linear hysteretic.

Based on current studies which includes SSI, two methods have been used for calculating soil reactions: (i) adapting the experimentally verified impedance functions of Veletsos and his co-workers (Veletsos & Wei, 1971; Veletsos & Verbic, 1973) and then modifying them to be in compliance with the contributions from foundation shape, foundation embedment and heterogeneity of soil profiles, or (ii) adapting generalised impedances functions available from different papers such as can be found in Gazetas (1991) and Pais and Kausel (1988). The first method is known as the "Modified Veletsos Method" (Stewart, Fenves, *et al.*, 1999) and it has been adapted in different design provisions (e.g. ATC, 2005). The second approach has been applied in large scale studies such as the NEHRP Consultants Joint Venture (2012). In practice, each of these methods have their own merits in terms of simplicity. Hereafter both are reviewed and a commentary on both methods is given at the end of this section.

(1) The Modified Veletsos Method (MVM)

i. Evaluation of static stiffness (surface stiffness)

The soil reactions Q are stated in the following form:

$$Q_j = K_j\left[k_j(a_o, v_s) + ia_o c_j(a_o, v_s)\right] \tag{3.3}$$

Where *j* represents the direction of translation or rotation, a_o dimensionless frequency parameter (equation (2.8)), v_s Poisson's ratio of the soil, K_j the static stiffness and, k_j

Stellenbosch University https://scholar.sun.ac.za

and c_j are frequency dependent coefficients. The static stiffnesses K_j are given as follows

$$K_x = \frac{8Gr_x}{2-\nu_s} \tag{3.4}$$

$$K_{yy} = \frac{8Gr_{yy}^3}{3(1-\nu_s)} \tag{3.5}$$

Where $r_x = \sqrt{A_f/\pi}$ and $r_{yy} = \sqrt[4]{4I_{yy}/\pi}$.

- **Modification of static stiffness for foundation embedment**

To take into account for the effects of foundation embedment, the static stiffnesses K_{yy} and K_x of the soil have to be adjusted as follows.

$$(K_x)_E = K_x\left(1+\frac{2}{3}\frac{e}{r_x}\right) \tag{3.6}$$

$$(K_{yy})_E = K_{yy}\left(1+2\frac{e}{r_{yy}}\right) \tag{3.7}$$

Where *e* is foundation depth and $(K_x)_E$ and $(K_{yy})_E$ are the new adjusted static stiffnesses for embedment effect. The applicability of this method is set to the embedment ratios $e/r_x < 0.5$. For embedment ratios greater than 0.5 , Kramer and Stewart (2004) have recommended to adopt the impedance functions of Apsel and Luco (1987) or Bielak (1975).

- **Extension of static stiffness to any foundation shape**

The static stiffness of any foundation shape is generally calculated by evaluating the equivalent radius of the foundation and then substituting it into static stiffness equations accordingly as illustrated (equation 3.4 and 3.5). Clearly, the equivalent radius for translation stiffness (translation radius) is assessed by matching foundations areas whereas the equivalent radius for rotational stiffness (rotational radius) is assessed by matching foundations moments of inertia. This procedure is effective for a rectangular

Stellenbosch University https://scholar.sun.ac.za

foundation shape with sides ratio (larger dimension over smaller dimension) less than four (Roesset, 1981).

- **Adjustment of static stiffness for heterogeneity of soil profile**

Mechanical properties of the soil profile increase progressively with depth, therefore Stewart *et al.*, (2003) have recommended the use of average values of soil properties underneath the foundation up to the depth of $0.57r_x$ or $0.75r_{yy}$ (r_x and r_{yy} are the translational and rotational radiuses of the foundation, respectively). For the case of homogeneous half space soil lying over bedrock material, the static stiffnesses are modified as follows (Kausel, 1974):

$$(K_x)_B = K_x\left(1+\frac{1}{2}\frac{r_x}{d_s}\right) \tag{3.8}$$

$$(K_{yy})_B = K_{yy}\left(1+\frac{1}{6}\frac{r_{yy}}{d_s}\right) \tag{3.9}$$

Where $(K_x)_B$ and $(K_{yy})_B$ are adjusted horizontal translational and rotational static stiffnesses of the foundation due to the bedrock effect, and d_s is the depth of the bedrock.

ii. Evaluation of dynamic stiffness and damping value

The dynamic soil stiffness and dashpot values are $\overline{K}_j = \eta_j k_j$ and $\overline{C}_j = \eta_j c_j r_j / v_s$ where k_j and c_j are the dynamic stiffness and dashpot coefficients modifiers which depend on soil characteristics, r_j is the radius of the foundation, and η_j is the modified static stiffness for the relevant circumstances such as foundation embedment, heterogeneity of the soil or both.

Example: the dynamic stiffness $\overline{K}_j$ and damping value $\overline{C}_j$ of the foundation for horizontal translation along the x-axis and rotation about the y-axis are:

Stellenbosch University https://scholar.sun.ac.za

$$\left.\begin{aligned}\overline{K}_x &= \eta_x k_x \\ \overline{C}_x &= \eta_x c_x r_x / v_s\end{aligned}\right\} \text{Horizontal translation} \tag{3.10}$$

$$\left.\begin{aligned}\overline{K}_{yy} &= \eta_{yy} k_{yy} \\ \overline{C}_{yy} &= \eta_{yy} c_{yy} r_{yy} / v_s\end{aligned}\right\} \text{Rotation} \tag{3.11}$$

The coefficients k_x, c_x, k_{yy} and c_{yy} for a 0.33 soil Poison ratio (ν_s) and 0.3 soil hysteretic damping (β_s) are given in Table 3.2. They have been calculated from numerical equations available in Veletsos and Verbic (1973).

Table 3.2: Frequency dependent coefficients for horizontal translation and rotation

a_o	0	1	2	3	4	5	6	7	8	9	10
k_x	1.00	0.90	0.81	0.71	0.61	0.52	0.42	0.32	0.23	0.13	0.04
c_x	∞	0.96	0.81	0.76	0.73	0.72	0.71	0.70	0.69	0.69	0.69
k_{yy}	1.00	0.81	0.60	0.46	0.36	0.28	0.21	0.14	0.07	0.00	-0.06
c_{yy}	∞	0.43	0.40	0.41	0.41	0.41	0.42	0.42	0.41	0.41	0.41

(2) Generalized impedances functions

As it was mentioned earlier in this section, the soil reactions of Pais & Kausel, (1988) are currently the most simplified and easily usable. For this reason, they are the only ones reviewed herein and they are developed for a rigid rectangular foundation. With reference to Roesset (1981), the shape of the foundation does not matter because the parameters for a rectangular shape can be converted into a circular shape if a larger dimension over smaller dimension is less than four. Table 3.3 represents numerical equations for the static stiffnesses calculation of surface and embedded foundation whereas Table 3.4 to Table 3.6 represent the dynamic stiffnesses and their corresponding radiation damping coefficients for surface foundations as well as embedded foundations. The radiation damping coefficient of the foundation $\beta_{fr,j}$ (Table 3.5 and Table 3.6) is related to the dashpot coefficient $\overline{C}_j$ as follows (NEHRP Consultants Joint Venture, 2012):

Stellenbosch University https://scholar.sun.ac.za

$$\begin{aligned}\overline{C}_j &= 2\overline{K}_j\left(\frac{\beta_{fr,j}+\beta_s}{\omega}\right)\\ &= 2\overline{K}_j\left(\frac{\beta_{f,j}}{\omega}\right)\end{aligned} \tag{3.12}$$

Where $\overline{K}_j$ is dynamic stiffness and β_s is the soil hysteretic damping coefficient. The indices j denotes excitation direction of interest.

Stellenbosch University https://scholar.sun.ac.za

Table 3.3: Static stiffnesses of surface and embedded rectangular foundations (adapted from Pais & Kausel; 1988)

Vibration direction	Surface foundations	Embedded Foundations
Vertical, Z-axis	$K_{z,sur} = \frac{GB}{1-\nu}\left[3.1\left(\frac{L}{B}\right)^{0.75} + 1.6\right]$	$K_{z,emb} = K_{z,sur}\left[1.0 + \left(0.25 + \frac{0.25}{L/B}\right)\left(\frac{e}{B}\right)^{0.8}\right]$
Horizontal, X-axis (long direction)	$K_{x,sur} = \frac{GB}{2-\nu}\left[6.8\left(\frac{L}{B}\right)^{0.65} + 2.4\right]$	$K_{x,emb} = K_{x,sur}\left[1.0 + \left(0.33 + \frac{1.34}{1+L/B}\right)\left(\frac{e}{B}\right)^{0.8}\right]$
Horizontal, Y-axis (short direction)	$K_{y,sur} = \frac{GB}{2-\nu}\left[6.8\left(\frac{L}{B}\right)^{0.65} + 0.8\left(\frac{L}{B}\right) + 1.6\right]$	$K_{y,emb} = K_{y,sur}\left[1.0 + \left(0.33 + \frac{1.34}{1+L/B}\right)\left(\frac{e}{B}\right)^{0.8}\right]$
Rocking, around longitudinal X-axis	$K_{xx,sur} = \frac{GB^3}{1-\nu}\left[3.2\left(\frac{L}{B}\right) + 0.8\right]$	$K_{xx,emb} = K_{xx,sur}\left[1.0 + \frac{e}{B} + \left(\frac{1.6}{0.35 + (L/B)}\right)\left(\frac{e}{B}\right)^2\right]$
Rocking, around transversal Y-axis	$K_{yy,sur} = \frac{GB^3}{1-\nu}\left[3.73\left(\frac{L}{B}\right)^{2.4} + 0.27\right]$	$K_{yy,emb} = K_{yy,sur}\left[1.0 + \frac{e}{B} + \left(\frac{1.6}{0.35 + (L/B)^4}\right)\left(\frac{e}{B}\right)^2\right]$
Torsional	$K_{zz,sur} = GB^3\left[4.25\left(\frac{L}{B}\right)^{2.45} + 4.06\right]$	$K_{zz,emb} = K_{zz,sur}\left[1.0 + \left(1.3 + \frac{1.32}{L/B}\right)\left(\frac{e}{B}\right)^{0.9}\right]$

Note:

1. *G* is the shear modulus of the soil at large strain level

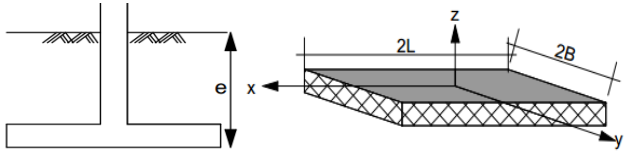

Stellenbosch University https://scholar.sun.ac.za

Table 3.4:Dynamic stiffnesses of surface and embedded rectangular foundations (adapted from Pais & Kausel; 1988)

Vibration direction	Dynamic modifier	Surface Foundations	Embedded Foundations
Vertical, Z-axis	$\alpha_z = 1.0 - \left[\frac{\left(0.4 + \frac{0.2}{L/B}\right) a_o^2}{\left(\frac{10}{1+3(L/B-1)}\right) + a_o^2} \right]$	$\frac{\overline{K}_{z,sur}}{K_{z,sur}} = \alpha_z$	$\frac{\overline{K}_{z,emb}}{K_{z,emb}} = \alpha_z$
Horizontal, X-axis (long direction)	$\alpha_x = 1.0$	$\frac{\overline{K}_{x,sur}}{K_{x,sur}} = \alpha_x$	$\frac{\overline{K}_{x,emb}}{K_{x,emb}} = \alpha_x$
Horizontal, Y-axis (short direction)	$\alpha_y = 1.0$	$\frac{\overline{K}_{y,sur}}{K_{y,sur}} = \alpha_x$	$\frac{\overline{K}_{y,emb}}{K_{y,emb}} = \alpha_x$
Rocking, around longitudinal X-axis	$\alpha_{xx} = 1.0 - \left[\frac{\left(0.55 + 0.01\sqrt{L/B-1}\right) a_o^2}{\left(2.4 - \frac{0.4}{(L/B)^3}\right) + a_o^2} \right]$	$\frac{\overline{K}_{xx,sur}}{K_{xx,sur}} = \alpha_{xx}$	$\frac{\overline{K}_{xx,emb}}{K_{xx,emb}} = \alpha_{xx}$
Rocking, around transversal Y-axis	$\alpha_{yy} = 1.0 - \left[\frac{0.55 a_o^2}{\left(0.6 + \frac{1.4}{(L/B)^3}\right) + a_o^2} \right]$	$\frac{\overline{K}_{yy,sur}}{K_{yy,sur}} = \alpha_{yy}$	$\frac{\overline{K}_{yy,emb}}{K_{yy,emb}} = \alpha_{yy}$
Torsional	$\alpha_{zz} = 1.0 - \left[\frac{\left(0.33 - 0.03\sqrt{L/B-1}\right) a_o^2}{\left(\frac{0.8}{1+0.33(L/B-1)}\right) + a_o^2} \right]$	$\frac{\overline{K}_{zz,sur}}{K_{zz,sur}} = \alpha_{zz}$	$\frac{\overline{K}_{zz,emb}}{K_{zz,emb}} = \alpha_{zz}$
Note: $a_0 = \omega B / V_s$			

Stellenbosch University https://scholar.sun.ac.za

Table 3.5: Radiation damping values of surface rectangular foundations (adapted from Pais & Kausel; 1988)

Vibration direction	Radiation Damping $\beta_{fr,j}$
Vertical, Z-axis	$\beta_{fr,z} = \left[\frac{4\psi(L/B)}{(K_{z,sur}/GB)}\right]\left[\frac{a_o}{2\alpha_z}\right]$
Horizontal, X-axis (long direction)	$\beta_{fr,x} = \left[\frac{4(L/B)}{(K_{x,sur}/GB)}\right]\left[\frac{a_o}{2\alpha_x}\right]$
Horizontal, Y-axis (short direction)	$\beta_{fr,y} = \left[\frac{4(L/B)}{(K_{y,sur}/GB)}\right]\left[\frac{a_o}{2\alpha_y}\right]$
Rocking, around longitudinal X-axis	$\beta_{fr,xx} = \left[\frac{(4\psi/3)(L/B)a_o^2}{(K_{xx,sur}/GB^3)\left[\left(2.2-\frac{0.4}{(L/B)^3}\right)+a_o^2\right]}\right]\left[\frac{a_o}{2\alpha_{xx}}\right]$
Rocking, around transversal Y-axis	$\beta_{fr,yy} = \left[\frac{(4\psi/3)(L/B)^3 a_o^2}{(K_{yy,sur}/GB^3)\left[\left(\frac{1.8}{1+1.75(L/B-1)^{0.7}}\right)+a_o^2\right]}\right]\left[\frac{a_o}{2\alpha_{yy}}\right]$
Torsional	$\beta_{fr,zz} = \left[\frac{(4/3)\left[(L/B)^3+(L/B)\right]a_o^2}{(K_{zz,sur}/GB^3)\left[\left(\frac{1.4}{1+3(L/B-1)^{0.7}}\right)+a_o^2\right]}\right]\left[\frac{a_o}{2\alpha_{zz}}\right]$
Note: Soil hysteretic damping, β_s is additive to foundation radiation damping, $\beta_{fr,j}$; $a_0 = \omega B/V_s$ and $\psi = \sqrt{2(1-\nu_s)/(1-2\nu_s)} \le 2.5$	

Stellenbosch University https://scholar.sun.ac.za

Table 3.6: Radiation damping values for embedded rectangular foundations (Tabulated from Pais & Kausel; 1988)

Vibration direction	Radiation Damping $\beta_{fr,j}$
Vertical, Z-axis	$\beta_{fr,z} = \left[\frac{4\left[\psi(L/B)+(e/B)(1+L/B)\right]}{\left(K_{z,emb}/GB\right)}\right]\left[\frac{a_o}{2\alpha_z}\right]$
Horizontal, Y-axis (short direction)	$\beta_{fr,y} = \left[\frac{4\left[(L/B)+(e/B)(1+\psi L/B)\right]}{\left(K_{y,emb}/GB\right)}\right]\left[\frac{a_o}{2\alpha_y}\right]$
Horizontal, X-axis (long direction)	$\beta_{fr,x} = \left[\frac{4\left[(L/B)+(e/B)(\psi+L/B)\right]}{\left(K_{x,emb}/GB\right)}\right]\left[\frac{a_o}{2\alpha_x}\right]$
Torsion about z-axis	$\beta_{fr,zz} = \left[\frac{(4/3)\left[3(L/B)(e/B)+\psi(L/B)^3(e/B)+3(L/B)^2(e/B)+\psi(e/B)+(L/B)^3+(L/B)\right]a_o^2}{\left(K_{zz,emb}/GB^3\right)\left[\left(\frac{1.4}{1+3(L/B-1)^{0.7}}\right)+a_0^2\right]}\right]\left[\frac{a_o}{2\alpha_{zz}}\right]$
Rocking about y-axis	$\beta_{fr,yy} = \left[\frac{(4/3)\left[\left(\frac{L}{B}\right)^3\left(\frac{e}{B}\right)+\psi\left(\frac{e}{B}\right)^3\left(\frac{L}{B}\right)+\left(\frac{e}{B}\right)^3+3\left(\frac{e}{B}\right)\left(\frac{L}{B}\right)^2+\psi\left(\frac{L}{B}\right)^3\right]a_o^2}{\left(K_{yy,emb}/GB^3\right)\left[\left(\frac{1.8}{1+1.75(L/B-1)}\right)+a_0^2\right]}+\frac{\left(\frac{4}{3}\right)\left(\frac{L}{B}+\psi\right)\left(\frac{e}{B}\right)^3}{\left(K_{yy,emb}/GB^3\right)}\right]\left[\frac{a_o}{2\alpha_{yy}}\right]$
Rocking about x-axis	$\beta_{fr,xx} = \left[\frac{(4/3)\left[\left(\frac{e}{B}\right)+\left(\frac{e}{B}\right)^3+\psi\left(\frac{L}{B}\right)\left(\frac{e}{B}\right)^3+3\left(\frac{e}{B}\right)\left(\frac{L}{B}\right)+\psi\left(\frac{L}{B}\right)\right]a_o^2}{\left(K_{xx,emb}/GB^3\right)\left[\left(\frac{1.8}{1+1.75(L/B-1)}\right)+a_0^2\right]}+\frac{\left(\frac{4}{3}\right)\left(\psi\frac{L}{B}+1\right)\left(\frac{e}{B}\right)^3}{\left(K_{xx,emb}/GB^3\right)}\right]\left[\frac{a_o}{2\alpha_{xx}}\right]$
Note: Soil hysteretic damping, β_s is additive to foundation radiation damping, $\beta_{fr,j}$; $a_0 = \omega B/V_s$ and $\psi = \sqrt{2(1-\nu_s)/(1-2\nu_s)} \le 2.5$	

Stellenbosch University https://scholar.sun.ac.za

Commentary: The Modified Veletsos method (MVM) was developed for the purpose of incorporating the effects of SSI into the seismic design codes and standards using the response spectrum approach. The equations represent the soil reactions for horizontal translation and rocking only and do not represent vertical soil reactions. The latter are required for estimating the updated fundamental frequency as well as the updated damping ratio (see section 2.3.3).

Pais and Kausel's (1988) expressions of soil reactions are available for any degree of freedom. Therefore, they are suitable either for response spectrum analysis or nonlinear static or dynamic analysis. Thus, for the purpose of comparing the results of different analysis methods the equations of Pais and Kausel (1988) are suitable.

(b) Integration of soil reactions into analysis process

In this section dynamic modelling using SSI is discussed. Response spectrum analysis is dealt with in section 3.2.3(B).

i. SSI analysis model

With reference to PEER (2010), the recommended model for SSI analysis is shown in Figure 3.4. It was first introduced by Stewart & Tileylioglu (2007) and later Naeim, Tileylioglu, Alimoradi & Stewart (2008) proved that the model agrees with recorded results from the field. It was developed for buildings with levels below the ground, but it can be modified for meeting different levels of foundation embedment (NEHRP Consultants Joint Venture, 2012). There is also the classical model of Veletsos and Wei (1971) (see Figure 2.9) which is based on the principle of modifying the fixity of the foundation base. Currently, this latter model is not used. One reason for this might be the fact that it is limited to 2D analysis of surface foundations.

Stellenbosch University https://scholar.sun.ac.za

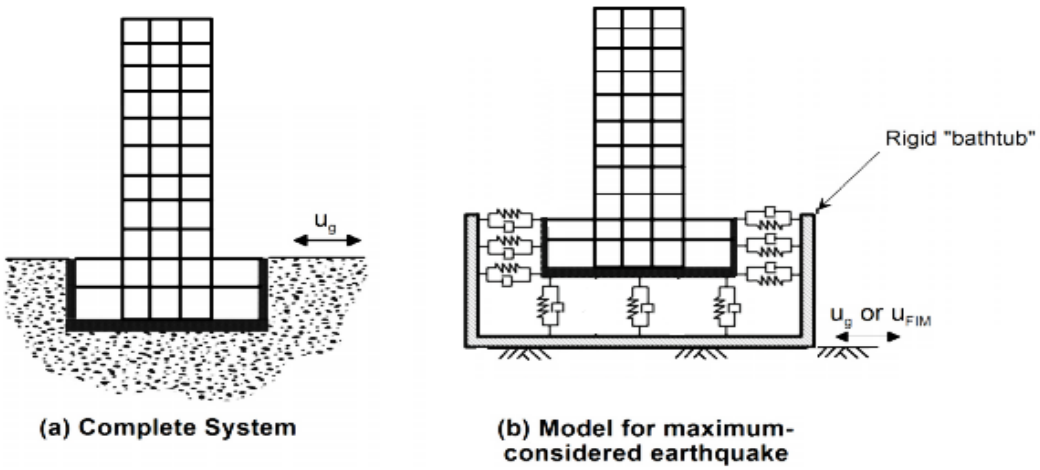

Figure 3.4: Modelling approach (modified from PEER 2010)

In this model, the horizontal stiffnesses and dashpots evaluated from foundation embedment are modelled and are fixed to a surrounding rigid wall (the "bathtub"). The dynamic loading in the form of a free field motion or foundation input motion is then applied to the bathtub.

ii. Linking of soil reactions to the foundation

As noted in section 2.3.2.3, the approach of distributing the soil reactions around and underneath the foundation is only one of the approaches which are currently available for implementing foundation flexibility effects into analysis process. The procedures described in this section are extracted from NEHRP Consultants Joint Venture (2012) and they are based on the Harden and Hutchinson's (2009) approach.

Computation of vertical foundation reactions:

Step 1: Calculate vertical soil parameters $\overline{K}_z$ and $\overline{C}_z$ as discussed in the previous section.

Step 2: Calculate vertical soil reactions intensities k_z^i and c_z^i by dividing soil reactions by corresponding foundation area.

$$k_z^i = \frac{\overline{K}_z}{4BL} \tag{3.13}$$

Stellenbosch University https://scholar.sun.ac.za

$$c_z^i = \frac{\overline{C}_z}{4BL} \tag{3.14}$$

Step 3: Calculate the individual vertical soil reactions by multiplying soil reaction intensity by the tributary area of each modelled spring and dashpot elements to obtain properties for both spring and dashpot elements.

Step 4: Multiply the edge soil reactions by the following ratios to account for the rocking effect.

$$R_{k,yy} = \frac{\left(\frac{3\overline{K}_{yy}}{4k_z^i BL^3}\right) - (1-R_e)^3}{1-(1-R_e)^3} \tag{3.15}$$

$$R_{k,xx} = \frac{\left(\frac{3\overline{K}_{xx}}{4k_z^i B^3 L}\right) - (1-R_e)^3}{1-(1-R_e)^3} \tag{3.16}$$

$$R_{c,yy} = \frac{\frac{3\overline{C}_{yy}}{4c_z^i BL^3}}{R_{k,yy}\left(1-(1-R_e)^3\right)+(1-R_e)^3} \tag{3.17}$$

$$R_{c,xx} = \frac{\frac{3\overline{C}_{xx}}{4c_z^i B^3 L}}{R_{k,xx}\left(1-(1-R_e)^3\right)+(1-R_e)^3} \tag{3.18}$$

Where R_e is the length ratio, which can be set at any value between 0.3 and 0.5 (see Figure 3.5).

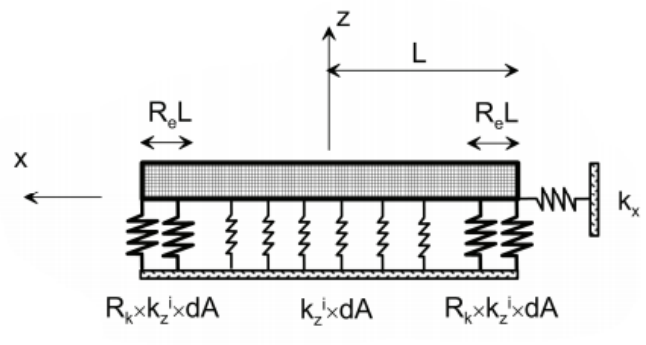

Figure 3.5:Allocation of vertical spring and dashpot forces to the foundation base (modified from NEHRP Consultants Joint Venture, 2012)

Stellenbosch University https://scholar.sun.ac.za

Computation of horizontal foundation reactions:

- Surface footings with two-dimension analysis: horizontal soil reactions are applied directly at the base of footing (see Figure 3.6(a));
- Embedded footings with two-dimension analysis: the horizontal soil reactions are evaluated in two steps. Firstly, the soil reactions are calculated by assuming a surface foundation condition. These are then applied directly at the base of footing. Secondly the embedded footing is analysed and then the difference between the surface and embedded horizontal soil reactions is distributed along the foundation depth (see Figure 3.6(b));
- For three-dimension analysis; the procedures are the same except that the horizontal soil reactions are distributed around the perimeter of the foundation depth (see Figure 3.6(c)).

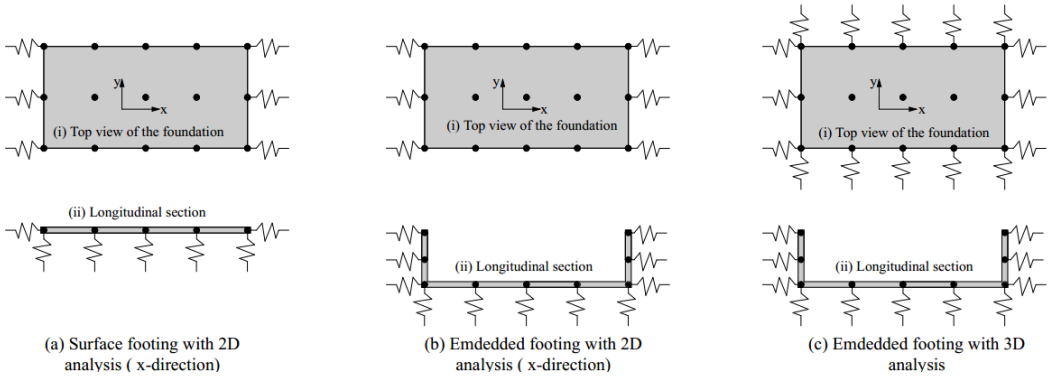

Figure 3.6: Typical example of soil reaction (stiffness) distribution (modified from NEHRP Consultants Joint Venture, 2012)

- **a response analysis of the combined soil reactions and the structure**

Once the mass of the water in the tank has been replaced by the impulse and convective masses, as discussed in section 3.2.1, and the flexibility of the soil has been replaced by soil springs and dashpots, as calculated from section 3.2.2; these parameters are then included in the numerical model of either a surface water tank or an elevated water tank depending on the case in hand. The next step consists of selecting the numerical analysis method, which depends on the applicable analysis options (e.g. P-delta effects, nonlinearity of material) and the required output. The output of the analyses included in this study are limited to the seismic demand and seismic capacity of water towers. This is discussed further in the next section.

Stellenbosch University https://scholar.sun.ac.za

3.2.3 Estimation of the seismic demand of the structure

A. Nonlinear dynamic approach

After implementing the sloshing and soil structure interaction effects into the analysis process, as discussed in sections 3.2.1 and 3.2.2, the seismic demand on the steel framed water tower is estimated from a nonlinear dynamic analysis. This analysis approach requires numerical integration of the governing dynamic equations of the structure at each time history point of the input ground motion. The advantage of the nonlinear dynamic approach is that it takes excessive lateral displacement resulting from SSI and the local yield and buckling of the frame elements into account. This is highly likely to affect the overall stability of the steel frame even before it is disturbed by seismic activity.

To estimate the maximum base shear force which can be induced by an earthquake on the structure, a code design approach could also be used.

B. Code design approach

A review of seismic designs for water tanks with consideration of SSI was presented in section 2.3.3.2. Most standards do not contain analysis procedures for elevated tanks. Since the analysis recommendations of the European standard EN 1998-4 (EC8-4, 2006) do not contain enough information on elevated water tanks, it was decided to use them in conjunction with the guidelines of Sudhir and Jaiswal (2007). The EN 1998-4 (EC8-4, 2006) contains various approaches to be used for the SSI analysis of water tanks; since Malhotra *et al.*'s (2000) approach is among those approaches, is presented herein. It was also discussed briefly in section 3.2.1.

(1) Water tanks founded on soil

With reference to Malhotra *et al.* (2000), the maximum seismic base shear force V which can be induced on the base of this type of water tank is given by

$$V = (m_i + m_{em}) * S_e(T_{imp}) + m_c * S_e(T_{con}) \tag{3.19}$$

where $S_e(T_{imp})$ is the impulse spectral acceleration, $S_e(T_{con})$ is the convective spectral acceleration and m_{em} is the mass of the container (i.e. empty tank). Other parameters were

Stellenbosch University https://scholar.sun.ac.za

previously defined. The impulse and convective spectral accelerations are dependent on damping and the natural period of the structure as well as the maximum ground acceleration and soil type (refer to section 3.2.2.2 of EC8, 2004). The damping ratios for the impulse mass and convective mass are 2% and 0.5%, respectively. The natural periods of the impulse and convective masses, T_{imp} and T_{con}, are obtained from equations 3.1 and 3.2.

(2) Elevated water tanks

The height of the water tank only influences the impulse mode and not the convective mode. With reference to Sudhir and Jaiswal (2007), the impulse period T_{imp} for elevated water tanks is given by

$$T_{imp} = 2\pi\sqrt{\frac{m_i + m_s}{K}} \tag{3.20}$$

where m_i is the impulse mass, m_s is the mass of the container and one third of the mass of the steel frame, and K is the lateral static stiffness of the steel frame. The total base shear force is obtained from the same equation as equation 3.19, by replacing m_c with m_s.

The above analysis procedures for both ground supported and elevated water tanks, the effect of SSI is not implemented in. In order to implement the SSI effect into the above procedures, the impulse period T_{imp} should be modified, as stated in equation 2.23. For elevated water tanks, the SSI effect can be alternatively included into the analysis process by modifying the lateral stiffness K for the fixed base condition of the tower to the flexible base condition.

3.2.4 Estimation of the seismic capacity of the structure

Generally, the seismic capacity of the structure is estimated by a pushover analysis. With reference to the summary of section 2.4.2.3, the modal pushover analysis was shown to be more accurate than others. Therefore, it better to use the modal pushover approach for estimating the seismic capacity of steel framed water towers. However, any other pushover method could be used, depending on the accuracy required and the analysis tool used.

Stellenbosch University https://scholar.sun.ac.za

3.3 Design criteria of frame members

According to Haroun and Temraz (1992) the maximum axial stress σ_{ax} in any frame element is limited as follows:

$$\sigma_{ax} \leq \begin{cases} \dfrac{18000}{\left[1+\left(l/18000r_g^2\right)\right]} \\ 103MPa \end{cases} \tag{3.21}$$

The local buckling of frame members is limited as stated by equation 3.22. Here l defines the length of the frame member and r_g is its radius of gyration.

$$\frac{l}{r_g} \leq 175 \tag{3.22}$$

3.4 Case study layout

The numerical method for the seismic assessment of a steel framed water tower, illustrated in the above sections, was applied to the case study of this research, the Engen Winelands 1-Stop water tower, in order to evaluate its seismic performance. This section describes in detail the structural characteristics, site soil characteristics and site seismic characteristics used for the case study.

3.4.1 Structural characteristics

3.4.1.1 Description of the water tower

The system is composed of a steel tank container supported by a steel frame (see Figure 3.7). The steel tank is a square tank made of square steel plates 1.22m in length and 3.0mm thick which are connected to each other in order to achieve the total volume of the tank. The tank is 2.44m high and 6.1m wide with a total capacity of 90,793 litres of water.

Stellenbosch University https://scholar.sun.ac.za

Figure 3.7: Engen Winelands 1-Stop elevated water tower

The steel frame is a combination of I-section column elements, and angles as horizontal and diagonal elements. The column elements are spaced at 4.5m from each other and braced both horizontally and diagonally with angles which are vertically spaced at 4m (see appendix **A**). The overall height of the steel frame is 20m. The connection of the horizontal and diagonal angles to the columns is provided by gusset plates of 320x150x6 mm which are welded to the columns and connected to angles by bolts of 18mm diameter. All columns are welded to base plates of 420x420x25mm which is connected to the foundation base by bolts with a diameter of 22mm.

3.4.1.2 Description of the foundation

No information was available on the foundation base, therefore, in the next section it is assumed as being a rigid raft foundation supported at ground level. This represents a conservative approach for SSI analysis (Avilés & Pérez-Rocha, 1996; Avilés & Pérez-Rocha, 1998). More information on how the size of the foundation was determined is presented in section 4.2.2.1(A).

Stellenbosch University https://scholar.sun.ac.za

Table 3.7: Lattice steel frame characteristics

Element Type	Type of section	Size [mm]	
Columns	I-section	200x200	
		Flange	web
		11	7.3
Horizontal tie beams	Equal angle	120x120x8	
Diagonal bracings	Equal angle	60x60x5	

(a) (b)

Figure 3.8: (a) Connection of the columns to foundation; (a) Connection of frame elements to the column

3.4.1.3 Mechanical characteristics of structural materials

All system elements are of grade 300WA steel with the mechanical properties given in Table 3.8.

Table 3.8: Mechanical properties of the system

Ultimate tensile strength σ_u [MPa]	Yield stress σ_y [MPa]	Yield strain [%]	Density [kg/m^3]	Elastic Modulus [*G*Pa]	Poisson's ratio	Shear Modulus [*G*Pa]
450/620	300	0.2	7850	200	0.3	77

Stellenbosch University https://scholar.sun.ac.za

3.4.2 Site soil Characteristics

The South African seismic design code (SANS 10160-4, 2011) classifies soil into four categories as shown in Table 3.9. According to Jeffares and Green Consulting Engineers (2008) and Bardet (1997), the soil of the site under consideration is classified as type 3: Sandy clay with the following properties.

Soil density, ρ_s = 18.45kN/m^3

Poisson ratio ν_s =0.25

Young's modulus, E_s = 250MPa

Table 3.9 : South African soil categories for seismic analysis and design (SANS 10160-4, 2011)

Ground type	Description of stratigraphic profile	Parameters		
		$v_{s,30}$ [m/s]	N_{SPT} [blows/ 30cm]	C_u [kPa]
1	Rock or other rock like geological formation, including at most 5m of weaker material at the surface	>800	-	-
2	Deposits of very dense sand, gravel, or very stiff clay, at least several tens of metres in thickness, characterized by a gradual increase of mechanical properties with depth	360-800	>50	>250
3	Deep deposits of dense or medium dense sand, gravel or stiff clay with thickness from several tens to many hundreds of metres	180-360	15-50	70-250
4	Deposits of loose to medium cohesion-less soil (with or without some soft cohesive layers), or of predominantly soft to firm cohesive soil	<80	<15	<70

$v_{s,30}$ -average value of propagation of S-waves in the upper 30m of the soil profile at shear strains of 10-5or less;

N_{SPT} -standard penetration test blow-count; and

C_u -un-drained shear strength of soil

Stellenbosch University https://scholar.sun.ac.za

3.4.3 Seismic characteristics of the site

3.4.3.1 Peak ground acceleration

With regard to the site location of the Engen Winelands 1-Stop and the seismic hazard map of South Africa (Figure 3.9), the structure is situated in seismic hazard zone I for which a peak ground acceleration of 0.1g applies. For design purposes, the South African seismic design code (SANS 10160-4, 2011) allows the increase of the peak ground acceleration obtained from the seismic hazard map by an importance factor of the corresponding importance class of the structure. As the main purpose of a water tank is to maintain the retained water and supply it even after a seismic hazard, it has been classified as a class IV structure which translates to an importance factor of 1.40 based on table 3 of SANS 10160-4 (2011). Thus, the maximum peak ground acceleration becomes 0.1g times 1.4 which gives the peak ground acceleration of 0.14g.

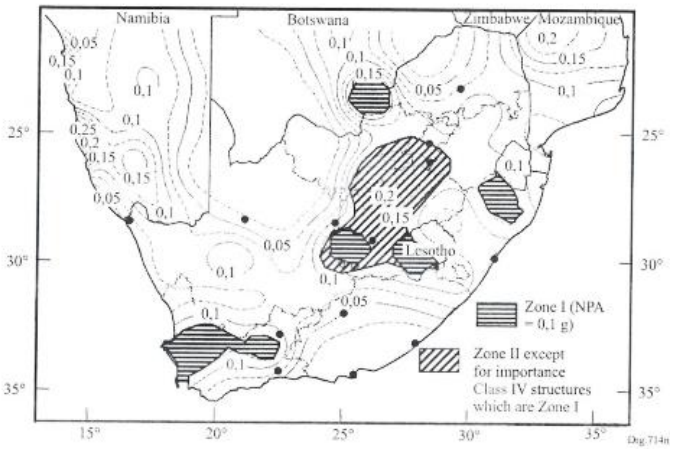

Figure 3.9: Seismic hazard map of South Africa (adapted from SANS 10160-4, 2011)

The maximum magnitude recorded for an earthquake in the Western Cape was 6.3 on the Richter scale. This magnitude falls into the moderate range with a peak ground acceleration of 0.1g to 0.15g (Jarvis, 2014). Therefore, in this study the design peak ground acceleration has been taken as 0.15g.

Stellenbosch University https://scholar.sun.ac.za

3.4.3.2 Ground motion

As stated in section 3.1, the adapted methodology for assessing seismic performance of the structure for this case study is to estimate seismic demand as well as seismic capacity of the structure from a nonlinear dynamic time history analysis and Modal Pushover Analysis, and compare the results afterwards. In the case of the time history analysis approach, one needs time history data to be implemented into analysis software (ABAQUS) in order to perform the time history analysis. For this reason, different ground motions of the same characteristics (soil characteristics and earthquake magnitude) at the site under consideration were compiled and reviewed from the Pacific Earthquake Engineering Research Center Ground Motion Database (PEER, 2013). From this reference, ten ground motions were obtained (see Table 3.10).

For this assessment, the selected ground motion is that of the "Victoria Mexico earthquake". This selection is based on the time duration and the maximum peak ground acceleration (PGA) of the earthquake. These two parameters are of interest due to the maximum allowable PGA of the site under consideration and the computational power of the analysis tool available to use for this analysis. The increase of the time duration of the ground motion implies the increase of the required number of analysis iterations which can subsequently result in a lengthy computational time. The PGA of Victoria Mexico ground motion matches the specified PGA of the site, and its time duration, among others, does not require much computational time. The ground acceleration and the ground displacement time history of the Victoria Mexico earthquake are shown in Figure 3.10.

Table 3.10: Available earthquake records corresponding to the specifications of the site (magnitude and the class of the soil)

S/N	Earthquake Name	Year	Station Name	Duration (sec)	Magnitude	PGA (g)	Mechanism	Vs30 (m/sec)	Lowest Useable Frequency (Hz)
1	Victoria_ Mexico	1980	Chihuahua	26.99	6.33	0.15	strike slip	242.05	0.0625
2	Coalinga-01	1983	Cantua Creek School	64.98	6.36	0.23	Reverse	274.73	0.1
3	Coalinga-01	1983	Parkfield - Fault Zone 12	59.98	6.36	0.11	Reverse	265.21	0.25
4	Coalinga-01	1983	Parkfield - Fault Zone 14	64.98	6.36	0.26	Reverse	246.07	0.1625
5	Coalinga-01	1983	Parkfield - Fault Zone 15	64.98	6.36	0.19	Reverse	307.59	0.25
6	Coalinga-01	1983	Parkfield - Fault Zone 7	59.98	6.36	0.12	Reverse	297.46	0.1875
7	Coalinga-01	1983	Parkfield - Fault Zone 8	59.98	6.36	0.13	Reverse	308.84	0.175
8	Coalinga-01	1983	Parkfield - Vineyard Cany 1W	59.98	6.36	0.09	Reverse	284.21	0.2625
9	Chi-Chi_ Taiwan-06	1999	TCU065	89.99	6.3	0.14	Reverse	305.85	0.06
10	L'Aquila_ Italy	2009	Avezzano	60	6.3	0.06	Normal	199	0.05

Stellenbosch University https://scholar.sun.ac.za

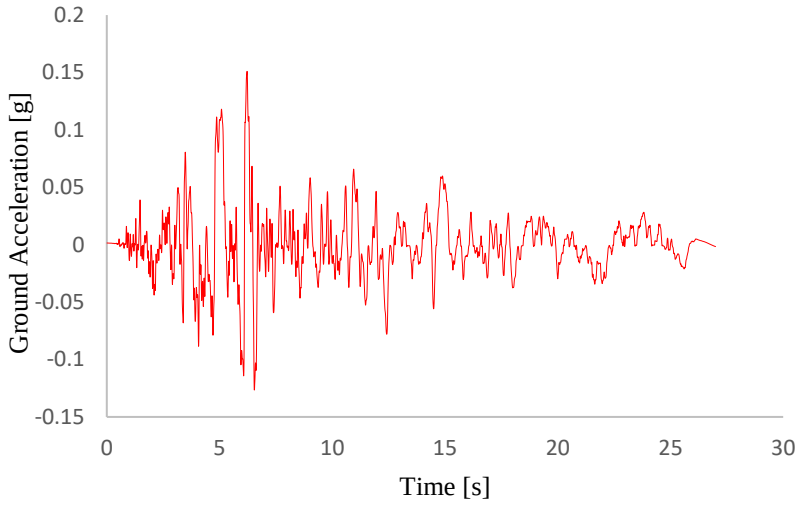

(a) Victoria Mexico Earthquake, ground acceleration

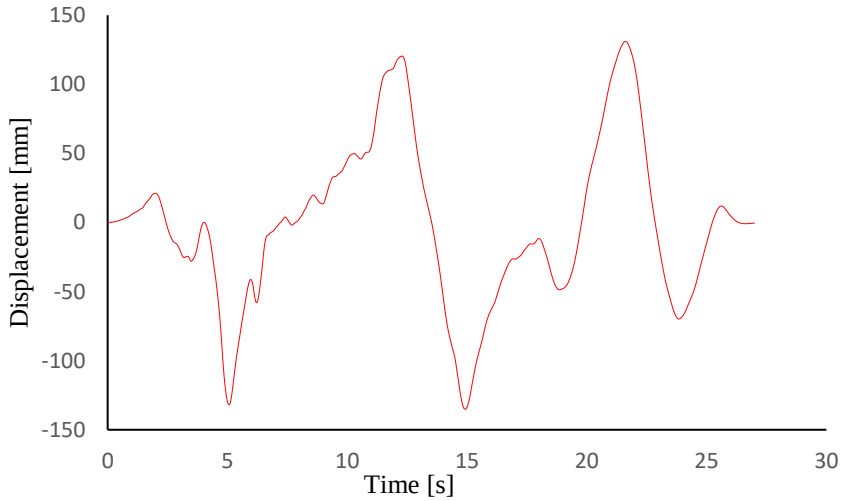

(a) Victoria Mexico earquake, displacement

Figure 3.10: Selected ground motion characteristics

Stellenbosch University https://scholar.sun.ac.za

Chapter 4

Analysis and testing of the structure

This chapter contains two main sections i.e. the analysis and results of the test structure as well as the analysis and results of the existing water tower. The test structure was a lattice steel frame with the same characteristics as the existing water tower under investigation. It was built in the laboratory for the main purpose of obtaining the damping ratio of the tower as well as validating the numerical analysis model of the tower.

The test structure was subjected to the same seismic excitation in both laboratory and ABAQUS finite element software. From a comparison of the two, the damping ratio was obtained. The analysis model of the existing water tower was validated through the use of the damping coefficient determined from the test structure inserted into the analysis software data.

After the analysis model was validated, the seismic behaviour of the water tower was assessed. Two boundary conditions were considered i.e. whether the water tower was perfectly fixed at ground level and whether it was flexibly supported at ground level. With respect to the boundary conditions, the seismic assessment of the tower was divided into two parts. For the first part the seismic behaviour of the tower with a fixed base condition was considered while for the second part a flexible base condition was considered. In each part, the assessment was conducted by estimating the seismic demand of the tower using the nonlinear dynamic approach, the code design approach as presented in the previous chapter and estimating the seismic capacity of the tower using the pushover approach. Later on, the seismic performance of the tower was found by comparing the seismic demand to the seismic capacity. In addition, the global stability of the tower was also checked.

Stellenbosch University https://scholar.sun.ac.za

4.1 Analysis of test structure

4.1.1 Experimental testing of the test structure

1. Test structure description

The test structure was a cross-braced steel frame 2m in height with a square cross section 0.6m wide. The cross-braced steel frame was made of four columns, with three levels of horizontal members braced diagonally in all panels (Figure 4.1).

Figure 4.1: Typical test structure

The orientation of the diagonal bracings was back-to-back. They were not directly connected and were free to slide relative to each other.

Stellenbosch University https://scholar.sun.ac.za

The connection of the horizontal and diagonal bracings to the vertical columns was provided by the plates welded to the columns and bolted to the bracings (Figure 4.2). The orientation of all bracings and the type of connection was chosen based on the characteristics of the Engen 1-Stop water tower. All of the frame elements were set at square angles. The diagonal bracings were 25x25x3mm, the horizontal bracings were 40x40x3mm and the columns were 60x60x4mm.The mechanical properties for each element are given in Table 4.1.

Table 4.1: Mechanical properties of test structure elements

Ultimate tensile strength σ_u [MPa]	Yield stress σ_y [MPa]	Yield strain [%]	Density [kg/m^3]	Elastic Modulus [*G*Pa]	Poisson's ratio	Shear Modulus [*G*Pa]
365	200	0.2	7850	200	0.3	77

A typical connection of the frame elements to the column is shown in Figure 4.2. 8mm and 10mm bolts were used to connect the horizontal and diagonal bracings to the columns. The 220x130x4mm plate was welded to the column.

Figure 4.2 : Column to beam and bracing connection

Figure 4.3 shows the connection of the footplates to the columns. The footplates, each 200x150x10mm in size, were welded to each column in order to facilitate the connection of the frame base to any given support structure.

Stellenbosch University https://scholar.sun.ac.za

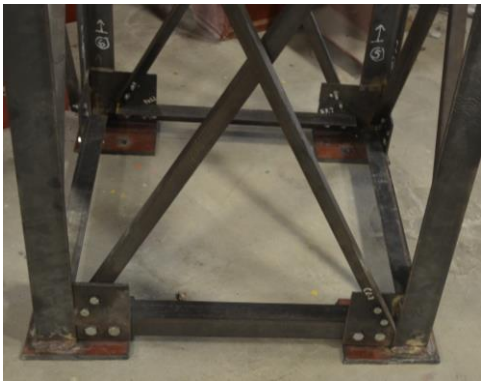

Figure 4.3:Footplates of the columns

2. Testing machine

The machine used for carrying out the experimental analysis is a shaking table (see Figure 4.4). The shaking table is a combination of a moving table and the Instron apparatus. The Instron apparatus is a machine capable of inducing unidirectional displacement to the moving table on which the test structure was fixed. The maximum absolute displacement of the Instron is 250mm. Based on various trial simulations conducted in laboratory it was found that the Instron machine does not correctly simulate an earthquake with a maximum acceleration greater than 0.1g.

Figure 4.4:Shaking table testing machine

3. Experimental test setup

The test structure was fixed to the shaking table in the laboratory as shown in Figure 4.6. A mass of 800kg consisting of eight lead plates, each with a mass of 100kg, were placed on the top apex of the steel frame and fixed to it. The steel frame was connected to the shaking table by 1xM16 high yield strength bolts per column base as shown in Figure 4.5.

Stellenbosch University https://scholar.sun.ac.za

Figure 4.5:Typical connection of the test structure to the shaking table

The earthquake chosen for simulation in the experimental work is the Kocaeli-Turkey earthquake (Table 4.2). It was selected based on the capacity of the testing machine. The time history data of the Kocaeli-Turkey earthquake is shown in Figure 4.7.

Table 4.2: Selected earthquake for test structure simulation

Earthquake Name	Kocaeli_Turkey
Year	1999
Station Name	Eregli
Duration (sec)	25.56
Magnitude (Richter scale)	7.51
PGA (g)	0.1015883
PGD (mm)	38.99385
Mechanism	strike slip
Vs30 (m/sec)	585.09
Lowest Useable Frequency (Hz)	0.0625

Stellenbosch University https://scholar.sun.ac.za

Figure 4.6: Loaded steel frame on shaking table

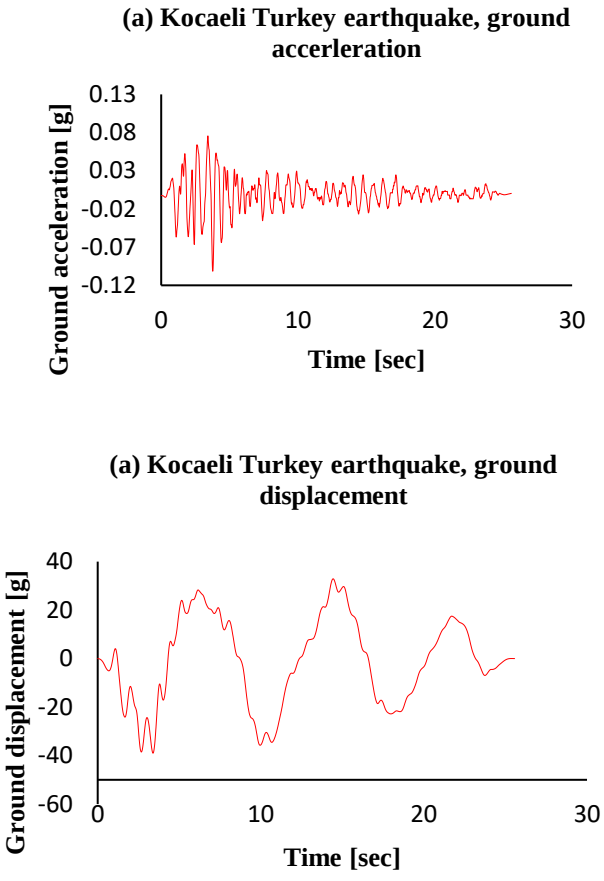

Figure 4.7: Experimental earthquake characteristics

Stellenbosch University https://scholar.sun.ac.za

In order to obtain the seismic response of the test structure, the linear variable displacement transducers (LVDTs) were mounted on the apex of the frame and connected to the computer through the Spider8 data acquisition system. The LVDTs were supported by steel columns fixed at the base and horizontally connected at the top. The shaking table moved in between and independent of the columns relative to the LVDTs, i.e. the LVDTs were kept fixed (refer to Figure 4.6). The latter were connected to the column at the apex of the frame (Figure 4.8).

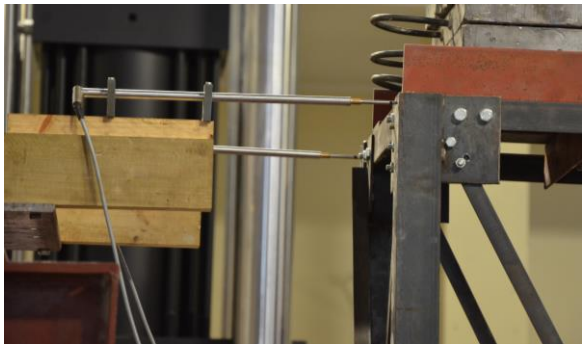

Figure 4.8: Connection of LVDTs to the apex of the test structure

4. Results

The test results obtained included the top displacement and the base shear force on the test structure. The former is shown in Figure 4.9 and the latter in Figure 4.10. The LVDTs mounted at the apex of the columns recorded the total displacement of the test structure, as they were fixed relative to the moving table. The top displacement shown in the graph was the difference between the average displacements of the two LVDTs and the base displacement, i.e. shaking table displacement. In this case, the shaking table displacement was the same as the input displacement. The base shear force was measured by the load-cell of the Instron. The load-cell measures the base shear force of the combined shaking table and attached structure. The base shear force of the test structure was obtained by computing the difference of the shear value for the test with and without the frame. The maximum displacement and base shear force obtained as shown in the figures were 0.170mm and 960N respectively.

Stellenbosch University https://scholar.sun.ac.za

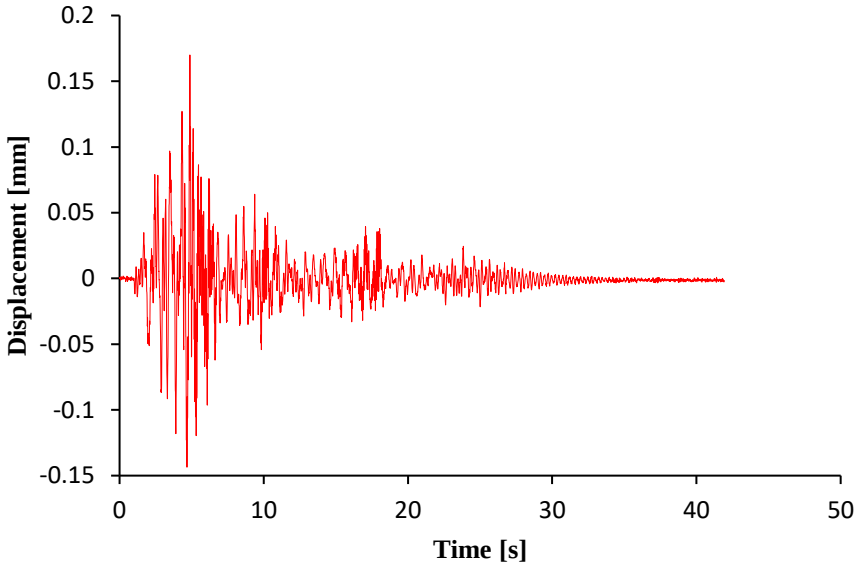

Figure 4.9: Top displacement for the test structure

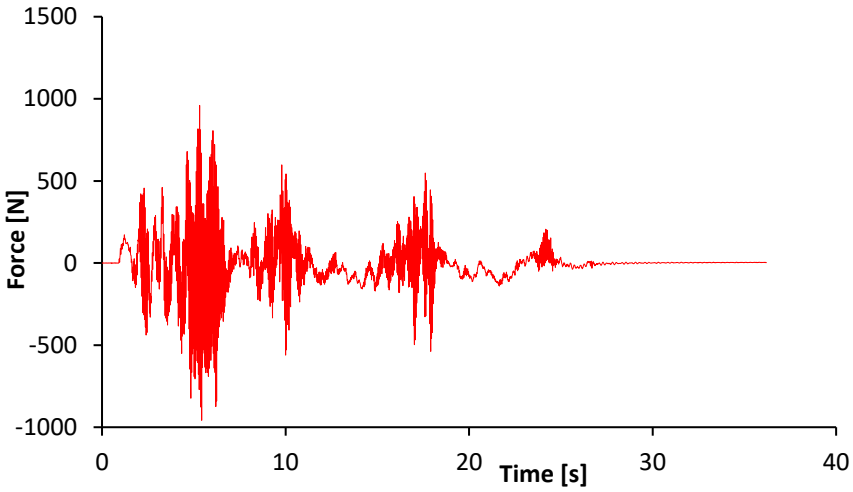

Figure 4.10: Base shear force for the test structure

4.1.2 Numerical analysis of the test structure

The numerical finite element analysis of the structure was done using the ABAQUS FEM software package. Figure 4.11 shows a 3D numerical model of the test structure. The section for the frame elements was defined as beam elements and their connection points were defined as pin joints. The sections were defined with the mechanical properties of steel: density ρ =7850kg/m^3, Young's modulus E=200GPa and Poisson ratio ν =0.3. The profiles were created based on the profiles used

Stellenbosch University https://scholar.sun.ac.za

in the experimental model i.e. equal angles of 60x60x4mm for columns, 40x40x3mm for horizontal bracings and 25x25x3mm for diagonal bracings. For the definition of the non-linear properties of the steel material a yield stress of 200MPa and strain of 0.2% were defined. The lumped mass of 800kg was assigned to the top of the model with a vertical offset of 0.2m from the apex of the columns. The effect of the lumped mass was transmitted to the apex of the columns through the massless rigid elements shown at the top of the steel frame in Figure 4.11. The offset of 0.2m corresponded to the centre of mass of the eight lead plates used during experimental work.

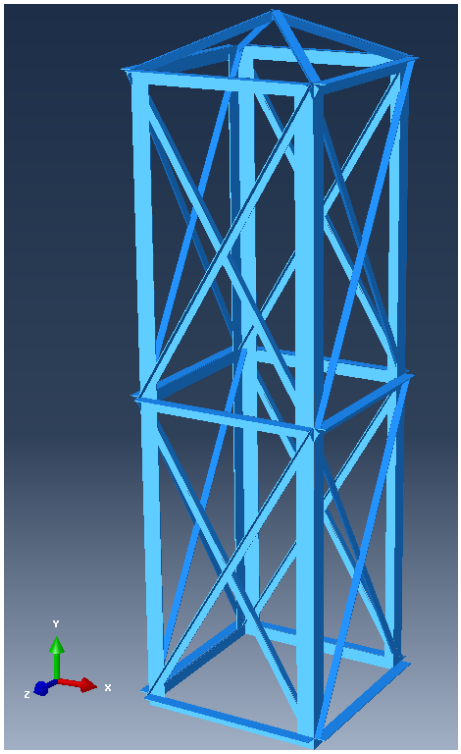

Figure 4.11: 3D numerical model of the test structure

The ABAQUS analysis consisted of a geometric and material nonlinear dynamic analysis for which two analysis steps were defined i.e. a static step and a dynamic step. The static step was defined first. In the static step, the gravity load was applied to the entire model. In the dynamic step, the ground acceleration was applied at the base of all four columns of the model as a boundary condition. The ground acceleration time history was entered as an amplitude in tabulated form. The boundary conditions of the model were initially defined as pinned in all three degrees of freedom. In the dynamic step, translational boundary conditions which were initially defined were released in the direction of excitation (i.e. the direction in which the ground acceleration was

Stellenbosch University https://scholar.sun.ac.za

applied) in order to allow the model to move at the required displacement. Moreover, the damping coefficient β was entered into the analysis software in the Rayleigh damping format. The damping coefficient β was related to Rayleigh mass damping coefficient γ_o and stiffness damping coefficient γ_1 by equation 4.1 (SIMULIA, 2012). ω was the fundamental natural frequency of the test structure.

$$\beta = \frac{\gamma_o}{2\omega} + \frac{\gamma_1 \omega}{2} \tag{4.1}$$

During analysis, the reaction forces, base displacement, and top displacements at the apex of two columns were selected as output. The base shear force was obtained by using the square root sum of squares (SRSS) of all reaction forces in the direction of the applied ground acceleration. In this analysis, the ground acceleration was applied is the x-direction. The latter direction was chosen arbitrarily because the geometry of the test structure is the same in both the x and y directions. The top displacement of the model was obtained from the difference between the average of the top displacements of two columns and the base displacement. The results of the numerical analysis at different damping factors are presented in Table 4.3.

Table 4.3: Numerical analysis results for test structure

Damping factor β [%]	γ_o	γ_1	Maximum displacement [mm]	Maximum base shear force [N]
1.0	0.0	4.53E-05	0.177	990
1.5	0.0	6.79E-05	0.175	981
2.0	0.0	9.06E-05	0.174	972
2.5	0.0	1.13E-04	0.171	965
3.0	0.0	1.36E-04	0.171	958
3.5	0.0	1.59E-04	0.170	951
4.0	0.0	1.81E-04	0.169	946

Comparison of the numerical results to the laboratory results showed that the latter are the same as the numerical results at a damping factor of 3%. The numerical results at a damping factor of 3% are 0.17mm displacement and 958N base shear force. In the laboratory analysis, a maximum displacement of 0.17mm and a maximum base shear force of 960N were obtained as shown in section 4.1.1(4). The small difference in the base shear force may come from the additional weight

Stellenbosch University https://scholar.sun.ac.za

of elements which were connected to the test structure but were not considered in the numerical analysis. Such elements include the footplates, bolts, the plates which were connecting the frame elements together, and the rod bolts used for tying the lead weights at top of the test structure. Therefore, in the summary of the results (section 4.1.4) the damping coefficient of the test structure was taken as 3% and the numerical analysis results are 0.17mm displacement and 958N base shear force. This damping coefficient is in good range of the damping values specified by Chopra (1995) for steel structures.

4.1.3 Analysis of test structure by the code design approach

The code design approach is a seismic design method by which the natural period of the structure is first determined for the purpose of getting the total base shear force of the structure. Once the natural period is obtained, the seismic design acceleration is then determined from the response spectrum of the applicable code. The total base shear force is given by the product of the seismic mass and the design acceleration. The total base shear force obtained is then multiplied by a correction factor, the value of which depends on the characteristics of the structure.

Using the code design approach (CDA), the total base shear force induced on the test structure from the ground acceleration used during both experimental and numerical analyses was evaluated. It was calculated firstly by determining experimentally the stiffness of the test structure. The natural period of the test structure was then calculated. Once the natural period of the test structure was obtained, the total base shear force was calculated with consideration of the requirements of European standard EN 1998-1: 2004 (EC8-1, 2004). For the calculation of this base shear force SANS 10160-4 would also be used, but since is not applicable in the analysis of the case study, EN 1998-1:2004 was adapted herein. The calculation procedures are as follows.

Stellenbosch University https://scholar.sun.ac.za

A. Determination of the lateral stiffness of the test structure

Figure 4.12 shows the test structure horizontally fixed as a cantilever beam.

Figure 4.12: Test structure horizontally fixed

The structure was statically loaded by monotonically increasing the point load applied at the tips of the columns (see Figure 4.13). The load was generated by the Instron machine at the rate of 1mm displacement per one minute.

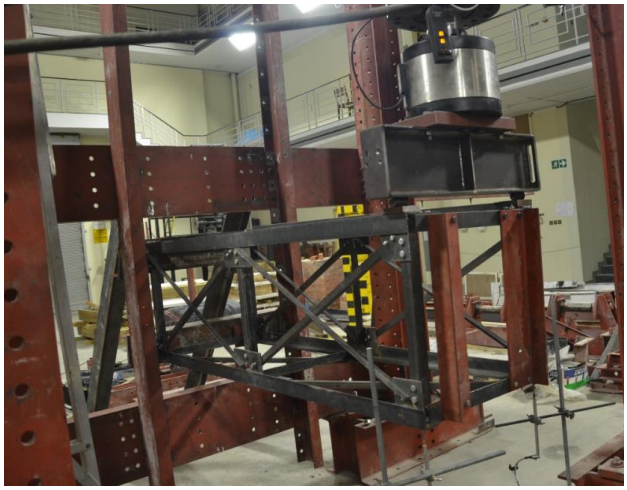

Figure 4.13: Test structure loaded at tip

Figure 4.14 shows the connection between the test structure and the rigid support beam. Each of the four foot-plates of the test structure was bolted to the rigid support beam by a 16mm high yield bolt.

Stellenbosch University https://scholar.sun.ac.za

Figure 4.14: Typical connection of test structure to the rigid support beam

The induced displacement due to the applied load was measured by LVDTs. The latter were connected to the tip of the columns at the opposite side of the applied load (Figure 4.15). The resultant displacement of the structure was taken as an average displacement of the two LVDTs.

Figure 4.15:Displacement measurement setup for test structure

The force displacement relationship curve of the test structure is shown in Figure 4.16. From this figure, the static secant stiffness of 339.2kN/m was derived.

Stellenbosch University https://scholar.sun.ac.za

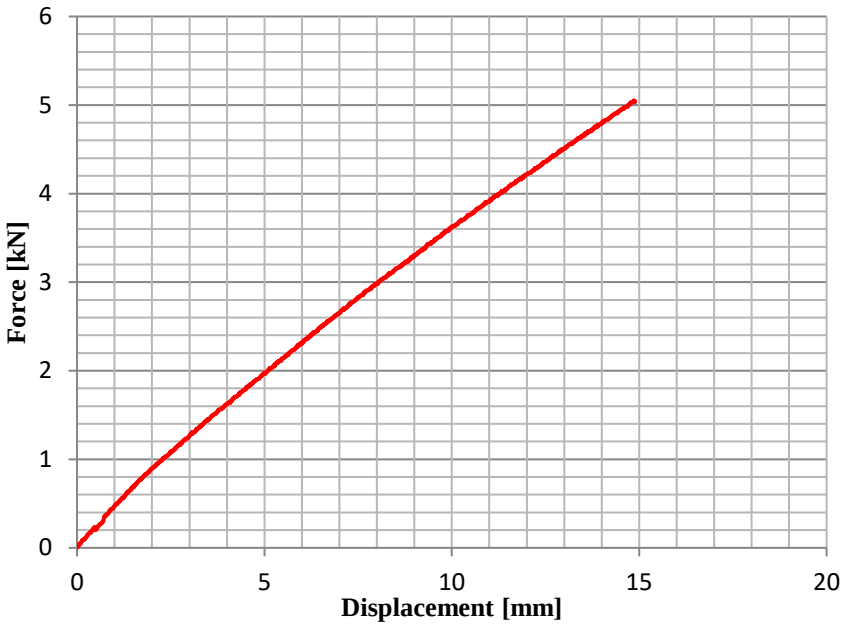

Figure 4.16: Force displacement relationship curve of the test structure

B. Determination of the natural period of the test structure

Once the static stiffness K of the test structure was obtained, its natural period T was calculated by equation 4.2. The mass of 880 kg used represents the total mass of the test structure i.e. the total mass of the experimental assembly plus the mass of the test structure itself. The resultant natural period T was 0.32s.

$$T = \frac{2\pi}{\sqrt{K/m}} \tag{4.2}$$

C. Determination of the total base shear force

The total base shear force was calculated based on Eurocode 8 (EN 1998-1:2004). The values obtained for different types of soil are tabulated in Table 4.4.

Stellenbosch University https://scholar.sun.ac.za

Table 4.4: Base shear force for the test structure

Ground Type	Damping factor (%)	Damping correction factor	T(s)	Mass [kg]	a_g[g]	S_e[g]	Base Shear force [N]
A	3.0	1.12	0.32	880	0.1	0.28	2194
B						0.34	2632
C						0.32	2523
D						0.38	2961
E						0.39	3071

Once the shear wave velocity (V_s) of the ground acceleration used for this analysis had been determined (Table 4.2), reference was made to table 3.1 of Eurocode 8 (EN 1998-1:2004) to determine the ground type. For this analysis, the shear wave velocity corresponded to ground type B. Therefore, from the above Table 4.4, the base shear force resulting from code design analysis is 2632N.

4.1.4 Summary and discussion of results

A summary of the results is presented in Table 4.5, the numerical analysis revealed a 3% damping coefficient and the results of code design approach are for ground type B. As can be seen in Table 4.5 the base shear value computed using the code approach is very conservative and much higher than the measured value. In addition, during numerical analysis of the water tower under investigation, the damping ratio of the tower β will be taken 3%, based on the results of both the laboratory and numerical analysis.

Table 4.5: Analysis results of the test structure

	Laboratory analysis	Numerical analysis	Code design analysis
Displacement [mm]	0.17	0.17	--
Base shear force [kN]	960	958	2632

Stellenbosch University https://scholar.sun.ac.za

4.2 Seismic assessment of the water tower

As addressed in section 3.1, the seismic assessment of the Engen Winelands 1-Stop water tower was done firstly by considering the foundation of the tower as a rigid foundation supported on the undeformable soil medium. This was referred to as the fixed base condition. Later on, the fixity of the base foundation was modified in order to incorporate the flexibility of the underlying soil to apply SSI analysis. This was referred to as the flexible base condition. Moreover, with reference to appendix **A**, the geometry of the columns supporting the water tower implies that the tower is better able to resist force from the x-direction than the y-direction. Because the columns are I-shaped, the column is sturdier when force is applied in the direction running from the top of the "I" to the bottom, rather than across the "I". The direction running across the "I" will be referred to as the weak direction of the water tower. Therefore, this study assessed the tower in its weak direction with respect to the geometry of the columns. Thus, the next section contains the assessment steps as well as the assessment results for both the fixed and the flexible base conditions.

4.2.1 Investigation of the behaviour of the tower for the fixed base condition

4.2.1.1 Development of the analysis model

1. Dynamic characteristics of the water tank

Various methods of dynamic modelling of water tanks have been discussed in section 2.2. They vary in terms of the mechanical characteristics of the tank. The water tank of the tower under investigation is made of a combination of steel plates, which allows it to be classified as a flexible container. The method used for this model was for a flexible container as has been discussed in section 3.2.1. Based on sections 3.2.1and 3.4.1.1, the dynamic characteristics of the water container were evaluated and are given in Table 4.6. As was mentioned in section 3.2.1, the values shown in the latter table are computed based on an equivalent circular tank of 2.3m in height and 7.1m in diameter.

Stellenbosch University https://scholar.sun.ac.za

Table 4.6: Dynamic characteristics of water tank

Total mass of water m_l [kg]	90,792
Impulse mass m_i [kg]	37,588
Convective mass m_c [kg]	53,204
Natural period of impulse mass T_i [sec]	0.004
Natural period of convective mass T_c [sec]	0.849
Stiffness of impulse mass K_i [N/m]	95,312,128,407
Stiffness of convective mass K_c[N/m]	291,2697
Height of impulse mass h_i [m]	0.9
Height of convective mass h_c [m]	1.3

2. Modelling of the water tower

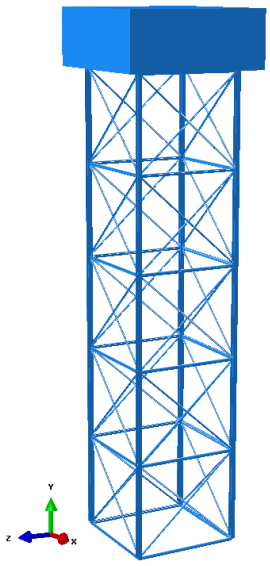

Figure 4.17: Fixed base model

Figure 4.17 shows a 3D numerical model of the water tower. The steel frame elements (columns and bracings) have been modelled as beam elements and the water container as shell elements. The connections between the frame elements were defined as pin joints and the connection of the tank to the steel frame was defined as a fixed connection. The sections were defined with the mechanical properties of steel: density ρ =7850kg/m^3, Young modulus E=200GPa and Poisson ratio ν =0.3.

Stellenbosch University https://scholar.sun.ac.za

The profiles were created based on the profiles of the steel frame at site (see Table 3.7). Based on Table 3.8, the yield stress-strain of 300MPa and 0.2% were considered as the yield point in the definition of the nonlinearity of the materials. Moreover, as the stress distribution throughout the water container is outside the scope of this study, the water container was considered as a rigid shell element in the analysis process, but it is crucial to remember that the equivalent dynamic properties of contained water were evaluated under consideration of its normal flexible state. The damping factor (β) of 3% was assigned to the materials in the Rayleigh damping format as stated by equation 4.1. This damping factor was experimentally determined as shown in section 4.1. The dynamic characteristics of the water tank shown in Table 4.6 were assigned to the analysis model as shown in Figure 4.18.

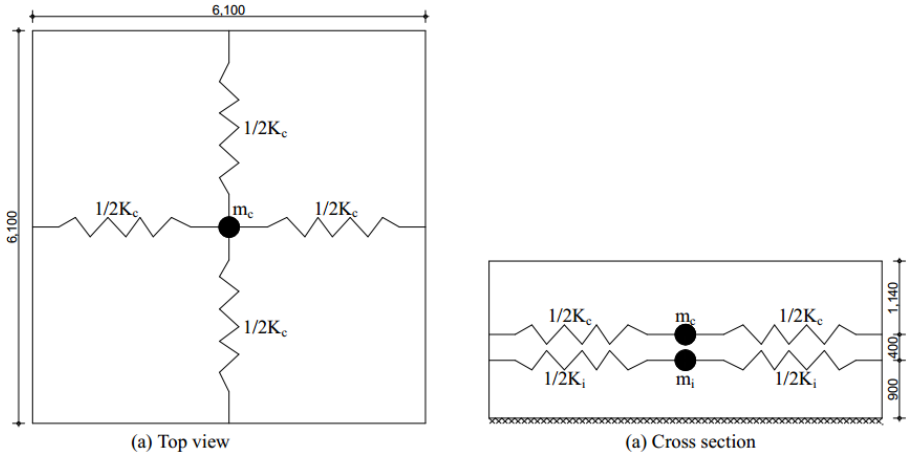

Figure 4.18: Allocation of dynamics characteristics into analysis model

4.2.1.2 Estimation of the seismic demand of the tower

A. Nonlinear dynamic approach (NLDA)

The nonlinear dynamic approach consists of a numerical analysis with consideration of the nonlinearity of the geometry and materials. This analysis was conducted by using ABAQUS Finite element software (SIMULIA, 2012) in which the analysis steps were defined, the gravity load applied, and the ground acceleration time history entered and applied, as was mentioned in section 4.1.2. The selected ground acceleration for this study was mentioned earlier in section 3.4.3.2. The boundary condition of the model was initially defined as pinned in all three degrees of freedom. In the dynamic step, the initial boundary condition was further defined as released in the direction

Stellenbosch University https://scholar.sun.ac.za

of excitation in order to facilitate the model to move at the input ground acceleration. The direction of excitation here refers to the direction in which the ground acceleration was applied and corresponds to the weak direction of the tower.

During the analysis process, the reaction forces, base displacement, and top displacements at the apex of two columns were selected as outputs. The base shear force was obtained by the square root of sum of squares (SRSS) of all reaction forces in the direction of the applied ground acceleration. The displacement result was obtained from the difference between the average top displacement measured at the apex of the two columns and the base displacement. The results of numerical analysis are presented in Table 4.7. The result of the displacement time history is shown in the Figure 4.19.

Table 4.7: NLDA results for perfectly fixed base condition

Displacement [mm]	39.84
Base shear force [kN]	158.59
Natural period [s]	0.73

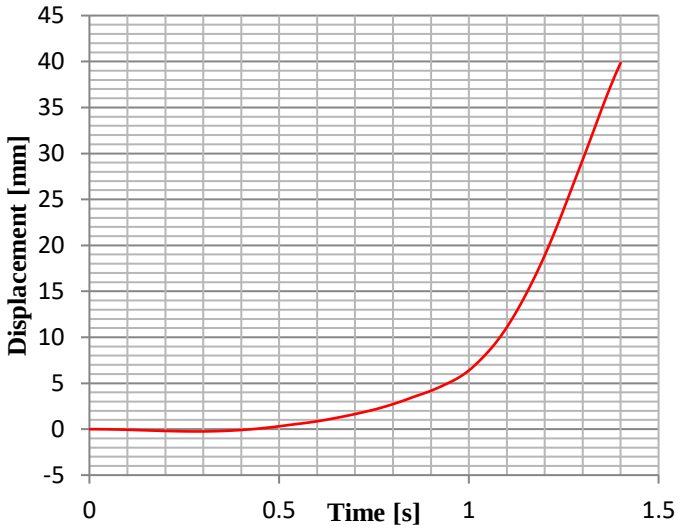

Figure 4.19: Displacement time history for perfectly fixed base condition

From the above displacement time history graph, it could be inferred that, during the time history analysis, the water tower collapsed (i.e. yielding of bracing elements) before the applied ground acceleration ended.

Stellenbosch University https://scholar.sun.ac.za

It collapsed at 1.4s, which corresponds to a ground acceleration of 0.0024g (red point in the Figure 4.20). The maximum ground acceleration in the interval of 0 to 1.4s was 0.023g.

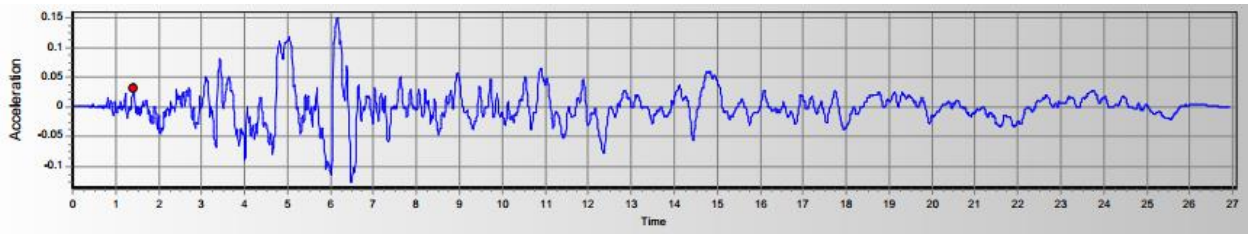

Figure 4.20: Collapse point of the water tower

B. Code design approach (CDA)

The CDA procedure is not discussed here and the reader is referred to the discussion on CDA in section 3.2.3(B).

i. Water tank characteristics

The description of the water tower under assessment was presented in section 3.4.1.1, the cross section of the water container is a square of 6.1x6.1m. The height and the thickness of the container are set to 2.44m and 3mm. The calculations of each mass component is shown below (Table 4.8). The density of water was taken as 1000kg/m^3 and that of steel as 7850kg/m^3.

Table 4.8: Mass components of the water tower

Component	Calculations	Mass (kg)
Total mass of the water, m_l	6.1x6.1x2.44x1000	90792.00
The mass of the tank walls, m_w	6.1x2.44x0.003x4x7850	1402.10
The mass of the tank roof and base, m_{rb}	6.1x6.1x0.003x7850x2	1752.59
The mass of the steel frame, m_f	------	6239.80

ii. Model properties

The equivalent circular tank dimension has a radius (r) of 3.55m and a height (H) of 2.3m.

- For H/r=0.7, C_i=6.97 and C_c=1.60 (table 3.1), the natural period of the convective mass T_{con} given by equation 3.2 is

$$T_{con} = 1.60 * \sqrt{3.55}$$
$$= 3.0\text{s}$$

Stellenbosch University https://scholar.sun.ac.za

- For H/r=0.7, m_i/m_l=*0.414* and m_c/m_l=0.586 (table 3.1); m_i=37588kg and m_c=53204kg.

With K=4185kN/m, $m_s=m_w+ m_{rb}+1/3m_f$ =5234.62kg, and equation 3.1920, the impulse period T_{imp} is

$$T_{imp} = 2\pi\sqrt{\frac{37588+5234.62}{4185000}} = 0.64s$$

iii. Seismic response

The seismic base shear force V induced at the base of the elevated water tank is given by equation 3.19. From EN1998-1 (2004), the damping ratios for the impulse mass and convective mass given in section 3.2.3(B) were corrected by applying a damping correction factor η, evaluated as follows:

$$\eta = \sqrt{10/(5+\beta)} \geq 0.55 \qquad (4.3)$$

where β is the damping ratio of the considered mass. Therefore, the damping correction factor for the impulse mass η_i and convective mass η_c had a value of 1.2 and 1.35 respectively.

For soil type C (section 3.4.2 of EN1998-1: 2004), the equations 3.4 and 3.5 of EN1998-1 (2004) give $S_e(T_{imp})$=0.49g and $S_e(T_{con})$=0.08g.

Hence, the base shear force obtained from equation 3.19 is

V =(37588+5234.62) x (0.49x9.81) + (53204x0.08x9.81) =247.6kN. Here, 5234.62kg represents the total mass of the empty tank plus one third of steel frame mass (m_s). To account for reliability differentiation, the code requires an increase of the seismic actions by a factor γ_I, where the factor γ_I is related to the importance of structure as stated in section 2.1.4(8) of EN 1998-4 (2006). From that section, the importance of the water tower is Class IV, which gives a value of the factor γ_I equal to 1.2. Hence, the design base shear force is 1.2*V which is equal to 297.10kN.

By comparing this result with that obtained from the previous section (section 4.2.1.2 A), it can be seen that the base shear force given by code design approach (297.10kN) exceeds far that given by nonlinear dynamic approach (158.90kN). The parameters which can be attributed to this difference in magnitude of the base shear force are: the analysis considerations of code design approach (e.g. consideration of peak ground acceleration) and failure point of the analysis model in nonlinear dynamic analysis. The analysis model of the water tower failed before the peak ground

Stellenbosch University https://scholar.sun.ac.za

acceleration of the applied earthquake was achieved, which means that the base shear force given by nonlinear dynamic approach represents the seismic capacity of the tower and the base shear force given by code design approach represents the seismic demand of the tower.

4.2.1.3 Estimation of seismic capacity of the water tower

In section 2.4.2.3, it was shown that the modal pushover approach is the most reliable method among currently available pushover approaches for seismic assessment of structures. However, for a single degree of freedom, the modal pushover approach reduces to N2 method or capacity spectrum method (CSM) depending on yield acceleration (Themelis, 2008). N2 method was selected in this section due to its simplicity.

Pushover approach (POA)

The nonlinear static analysis of the water tower was performed on the analysis model discussed in section 4.2.1.1 by applying a static load increasing monotonically at the centre of the masses calculated based on a weighted average of the three mass types (i.e. the impulse and convective masses as well as the empty tank mass) as shown the Figure 4.21. For this calculation of the centre of the mass of the tower; a mass representing one third of the weight of steel frame lumped at the bottom of the tank would also be considered, but since its influence was found small; the impulse, convective and empty tank masses were only ones considered. The static solutions were determined using the ABAQUS finite element software. The static load was assigned to the weak direction of the model through the dynamic implicit Quasi-static step. The POA results are described below.

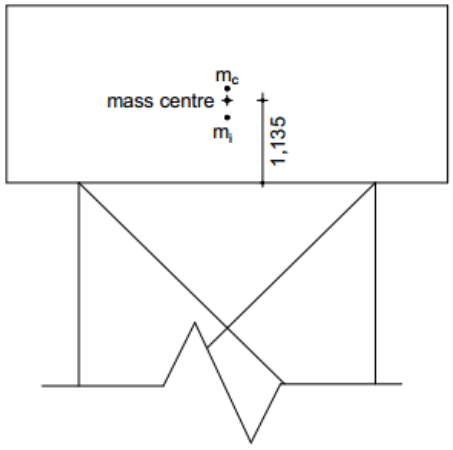

Figure 4.21: Top mass centre of the water tower

Stellenbosch University https://scholar.sun.ac.za

Figure 4.22 represents the nonlinear static analysis results (i.e. capacity curve) of the tower which is the base shear force-top displacement relationship. The top displacement was measured at the apex of the two columns of the steel frame located on the same side and in the direction of the applied load. The average value of the two displacements measured are presented.

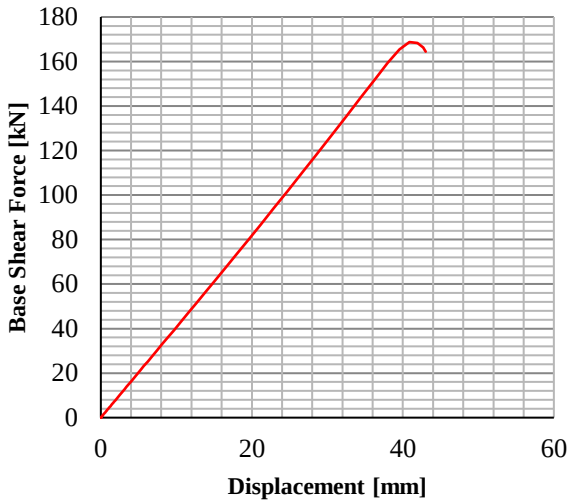

Figure 4.22: Base shear force-top displacement relationship (capacity curve)

The bilinearised capacity curve is shown in the Figure 4.23. The yield force and yield displacement are164.45kN and 39.30mm. Using this curve and equation 2.39, the elastic stiffness K^* of the tower is equal to 4185kN/m. As the mass of the tower is equal to 97066.65kg, the equation 2.38 gives an elastic period of the tower equal to 0.96s.

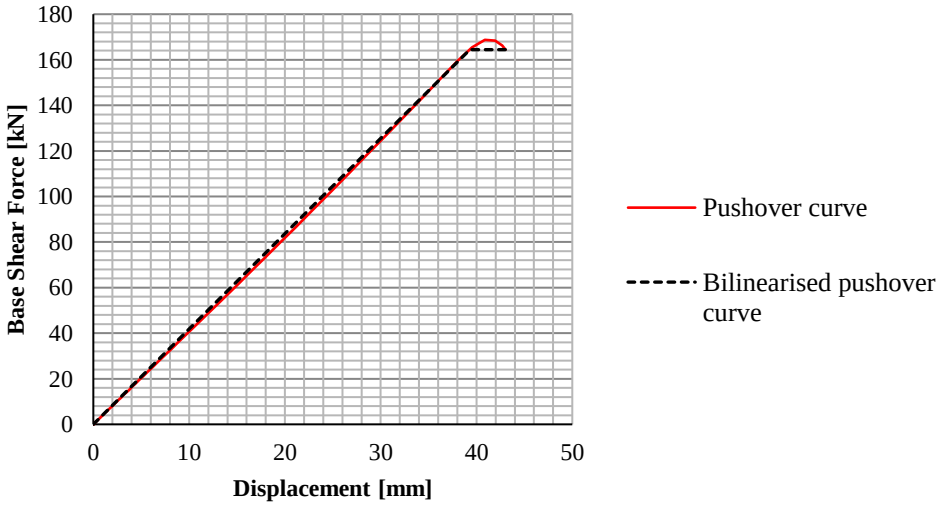

Figure 4.23: Bilinearised capacity curve

Stellenbosch University https://scholar.sun.ac.za

The capacity spectrum of the tower is shown in Figure 4.24. It was obtained by dividing the forces by the mass of the tower. The yield acceleration is equal to 0.17g.

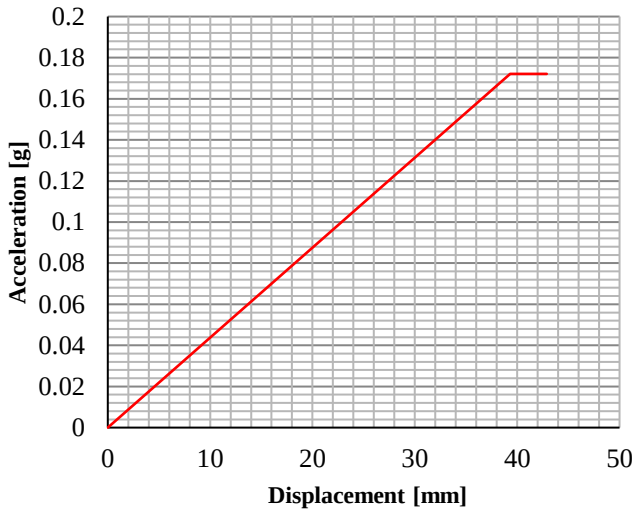

Figure 4.24: Capacity spectrum of the tower

The capacity spectrum and elastic seismic demand spectrum are combined in Figure 4.25. The elastic seismic demand spectrum was developed by using SeismoSpect software (SEiSMOSOFT, 2016) with the ground acceleration used for this study (section 3.4.3.2) as input. The calculation procedures of SeismoSpect are available from Chopra (2007), but they are also summarised in Appendix B of this thesis.

The resultant elastic acceleration S_{ae} and elastic displacement S_{de} are obtained from the intersection point of the elastic seismic demand spectrum and the line corresponding to the elastic period of the tower (T=0.96s). The values of $S_{ae} = 0.22g$ and $S_{de} = 42\,\text{mm}$ were obtained.

The reduction factor $R_{\mu} = S_{ae}/S_{ay} = 0.22g/0.17g = 1.3$ (equation 2.57). The period of the tower is greater than $T_c = 0.6s$; therefore; with equations 2.58 and 2.59, the ductility factor μ and the seismic inelastic displacement demand S_a are 1.3 and 42mm respectively.

Thereafter, the results of the pushover approach are summarized as follows:

Maximum allowable base shear force=164.45kN

Maximum allowable top displacement=42mm

Stellenbosch University https://scholar.sun.ac.za

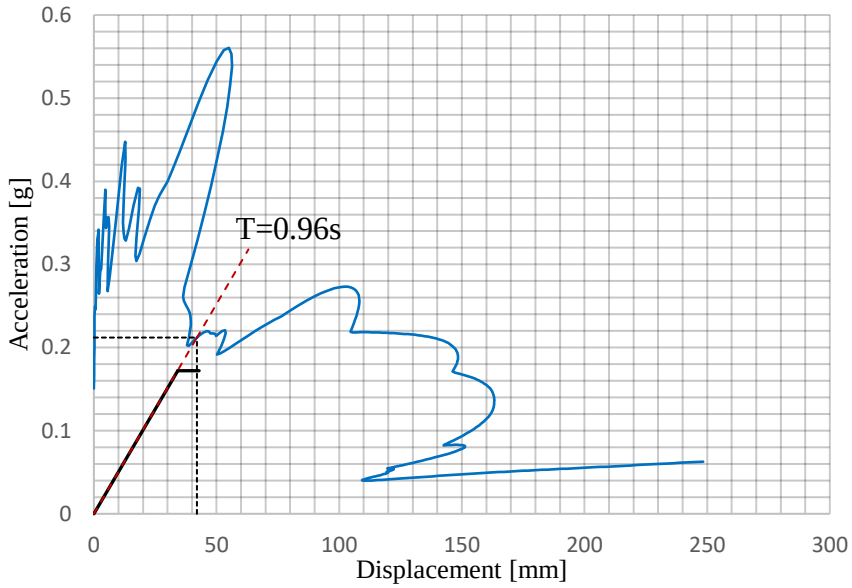

Figure 4.25: Combined capacity spectrum and seismic elastic demand

4.2.2 Investigation of the tower by consideration of flexible base condition

4.2.2.1 Development of the analysis model

The foundation base condition used in the general analysis model discussed in section 4.2.1.1 was subsequently on modified for the purpose of including the flexibility of the soil i.e. soil springs and dashpots. This section presents the characteristics of the flexible foundation (i.e. soil springs and dashpots values) as well as their assignment to the base of the tower, and a review of the new analysis model.

A. Development of the flexible foundation

1. Foundation characteristics of the tower

As mentioned in section 3.4.1.2, the analysis of the structure with consideration of the soil structure interaction is more conservative for a surface foundation than an embedded foundation. Hence, in the next section the foundation of the tower was taken to be a surface foundation. Because no detail drawings of the foundation were available, the dimensions of the foundation were estimated based on the gravity load of the tower (982.83kN) and the bearing capacity of the soil site available from Jeffares and Green Consulting Engineers (2008). It was obtained by dividing the gravity load by the bearing capacity of the soil. Thus, the dimension of the foundation was taken to be as massless

Stellenbosch University https://scholar.sun.ac.za

square mat foundation of 6.5x6.5 meters. The choice of mat foundation was based on the spacing of the columns of the tower, which is not sufficient to ensure that the stress bulbs underneath the pad foundation do not overlap at a certain depth. Therefore, since the stress bulbs overlap, the pad foundations behave as if they were a mat foundation.

2. Foundation springs and dashpots

The appropriate approach for calculating the foundation springs and dashpots of the tower was discussed in chapter 3. The calculation expressions of those foundation springs and dashpots are shown in Table 3.3 to Table 3.6 of the aforementioned chapter.

i. Shear waves velocity V_s

As stated in Table 3.9, the shear waves velocity of the site under consideration ranges from 180 to 360m/s. The shear waves velocity selected for this assessment is one corresponding to the used ground motion, which is equal to 242.05m/s (see section 3.4.3.2).

ii. Fundamental natural period of the tower *T*

The modal analysis of the tower was carried out and the results showed that the fundamental period of the tower T =0.73s. As was stated early in section 4.2.1.2; the selected mode shape corresponds to the weak direction of the tower. Moreover, the mass of the water was replaced by the equivalent impulse and convective masses as shown in Figure 4.18 and the analysis model was pinned at the base (see section 4.2.1.1).

iii. Structure-to-soil stiffness ratio $h/(V_sT)$

The ratio $h/(V_sT)$ for the water tower being assessed is 0.12 which is slightly greater than 0.1. This implies that the SSI influences the response of the tower (see summary of section 2.3.2.1). The height h was taken to be the height of the tower from base to the centre of the top mass (see Figure 4.21) and is equal to 21.135m. As the ratio $h/(V_sT)$ is close to 0.1, the effect of soil structure interaction might not be significant.

iv. Stiffness and dashpot coefficient calculation

The calculated stiffness and damping coefficient for the foundation of the water tower are given in Table 4.10. The shear modulus G_0 of the soil was calculated based on equation 2.7, but it was later modified with a modification ratio of $G/G_0 = 0.6825$(EN 1998-5, 2004) in order to consider

Stellenbosch University https://scholar.sun.ac.za

the effect of large strain. The frequency dependent parameter a_o was also calculated, as was stated underneath Table 3.4, with the natural frequency ω equal to the frequency of the flexibly supported water tower obtained from equation 2.23. Moreover, the dashpot coefficient was evaluated based on equation 3.3. The soil hysteretic damping β_s was taken as 0.03825 (EN 1998-5, 2004). Additional input parameters are shown in Table 4.9.

Table 4.9: Input parameters for stiffness and dashpot calculation

Poisson's ratio		0.25
Soil density [kN/m^3]		18.45
Soil mass density [kg/m3]		1880.73
Shear waves velocity V_s [m/s]		242.05
Shear modulus at small strain G_o [MPa]		110.19
Soil factor S (EN 1998-1:2004)		1.15
Maximum peak ground acceleration [g]		0.15
Earthquake Magnitude		6.30
G/G_o (EN 1998-5:2005)		0.68
Shear modulus at large strain G [MPa]		75.20
Foundation dimensions	Half-width B	3.25
	Half-length L	3.25
Water tower stiffness [N/m]		4185000
Natural period T of the tower (pinned base) [s]		0.73
Height h of the tower (mass centre) [m]		21.135
Natural period $\widetilde{T}$ of the tower (flexible base) [s]		1.07
Natural frequency $\widetilde{\omega}$ of the tower (flexible base) [s]		5.88
Coefficient Ψ		1.73

Stellenbosch University https://scholar.sun.ac.za

Table 4.10 : Foundation stiffness and damping values for the Engen 1-stop water tower

Degree of freedom	**G [MPa]**	**K_{static} [N/m]**	**a_o**	**α**	**$K_{dynamic}$ [N/m]**	**β_{fr}**	**Dashpot factor *C* (N-sec/m)**
Horizontal x-direction	75.204	1284911844	0.0790	1	1284911844	0.120	69217277.6
Horizontal y-direction	75.204	1284911844	0.0790	1	1284911844	0.120	69217277.6
Vertical Z-direction	75.204	1531652162	0.0790	0.9996	1531079197	0.175	110788746.7
Rocking about x-direction	75.204	13768575287	0.0790	0.9983	13745027136	0.000	179850295.1
Rocking about y-direction	75.204	13768575287	0.0790	0.9983	13745027136	0.000	179850295.1

Stellenbosch University https://scholar.sun.ac.za

v. Assignment of dynamic springs and dashpots to the foundation

Vertical springs and dashpots

The vertical stiffness and dashpot were assigned to the foundation as shown in Figure 4.26.The corresponding spring and dashpot intensities calculated by equations 3.13 and 3.14 are shown in Table 4.11. The edge stiffness intensity was adjusted in order to correct the underestimation of the rotation of the foundation i.e. it was increased in both directions by a factor R_k=2.89 which is an average value between allowable limits of the foundation length ratio, see section 3.2.2 (2). The latter was obtained by equations 3.15 and 3.16 with the length ratio R_e=0.4. The dashpot intensity was also decreased by a factor R_c=0.18 (equations 3.17 and 3.18) for the purpose of decreasing overestimated edge damping. The corner intensities were obtained by averaging both the x and y-directions intensities. In the analysis model, the stiffness and dashpot were assigned to each node and their values were calculated based on the stiffness and dashpot intensities as well as the area attributed to each node. The nodes are spaced at 1.3m.

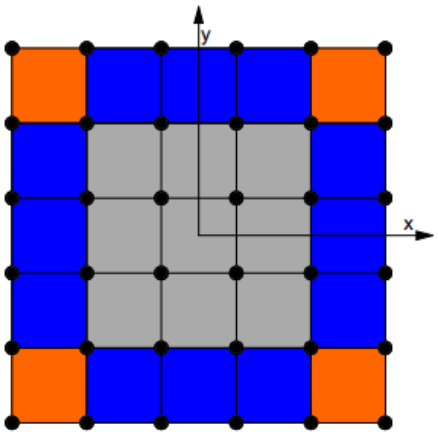

Figure 4.26: Assignment of vertical springs and dashpots to the footprint of foundation

Table 4.11: Soil foundation stiffness and dashpot intensities

Zone	k_z^i (kNm/m^3)	c_z^i (kN-sec/m^3)
	36239	2622
	107992	1411
	107992	1411

Stellenbosch University https://scholar.sun.ac.za

Horizontal springs and dashpots

The dynamic stiffness and the dashpot coefficient of 107076kN/m and 5768kN-sec/m were assigned to each perimeter node of the foundation. These were obtained by dividing the total dynamic stiffness and dashpot coefficient of Table 4.10 by the total number of the nodes in each direction, i.e. 12 nodes. The final values of soil springs and dashpots were assigned to the foundation as shown in Figure 4.27. This figure presents only the distribution of the springs, but the dashpots were also allocated to the foundation in the same way as the springs and their corresponding values are tabulated in the mentioned figure.

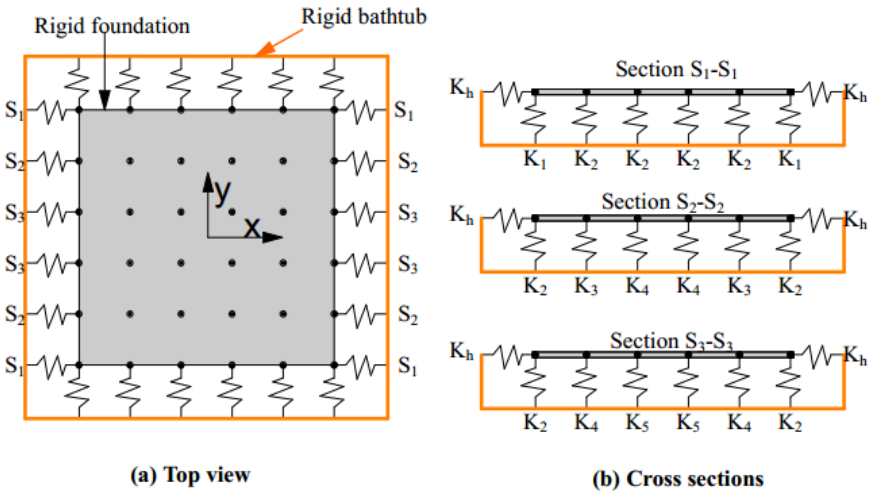

(a) Top view (b) Cross sections

K_i/C_i	kN/m	kN-sec/m
K_h/C_h	107076	5768
K_1/C_1	45627	596
K_2/C_2	91253	1192
K_3/C_3	152191	3492
K_4/C_4	121875	4601
K_5/C_5	61244	6817

Figure 4.27: Assignment of springs and dashpots to the base of the water tower

Stellenbosch University https://scholar.sun.ac.za

B. Numerical analysis model

The analysis model of the tank with water is shown in Figure 4.28. It represents the model discussed in section 4.2.1.1, which was modified by assigning the soil springs and dashpot values to its base as calculated in the previous section as shown in Figure 4.27.

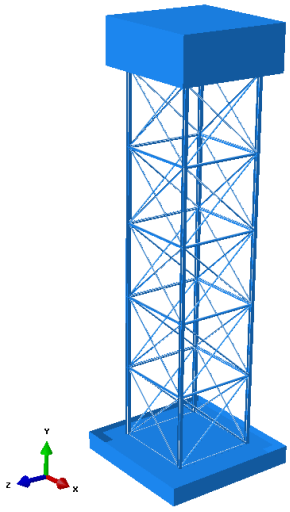

Figure 4.28: Numerical analysis model for flexible base condition

4.2.2.2 Estimation of the seismic demand

A. Nonlinear dynamic approach

The analysis was carried out in the same way as in section 4.2.1.2 (A), with the ground acceleration applied at the rigid bathtub. The Table 4.12 shows the numerical results of a nonlinear dynamic analysis of a flexibly supported water tower. The top displacement time history is also shown in Figure 4.29. The analysis model collapsed (i.e. yielding of bracing elements) at the same point of the applied ground acceleration as in the nonlinear dynamic analysis of the perfectly fixed base condition (see Figure 4.20).

Table 4.12: NLDA results for flexible base condition

Displacement [mm]	43.89
Base shear force [kN]	156.12
Natural period [s]	0.78

Stellenbosch University https://scholar.sun.ac.za

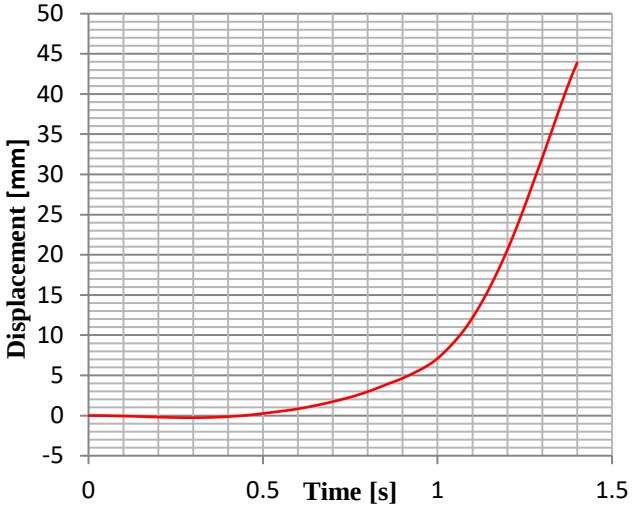

Figure 4.29: Top displacement time history

B. Code design approach

This section is the same as section 4.2.1.2 (B) except that the reduction in stiffness of the structural steel system due to the flexibility of the soil increased the natural period of the impulse mass. The new stiffness *K* determined from section 4.2.2.3 is equal to 3696kN/m. With reference to equation 3.19, the new natural period of impulse mass was calculated as:

$$T_{imp} = 2\pi\sqrt{\frac{37588+5234.62}{3696000}} = 0.68s$$

Therefore, the new impulse spectral acceleration $S_e(T_{imp})$ is equal to 0.46g. Hence, the new base shear force is V =(37588+5234.62) * (0.46*9.81) + (53204*0.08*9.81) =235.00kN. Other parameters were previously determined. With the reliability differentiation factor of 1.2 (section 4.2.1.2 (B)), the design base shear force becomes 1.2*V=282kN. Therefore, the ultimate base shear force which can be obtained from code design analysis of the flexibly supported water tower is 282kN.

Stellenbosch University https://scholar.sun.ac.za

4.2.2.3 Estimation of seismic capacity of the tower

Pushover approach

The soil reactions assigned to the nonlinear dynamic model in section 4.2.2.1 are dynamic springs and dashpots. In the pushover analysis, only the static springs should be considered (ATC, 2005). As could be seen from Table 4.10, the dynamic modifiers from static springs to dynamic springs are all close to one. For engineering purposes, this means that the static and dynamic springs could be considered to be the same. For this reason, the nonlinear dynamic model was taken as the pushover analysis model, except that in the latter model, the dashpots were removed. The pushover approach was conducted and performed in the same way as in section 4.2.1.3 (0) and the subsequent results are presented in the section below.

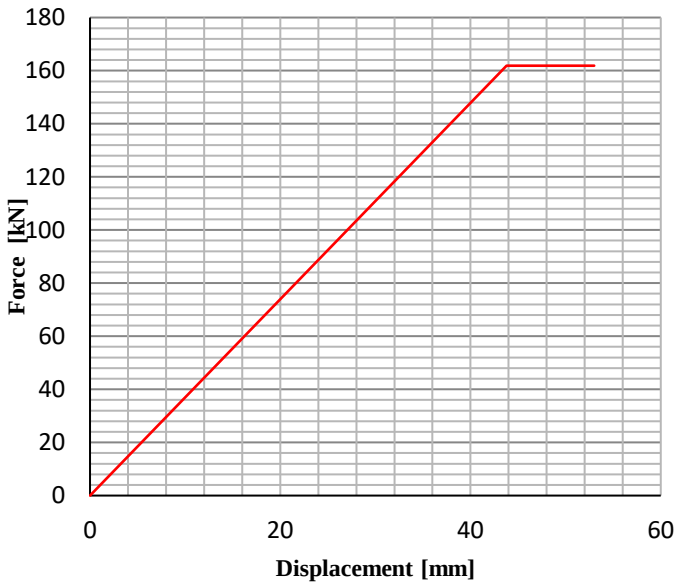

Figure 4.30: Bilinearized capacity curve

Figure 4.30 shows a bilinearized capacity curve of the tower flexibly supported at the foundation base. The yield force and yield displacement are161.87kN and 43.8mm. Equation 2.39 gives an elastic stiffness K^* of the tower equal to 3696kN/m. Along with equation 2.38, the elastic period of the tower was found equal to 1.02s.

Stellenbosch University https://scholar.sun.ac.za

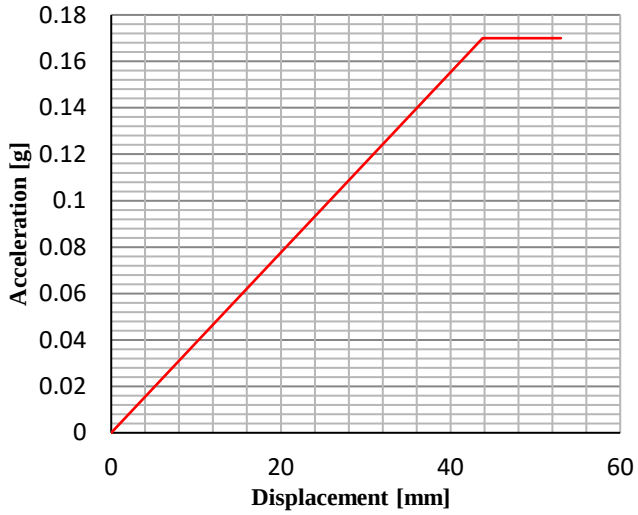

Figure 4.31: Capacity spectrum of the tower

From the capacity spectrum shown in Figure 4.31, the yield acceleration is equal to 0.17g.

The capacity spectrum and elastic seismic demand spectrum are combined in Figure 4.32.The resultant elastic acceleration S_{ae} and elastic displacement S_{de} are obtained from the intersection point of the elastic seismic demand spectrum and the line corresponding to the elastic period of the tower (T=1.02s). The values of $S_{ae}=0.20g$ and $S_{de}=52mm$ were obtained.

The reduction factor $R_{\mu} = S_{ae}/S_{ay} = 0.20g/0.17g = 1.2$ (equation 2.57). The period of the tower is greater than $T_c=0.6s$; therefore with equations 2.58 and 2.59, the ductility factor μ and the seismic inelastic displacement demand S_a are 1.2 and 52mm respectively.

Thereafter, the results of the pushover analysis are summarized as follows:

Maximum allowable base shear force = 161.87kN

Maximum allowable top displacement = 52mm

Stellenbosch University https://scholar.sun.ac.za

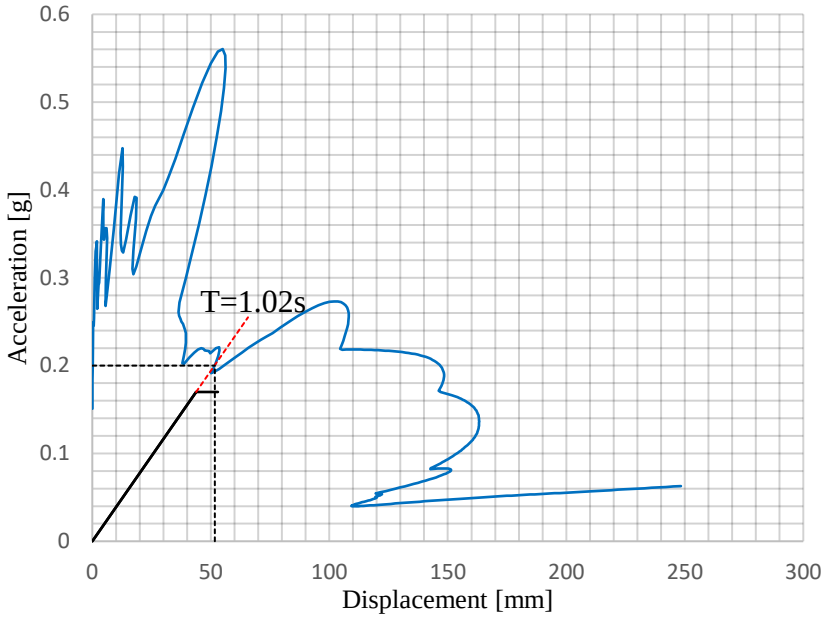

Figure 4.32: Combined capacity spectrum and seismic elastic demand

4.3 Stability of the water tower

4.3.1 Local stability

Local stability refers to the buckling and yield of internal elements of the steel frame of the tower. It was taken into consideration in all analyses done previously in the whole of section 4.2, excluding subsections 4.2.1.2(B) and 4.2.2.2(B), by including the nonlinearity of the geometry and materials into the analysis models. The presented results in that section included the local stability of the water tower. This was also mentioned early in section 4.2.1.1.

4.3.2 Global stability

The global stability of the tower against overturning was checked at the base connection of the columns to the foundation level. As was stated in section 3.4.1.1 and Figure 3.8, the columns of the water tower are connected to the foundation by bolts 22mm in diameter. The global stability was verified by checking whether the bolts would be able to hold down the tower against the overturning inertia moment generated at the top mass of the tower. The evaluation procedures are shown in the next section.

Stellenbosch University https://scholar.sun.ac.za

4.3.2.1 Global stability requirement

With reference to SAISC (2012), equation 4.4 should be verified for a bolt subjected to the combination of the ultimate shear force V_u and ultimate tension force T_u.

$$\frac{V_u}{V_r}+\frac{T_u}{T_r}\leq 1.4 \tag{4.4}$$

V_r and T_r are the shear and tension capacities of the bolt.

From table 3.7 of SAISC (2012) $V_r = 44.3\,\text{kN}$ and $T_r = 79.2\,\text{kN}$ for one single bolt. With reference to Figure 4.33, the ultimate tension force T_u, which could be obtained at the base of the tower, is given by equation 4.5. It was obtained by evaluating the overturning moment at the point B.

$$T_u = \frac{Vh}{S} \qquad \textit{per two columns} \tag{4.5}$$

where h is the height of the tower from the base to the mass centre (h=21.135m), and S is the spacing of the columns which is equal to 4.5m (appendix A). The substitution of the equation 4.5 into equation 4.4 gives equation 4.6, which is the ultimate base shear force which could be transmitted to the base of the columns before the bolts connecting the columns to the base fail.

$$V \leq 1.4\left[\frac{1}{V_r}+\frac{h}{ST_r}\right]^{-1} \tag{4.6}$$

One column is pinned at the base by four bolts of 22mm diameter. For one tension side there are two columns which gives a total of eight bolts. The base shear force is shared by four base connections which also gives a total of sixteen bolts. Therefore, the total shear and tension resistances for all bolts, eight bolts to resist tension and sixteen bolts to resist shear, are V_r=708.80kN and T_r=633.60kN. The substitution of the latter values into equation 4.6 gives the ultimate shear force V=152.66kN. Thus, the base shear force required to maintain the global stability of the water tower should not exceed 152.66kN.

Stellenbosch University https://scholar.sun.ac.za

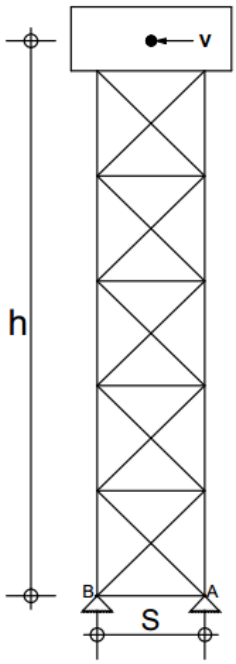

Figure 4.33: Tension force induced by the base shear *V* at point A

Stellenbosch University https://scholar.sun.ac.za

Chapter 5
Results summary and discussions

5.1 Summary of the results

The aim of this thesis was to study and document techniques to assess the dynamic structural performance of typical water tower structures and apply this to investigate whether the Engen 1-Stop water tower would be able to withstand an earthquake of a magnitude appropriate to its site location. In overview, the seismic assessment was conducted by estimating the seismic demand and seismic capacity of the structure and comparing both these results. The state of the structure under dynamic seismic loading is assessed by comparing whether the base shear force of the seismic demand is greater than the base shear force of the seismic capacity. A greater seismic demand relative to the seismic capacity implies a high probability that the structure will fail during seismic activity; a greater seismic capacity relative to seismic demand implies that the structure is less likely to fail and will be able to resist the earthquake.

Three approaches were used for achieving the objectives of the study: the nonlinear dynamic approach (NLDA), the code design approach (CDA) and the pushover approach (POA). The NLDA and CDA were used for estimating the seismic demand of the tower, and the POA was used for evaluating the seismic capacity of the water tower. Two boundary conditions were considered: one in which the water tower was flexibly supported at ground level and one in which the water tower was perfectly fixed at ground level. The former was referred to as the flexible base condition and the latter as the perfectly fixed base condition. The flexible base condition was analysed by considering the soil structure interaction (SSI). Consequently, there is no SSI for the perfectly fixed base condition. The analysis steps and the results for each approach were presented in chapter four. In addition, the global stability requirement (GSR) of the tower was checked and the resultant seismic demand from the GSR was also presented.

Chapter 4 concluded that, during the NLDA for both perfectly and flexibly fixed base conditions, the analysis models of the water tower failed before the applied earthquake ended. In both cases, the tower failed after 1.4s, whereas the ground acceleration used has a time duration of 27s (see Figure 4.20). This implies that the water tower cannot withstand an earthquake of a magnitude expected at its site location. Consequently, the NLDA results represent the seismic capacity of the

Stellenbosch University https://scholar.sun.ac.za

tower and not the seismic demand under the seismic activity of the location of the water tower. The seismic demand is therefore only given by CDA. Since the tower failed in both models and the NLDA represents the seismic capacity of the structure, the results between the NLDA and the POA should be similar because the POA also represents the seismic capacity of the structure. It is important to remember that the principle of the POA is to apply a constantly increasing static load until the failure point of the structure is achieved. Based on these results, the seismic capacity is evaluated. The summary of results is presented in Table 5.1 and a discussion of the results in follows section 5.2.

Stellenbosch University https://scholar.sun.ac.za

Table 5.1: Analysis results summary

	Fixed base condition				Flexible base condition			
	Seismic capacity			Seismic demand	Seismic capacity			Seismic demand
	POA	NLDA	GSR	CDA	POA	NLDA	GSR	CDA
Displacement [mm]	42.00	39.84	--	--	52.00	43.89	--	--
Base shear force [kN]	164.45	158.59	152.66	297.10	161.87	156.12	152.66	282.00
Natural period [s]	0.96	0.73	--	--	1.02	0.78	--	--

Stellenbosch University https://scholar.sun.ac.za

5.2 Discussions

5.2.1 Seismic capacity of the tower

The POA was carried out on the water tower structure to determine the capacity of the tower under seismic loading in addition to the GSR, which also gave values for the base shear force capacity of the water tower. However, the values from the NLDA also represent the base shear force capacity of the tower since the water tower failed during the analysis. Since both the POA and NLDA gave values for the seismic capacity of the tower, the values were expected to be the similar. From Table 5.1 it can be seen that the values are indeed similar, with the POA giving a base shear force capacity of 164.45 kN compared to the 158.59 kN provided by the NLDA. The small difference in these values could be attributed to the inertia force and the effect of sloshing that was considered in the NLDA, but ignored in the POA. In conclusion, the controlling base shear force which represents the capacity of the water tower structure model is the minimum from among the POA, NLDA and GSR. From the results in Table 5.1, it can be seen that the GSR provided the lowest value at 152.66 kN.

5.2.2 Seismic demand of the tower

At the start of this study, the seismic demand of the tower was expected to be given by the NLDA as well as the CDA. However, during the NLDA, the maximum resistance of the tower was achieved, which implied that the NLDA results represented the seismic capacity of the tower instead. Therefore, the seismic demand was only given by the CDA. From Table 5.1 it is shown that the seismic demand for the structure for the perfectly fixed and flexible base conditions is 297.1 and 282 kN, respectively.

5.2.3 The soil structure interaction effect

For the purpose of assessing the effect of Soil Structure Interaction (SSI) on the seismic response of the tower, Table 5.2 was developed from the results of the Non-Linear Dynamic Analysis (NLDA) presented in Table 5.1. The effect of the SSI on the CDA results was also evaluated and is equal to -5.1%, i.e. the base shear force in the perfectly fixed base condition was 5.1% less that the base shear force obtained when SSI was considered.

Stellenbosch University https://scholar.sun.ac.za

Table 5.2: Increase/decrease from fixed to flexible base conditions

	Perfectly fixed base condition	Flexible base condition	Percentage increase/decrease
Displacement	39.84 mm	43.89 mm	9.2
Base shear force	158.59 kN	156.12 kN	-1.6
Natural period	0.73 s	0.78 s	6.4

From the above results, it could be concluded that the effects of SSI did not significantly influence the response of the tower. This corresponds to the predicted result in section 4.2.2.1(2)iii, since the calculated ratio $h/(V_sT)$ was close to 0.1.

Stellenbosch University https://scholar.sun.ac.za

Chapter 6
Conclusion and recommendation

6.1 General conclusion

Elevated water tanks are classified as important structures. There are different reasons for this classification, such as the importance of water tanks in lifeline and industrial area, the vulnerability of elevated tanks to horizontal lateral loads and the negative consequences associated with the failure of the water supply system. In the past, the value of the lateral seismic load which could be induced on a particular elevated water tank was estimated based on the static approach, which was carried out by taking the mass of the structure as the total mass of the tank filled by water.

The report on the catastrophic failure of water tanks during the Chilean earthquake of May, 1960 (Steinbrugge & Flores, 1963) caused uncertainty about the accuracy of this approach. Subsequently, much research on seismic behaviour of water tanks has been conducted. As a result, it has been shown that the static approach does not represent the realistic response of water tanks to a given earthquake excitation. Housner's (1963) research was among the first to show that the static approach is reliable only for the case in which the water tank is full of water, which is not practically useful as water tanks are rarely kept full. For a rigid wall tank full of water with a freeboard, it has been shown that the seismic excitation of water tanks is best represented if one understands the mass of the tank as made up of two components, the impulsive mass and the convective mass.

The impulsive mass represents the portion of the water tank which responds as a solid mass attached to the bottom of the tank. The convective mass represents the portion of the water which contributes to the sloshing of the surface water during a given excitation. The seismic responses of these masses are obtained based on standard structural dynamic procedures, and their natural periods should be separated so that the seismic response of each mass can be modelled separately, each with its respective stiffness. The total seismic response of the tank is then obtained by the combination (e.g. absolute sum) of each mass's response. This analysis concept is known as "dynamic analysis" and correlates to laboratory results (Sonobe & Nishikawa, 1969). Dynamic analysis gives a lower base shear force and higher hydrodynamic pressure on the wall of the tank when compared to the static approach (Gaikwad & Mangulkar, 2013).

Stellenbosch University https://scholar.sun.ac.za

Later on, Haroun & Housner (1981) found that the flexibility of the walls of the tank influences the response of the impulse mass. Consequently, Malhotra *et al*. (2000) updated Housner's analytical equations in order to consider the flexibility of the wall of the tank. At present, the dynamic analysis for water tanks has been adopted in various design codes and standards (e.g. EN 1998-4, 2006, Priestley *et al.*, 1986). However, standards such as SANS 10160-4:2011 have not yet been implemented in any design provisions for water tanks.

Another factor which contributes to the seismic response of the structure is the mechanical properties of the soil. The literature showed that when a structure is analysed with consideration of the soil properties of the medium under the foundation, the resultant seismic base shear force is reduced and the resultant internal forces are increased compared to that obtained from the same structure analysed with a perfectly fixed foundation. These changes are attributed to the Soil Structure Interaction (SSI) effect. Three forms of SSI occur when the seismic waves strike the foundation of the structure. The first is associated with the difference between the foundation input motion and the free field ground motion, which is caused by the dissimilarity between the mechanic properties of the foundation unit and the soil. This dissimilarity causes reflection and refraction of the incident seismic waves at the soil-foundation interface back to the soil medium, and the resultant foundation input motion is reduced compared to the free field ground motion. This mechanism is known as kinematic interaction and its effect is small enough so that it can be practically ignored (Kramer & Stewart, 2004:4-34).

The second form of SSI occurs when the structure starts oscillating as a result of the inertial force generated over the height of the superstructure, which in turn induces the shear force and overturning moment at the foundation base resulting in translation and rotation of the foundation. The translation and rotation of the foundation induce the deformation of the soil and radiate energy into the soil medium. The radiated energy dissipates part of the incoming seismic waves, and, as a result, the incoming seismic waves are reduced. This mechanism is considered to be an additional source of energy dissipation to the inherent damping of the system. In addition, the rotation of the foundation base induces excessive lateral displacement on the superstructure compared to the displacement estimated based on a perfectly fixed foundation, which results in lengthening of the fundamental natural period of the structure. All mechanisms associated with the modification of the damping and lengthening of the fundamental natural period of the system are referred to as

Stellenbosch University https://scholar.sun.ac.za

inertia interaction. The inertia interaction has been implemented into design codes and standards (e.g. ASCE, 2014; ATC,2005) by modifying the fundamental natural period and the damping coefficient of the structure calculated based on the fixed foundation. However, the displacement based approach has been critiqued on the basis that during the evaluation of the internal forces, it does not take into account the effect of the lateral displacement induced by the rotation of the foundation on the superstructure, which was proven to increase the internal forces in the superstructure elements. Therefore, updated codes and standards containing the design considerations for the evaluation of the internal forces with consideration of this lateral displacement are needed.

The third form of SSI is associated with the flexibility of the foundation unit. Iguchi and Luco (1982) have demonstrated that the flexibility of the foundation decreases the damping value of the system compared to a rigid foundation. For low frequencies of excitation, the effective stiffness of the system is lower than that obtained with consideration of a rigid foundation, and higher for high frequencies of excitation. However, the literature shows that there are no analytical equations for design of the structures with consideration of the foundation flexibility.

The concern of this research was to illustrate a numerical method for seismic design and performance assessment of steel framed water tower structures which could take into account all of the aforementioned factors influencing the seismic response. This method was applied to investigate a particular case study, the Engen 1-Stop water tower. A review of relevant publications for achieving these objectives were presented in chapter 2, and the numerical method developed in this study was described in section 3.2. In addition, the general characteristics of the water tower were also discussed in section 3.4 and an explanation of the application of the method to the assessment of the tower was given in section 4.2.

From sections 4.1 and 4.2, the first step before assessment of the mentioned structure was to validate the analysis model. This was done by building in a laboratory a steel frame structure, which was referred to as the test structure. The test structure had the same characteristics as the steel frame of the tower, scaled down by a factor of 12. Once the test structure was built, it was then subjected to a simulation of ground acceleration in the laboratory and in ABAQUS finite element software. The analysis model for the water tower was calibrated by comparing both the numerical and laboratory results of the test structure. Furthermore, this analysis model was

Stellenbosch University https://scholar.sun.ac.za

modified in order to conform to the boundary conditions used to implement SSI in the assessment process.

The seismic performance assessment of the tower was conducted by evaluating and comparing the seismic capacity of the tower to its seismic demand. The seismic performance of the tower was determined by whether or not demand exceeded capacity. If not, this implies that the structure is less likely to fail under a given ground motion. If demand exceeds capacity, however, the structure has a higher probability of failure during an earthquake. To achieve this, following approach was followed: the developed numerical method and the code design approach. The developed numerical method in this section refers to the documented method which considers all the discussed analysis considerations (i.e. the sloshing of the surface water, the SSI, etc.) for the seismic design of the water tower. The latter method consisted of the nonlinear dynamic and static analyses in which the soil medium characteristics were included into the analysis models through springs and dashpots. The code design approach is a response spectrum analysis which was performed based on the design provisions of EN 1998-4:2006.

The seismic demand was given by the nonlinear dynamic analysis and the code design analysis while the seismic capacity was obtained from the static pseudo-dynamic analysis (pushover analysis). The code design analysis was considered for the purpose of checking its accuracy in estimating the base shear force induced on the structure. It is important to remember that the current design codes and standards do not consider the effect of the flexibility of the foundation on the response of the structure, nor the influence of the lateral displacement on the internal forces induced in the superstructure. Two boundary conditions were considered: the water tower perfectly fixed at the base of the foundation and the water tower flexibly supported at the ground level. The latter was used in order to be able to include the properties of the soil medium on which the tower is supported into the analysis process, i.e. the SSI analysis. The former was considered in order to illustrate the effect of the SSI on the base shear force imposed on the tower. Additionally, the seismic capacity of the tower against overturning was checked.

With reference to sections 5.1 and 5.2, the results showed that during the nonlinear dynamic analysis for both perfectly fixed and flexibly supported base conditions, the analysis models of the water tower failed before the applied ground acceleration time history ended. This implied that the water tower on the site is not able to survive under the seismic activity expected for its site location.

Stellenbosch University https://scholar.sun.ac.za

Consequently, the resultant nonlinear dynamic results represented the seismic capacity instead of the expected seismic demand on the tower. Therefore, the seismic capacity was given by both the nonlinear dynamic analysis and pushover analysis while the seismic demand was only given by the code design approach. Subsequently, the accuracy of the code design analysis on the base shear force was not identified. This is due to the fact that, since the code design analysis (i.e. the response spectrum analysis) peaks only at the maximum value for a given ground acceleration and the nonlinear dynamic analysis models failed before that point, it was not reasonable to compare both results.

Moreover, the nonlinear dynamic and pushover analyses results were expecting to be the same because the maximum capacity of the tower was achieved during both analyses. The small difference in results can be attributed to the inertia force and sloshing effect which are basically not considered in the pushover analysis. By comparing the seismic capacity results given by both methods (the nonlinear dynamic and pushover analyses) against the global stability requirement, it was concluded that the global stability requirement controlled the seismic capacity. In other words, the seismic capacity of the water tower was considered as that given by the global stability requirement of the tower, as it gave the lowest value.

Therefore, the seismic demand and seismic capacity of the tower were taken as the values given by the code design analysis and global stability requirement, respectively. The comparison of these results causes serious uncertainty over whether the Engen 1-Stop water tower could withstand any seismic hazard. The effect of Soil Structure Interaction (SSI) on the response of the tower was interpreted by comparing the nonlinear dynamic results of the perfectly fixed and flexible base conditions. From these results, it was shown that the effect of SSI was not significant. The reason attributed to these observations are the system parameters, as the ratio $h/(V_sT)$ was close to 0.1.

As a final point, the Engen 1-Stop water tower would not be able to survive during seismic activity, therefore, retrofitting of the structure is required in order to ensure the safety of the tower. In addition, the computed effect of Soil Structure Interaction on the dynamic response of the structure appeared insignificant, but this does preclude further investigation, especially for the purpose of assessing the stress distribution throughout the steel frame elements, because the induced additional lateral displacement from SSI increases the internal forces.

Stellenbosch University https://scholar.sun.ac.za

6.2 Recommendations

- **Considered assumptions and analysis data**

  During the study, a number of assumptions were made, as presented in Chapter 1. Some of the data used was obtained from literature, as discussed in Chapter 3. For a more accurate analysis, further on-site investigation should be conducted to obtain specific data for the existing water tower. This could be achieved by evaluating the shear waves velocity of the soil at the site as well as the foundation characteristics of the tower. Although the member sizes and structure dimensions of the model are the same as the existing structure, the structural integrity of the two may differ. The existing water tower has been there for a number of years, whereas the water tower analysis model is made up of new elements. In order to consider the stiffness degradation of the steel frame which results from rusting and the weathering of elements on site, further study should introduce the imperfections of the elements into the analysis process.

- **Design seismic response**

  The earthquake ground motions used in this study were selected based on the soil characteristics of the site and the expected earthquake magnitude. These were considered as preliminary factors for the investigation of the tower. Factors such as the source mechanisms of the earthquakes, the epicenter distances relative to the site location of the water tower and the epicenter distances with respect to the recording station of the ground motions should be taken into account for better results. With reference to NEHRP Consultants Joint Venture (2011), this can be achieved by considering and grouping at least six different appropriate ground accelerations into three groups. The ground accelerations of each group should be scaled so that their average value, the square root sum of the squares, does not drop below 1.3 times the associated ordinate of the design response spectrum assigned to the site location of the structure for the periods in the range of $0.2T$ to $1.5T$. Here, T defines the fundamental natural period of the structure in the direction of interest. Next, if the analyses will be performed with consideration of more than seven ground accelerations, the seismic response of the structure will be obtained from an analysis giving the maximum values. In the other way around, the seismic response will be given by the average value of all analyses.

Stellenbosch University https://scholar.sun.ac.za

- **Seismic assessment methods**

  The literature showed that current pushover approaches were developed based on building structures. Since the behaviour of building structures is dynamically different than water retaining structures, further study is needed to determine whether these pushover approaches are applicable to water retaining structures. This is due to the fact that in the modelling of the water retaining structures, two mass components, solid mass and active mass, are considered because of the sloshing effect, while in building structures all masses are considered as a solid mass.

- **Soil Structure Interaction, SSI**

  More research is required in order to investigate the magnitude of the influence of foundation flexibility on the response of structures, as a review of the literature revealed little. Stewart and Tileylioglu (2007) also stated that analytical equations for the evaluation of this influence on the response of the structures are needed. It was also drawn from literature that the updated design codes and standards which are based on a "*displacement-based approach"* are required for accurate SSI analysis results. Since the presented numerical method requires high performance analysis tools, these will be helpful to design engineers who do not have access to those analysis tools.

Stellenbosch University https://scholar.sun.ac.za

References

Abrahamson, N.A., Schneider, J.F. & Stepp, J.C. 1991. Empirical Spatial Coherency Functions for Application to Soil Structure Interaction Analyses. *Earthquake Spectra*. 7(1):1–27.

Algreane, G.A.I., Osman, S.A., Karim, O.A. & Kasa, A. 2011. Behavior of Elevated Concrete Water Tank Subjected to Artificial Ground Motion. *Electronic Journal of Geotechnical Engineering*. 16:387–406.

Anastasopoulos, I., Gazetas, G., Loli, M., Apostolou, M. & Gerolymos, N. 2010. Soil failure can be used for seismic protection of structures. *Bulletin of Earthquake Engineering*. 8(2):309–326.

Apsel, R.J. & Luco, J.E. 1987. Impedance Functions for Foundations Embedded in A Layered Medium: An Integral Equation Approach. *Earthquake Engineering & Structural Dynamics*. 15(2):213–231.

Arefi, M.J. 2008. Effects of Soil-Structure Interaction on the Seismic Response of Existing R . C . Frame Buildings, Master's Thesis. Istituto Universitario di Studi Superiori di Pavia.

ASCE. 2000. *FEMA 356 Prestandard and Commentary for the Seismic Rehabilitation of Building*. Reston, Virginia: Prepared by American Society of Civil Engineers for Federal Emergency Management Agency.

ASCE. 2010. *Minimum Design Loads for Buildings and Other Structures, ASCE/SEI 7-10*. Reston, Virginia: American Society of Civil Engineers.

ASCE. 2013. *Seismic Analysis of Safety-Related Nuclear Structures and Commentary, ASCE 4-98*. Reston, Virginia: American Society of Civil Engineers.

ASCE. 2014. *Seismic Evaluation and Retrofit of Existing Buildings, ASCE/SEI 41-13*. Reston, Virginia: American Society of Civil Engineers.

ATC. 2005. *Improvement of Nonlinear Static Seismic Analysis Procedures, FEMA 440*. Redwood City, California: Prepared by the Applied Technology Council (ATC-55 Project) for the Federal Emergency Management Agency.

Stellenbosch University https://scholar.sun.ac.za

ATC-40. 1996. *ATC-40 report,Seismic Evaluation and Retrofit of Concrete Buildings*. Redwood City/ Califonia: Applied Technology Council.

Avilés, J. & Pérez-Rocha, L.E. 1996. Evaluation of Interaction Effects On the System Period and The System Damping Due to Foundation Embedment and Layer Depth. *Soil Dynamics and Earthquake Engineering*. 15(1):11–27.

Avilés, J. & Pérez-Rocha, L.E. 1998. Effects of Foundation Embedment During Building-Soil Interaction. *Earthquake Engineering and Structural Dynamics*. 27(12):1523–1540.

Avilés, J. & Pérez-Rocha, L.E. 2003. Soil-Structure Interaction in Yielding Systems. *Earthquake Engineering and Structural Dynamics*. 32(11):1749–1771.

Avilés, J. & Pérez-Rocha, L.E. 2005. Design Concepts for Yielding Structures On Flexible Foundation. *Engineering Structures*. 27(3):443–454.

Avilés, J. & Suárez, M. 2002. Effective Periods and Dampings of Building-Foundation Systems Including Seismic Wave Effects. *Engineering Structures*. 24(5):553–562.

Bardet, J. 1997. *Experimental Soil Mechanics*. Upper Saddle River, New Jersey 07458: Prentice Hall.

Beredugo, Y.O. & Novak, M. 1972. Coupled Horizontal and Rocking Vibration of Embedded Footings. *Canadian Geotechnical Journal*. 9(4):477–497.

Bielak, J. 1971. Earhquake Response of Building Foundation System. Califonia Institude of Technology.

Bielak, J. 1975. Dynamic Behaviour of Structures with Embedded Foundations. *Earthquake Engineering & Structural Dynamics*. 3(3):259–274.

Bielak, J. 1976. Modal Analysis for Building-Soil Interaction. *Journal of the Engineering Mechanics Division*. 102(5):771–786.

Birtharia, A. & Jain, S.K. 2015. Seismic Response of Elevated Water Tanks: an overview. *International Research Journal of Engineering and Technology (IRJET)*. 2(4):964–968.

Stellenbosch University https://scholar.sun.ac.za

BSSC. 2004a. *NEHRP Reccomended Provisions For Seismic Regulations for New Buildings and Other Structures, Part 1: Provisions, FEMA 450/2003 Edition*. Washington, D.C.: Prepared by the Building Seismic Safety Council for the Federal Emergency Management Agency.

BSSC. 2004b. *NEHRP Reccomended Provisions For Seismic Regulations for New Buildings and Other Structures, Part 2: Commentary, FEMA 450/2003 Edition*. Washington, D.C: Prepared by the Building Seismic Safety Council for the Federal Emergency Management Agency.

Bycroft, G.N. 1956. Forced Vibrations of a Rigid Circular Plate on a Semi-Infinite Elastic Space and on an Elastic Stratum. *Philosophical Transactions of the Royal Society A: Mathematical, Physical and Engineering Sciences*. 248(948):327–368.

Chen, J.Z. 2010. Generalized SDOF System for Dynamic Analysis of Concrete Rectangular Liquid Storage Tanks. Ryerson University.

Chopra, A.K. 2007. *Dynamics of Structures Theory and Applications to Earthquake Engineering*. Third Edit ed. Upper Saddle River, New Jersey: Prentice-Hall.

Chopra, A.K. & Goel, R.K. 2000. Evaluation of NSP to Estimate Seismic Deformation: SDF Systems. *Journal of Structural Engineering*. 126(4):482–490.

Chopra, A.K. & Goel, R.K. 2001. *A Modal Pushover Analysis Procedure for Estimating Seismic Demands for Buildings: Theory and Preliminary Evaluation*. PEER Report 2001/2003, Pacific Earthquake Engineering Research Center, College of Engineering, University of California, Berkeley.

Chopra, A.K. & Goel, R.K. 2002. A Modal Pushover Analysis Procedure for Estimating Seismic Demands for Buildings. *Earthquake Engineering and Structural Dynamics*. 31(3):561–582.

Day, S.M. 1978. *Seismic Response of Embedded Foundations. Volume 3450 of Preprint / ASCE National Convention*. (Preprint / ASCE National Convention). New York: American Society of Civil Engineers.

Dobry, R., Gazetas, G. & Stokoe, K.H. 1986. Dynamic Response of Arbitrarily Shaped Foundations. *Journal of Geotechnical Engineering*. 112(2):136–154.

Stellenbosch University https://scholar.sun.ac.za

EC8-1. 2004. *EN 1998-1: Design of structures for earthquake resistance - Part 1: General rules, seismic actions and rules for buildings*. London: British Stantard Institution.

EC8-4. 2006. *EN 1998-4: Design of Structures for Earthquake Resistance: Silos, Tanks and Pipelines*. Brussels: European Committee for Standardization.

Elsabee, F. & Morray, J.P. 1977. *Dynamic Behavior of Embedded Foundations. Issue 33 of Publication*. (Publication). Massachusetts: Massachusetts Institute of Technology, Department of Civil Engineering, Constructed Facilities Division.

EN 1998-5. 2004. *Design of structures for earthquake resistance Part 5: Foundations, retaining structures and geotechnical aspects*. Brussels: European Committee for Standardization.

Fajfar, P. 2000. A Nonlinear Analysis Method for Performance-Based Seismic Design. *Earthquake Spectra*. 16(3):573–592.

Freeman S.A., Nicoletti J.P. & Tyrell J.V. 1975. 'Evaluations of Existing Buildings for Seismic Risk - A Case Study of Puget Sound Naval Shipyard, Bremerton, Washington. *Proceedings of U.S. National Conference on Earthquake Engineering*. 113–122.

Gaikwad, M. V & Mangulkar, M.N. 2013. Comparison between Static and Dynamic Analysis of Elevated Water Tank. *International Journal of Scientific & Engineering Research*. 4(6):2043–2052.

Gazetas, G. 1991. Foundation Vibrations. In *Foundation Engineering Handbook, Second Edition*. H.-Y. Fang, Ed. New York: Chapman & Hall. 553–593.

Gazetas, G. & Tassoulas, J.L. 1987. Horizontal Stiffness of Arbitrarily Shaped Foundations. *Journal of Geotechnical Engineering*. 113(5):440–457.

Harden, C.W. & Hutchinson, T.C. 2009. Beam-on-Nonlinear-Winkler-Foundation Modeling of Shallow, Rocking-Dominated Footings. *Earthquake Spectra*. 25(2):277–300.

Haroun, M.A. & Housner, G.W. 1981. Seismic Design of Liquid Storage Tanks. *Journal of the Technical Councils of ASCE*. 107(1):191–207.

Stellenbosch University https://scholar.sun.ac.za

Haroun, M.A. & Temraz, M.K. 1992. Effects of Soil-Structure Interaction on Seismic Response of Elevated Tanks. *Soil Dynamics and Earthquake Engineering*. 11(2):73–86.

Hosseinzadeh, N. 2008. Seismic Vulnerability Analyses of Steel Storage Tanks in an Oil Refinery Complex Using Dynamic Analyses.

Housner, G.W. 1957. Dynamic Pressures on Accelerated Fluid Containers. *Bulletin of the Seismological Society of America*. 47(1):15–35.

Housner, G.W. 1963. The Dynamic Behavior of Water Tanks. *Bulletin of the Seismological Society of America*. 53(2):381–387.

Iguchi, M. & Luco, J.E. 1982. Vibration of Flexible Plate on Viscoelastic Medium. *Journal of the Engineering Mechanics Division*. 108(6):1103–1120.

Jaiswal, O.R., Rai, D.C. & Jain, S.K. 2007. Review of Seismic Codes On Liquid-Containing Tanks. *Earthquake Spectra*. 23(1):239–260.

Jarvis, W.J. 2014. The Effect of Seismic Activity on Reinforced Concrete Frame Structures with Infill Masonry Panels. Stellenbosch University.

Jeffares and Green Consulting Engineers. 2008. *Getechnical Report On Refuse Transfer Station, Winelands*. Camps Bay.

Jennings, P.C. & Bielak, J. 1973. Dynamics of building-Soil Interaction. *Bulletin of the Seismological Society of America*. 63(1):9–48.

Jones, K.C. 2013. Dynamic Soil-Structure-Interaction Analysis of Structures in Dense Urban Environments, Ph.D. Dissertation. University of Califonia, Berkely.

Kausel, E. 1974. *Forced Vibrations of Circular Foundations On Layered Media, Research Report No R74-11*. Cambridge, MA.

Kausel, E. 2010. Early History of Soil–Structure Interaction. *Soil Dynamics and Earthquake Engineering*. 30(9):822–832.

Stellenbosch University https://scholar.sun.ac.za

Kausel, E., Whitman, R. V., Morray, J.P. & Elsabee, F. 1978. The Spring Method for Embedded Foundations. *Nuclear Engineering and Design*. 48(2–3):377–392.

Kim, S. 2001. Calibration of Simple Models for Seismic Soil-Structure Interaction from Field Performance Data, Ph.D. Dissertation. University of Califonia, Los Angeles.

Kim, S. & Stewart, J.P. 2003. Kinematic Soil-Structure Interaction from Strong Motion Recordings. *Journal of Geotechnical and Geoenvironmental Engineering*. 129(4):323–335.

Kobori, T., Minai, R. & Suzuki, T. 1971. The Dynamical Ground Compliance of a Rectangular Foundation on a Viscoelastic Stratum. *Bulletin of the Disaster Prevention Research Institute*. 20(4):289–329.

Kotronis, P., Tamagnini, C. & Grange, S. 2013. *ALERT Doctoral School 2013: Soil-Structure Interaction.* Unpublished Class Notes. Germany: Technische Universitat Dresden.

Kramer, S.L. & Stewart, J.P. 2004. Geotechnical Aspects of Seismic Hazards. In *Earthquake Engineering: From Engineering Seismology to Performance-Based Engineering*. Y. Bozorgnia & V. V.Bertero, Eds. Boca Raton: CRC Press. 1–85 of chapter 4.

Lamb, H. 1904. On the Propagation of Tremors over the Surface of an Elastic Solid. *Proceedings of the Royal Society of London, Philosophical Transactions of the Royal Society*. 203:1–42.

Liou, G. & Huang, P. 1994. Effect of Flexibility on Impedance Functions for Circular Foundation. *Journal of Engineering Mechanics*. 120(7):1429–1446.

Lou, M., Wang, H., Chen, X. & Zhai, Y. 2011. Structure–Soil–Structure Interaction: Literature review. *Soil Dynamics and Earthquake Engineering*. 31(12):1724–1731.

Luco, J.E. 1980. Soil-Structure Interaction and Identification of Structural Models. In *Civil Engineering and Nuclear Power*. Knoxville, Tennessee: ASCE. 1–31.

Mahin, S.A. & Lin, J. 1983. *Construction of Inelastic Response spectra for SDOF Systems. Computer program and applications. Report No UCB/EERC-83/17,University of California, Berkeley.*

Stellenbosch University https://scholar.sun.ac.za

Malhotra, P.K., Wenk, T. & Wieland, M. 2000. Simple Procedure for Seismic Analysis of Liquid-Storage Tanks. *Structural Engineering International: Journal of the International Association for Bridge and Structural Engineering (IABSE)*. 10(3):197–201.

Mason, H.B. 2011. Seismic Performance Assessment in Dense Urban Environments, Ph.D. Dissertation. University of Califonia, Berkely.

Mehani, Youcef. 2012. Inelastic Response and Ductility Demand of Structures. *15th World Conference on Earthquake Engineering (15WCEE)*. (1991).

Mehrpouya, Siavash. 2012. Seismic Vulnerability of Cylindrical Steel Tanks Using Static and Dynamic Analysis and Fluid Wave Height Control. *15th World Conference on Earthquake Engineering (15WCEE)*.

Mita, A. & Luco, J.E. 1989a. Dynamic Response of a Square Foundation Embedded in an Elastic Half-Space. *Soil Dynamics and Earthquake Engineering*. 8(2):54–67.

Mita, A. & Luco, J.E. 1989b. Impedance Functions and Input Motions for Embedded Square Foundations. *Journal of Geotechnical Engineering*. 115(4):491–503.

Moghaddam, H. & Sangi, S. 2011. *Elephant's Foot Buckling of Cylindrical Steel Storage Tanks Subjected to Earthquake Excitation*. Semnan University, Semnan, Iran: 6th National Congress on Civil Engineering.

Moghaddasi, M., Carr, A., Cubrinovski, M., Pampanin, S. & Chase, J.G. 2012. The Effects of Soil-Foundation Interface Nonlinearity On Seismic Soil-Structure Interaction Analysis. *2012 NZSEE Conference*. (Xxx).

Mylonakis, G. & Gazetas, G. 2000. Seismic Soil-Structure Interaction: Beneficial or Detrimental? *Journal of Earthquake Engineering*. 4(3):277–301.

Mylonakis, G. & Nikolaou, A. 1997. Soil--Plie--Bridge Seismic Interaction: Kinematic and Inertial Effects. Part I: Soft Soil. *Earthquake Engineering & Structural Dynamics*. 26:337–359.

Stellenbosch University https://scholar.sun.ac.za

Mylonakis, G., Syngros, C., Gazetas, G. & Tazoh, T. 2006. The Role of Soil in The Collapse of 18 Piers of Hanshin Expressway in The Kobe Earthquake. *Earthquake Engineering and Structural Dynamics*. 35(5):547–575.

Mylonakisa, G., Nikolaoub, S. & Gazetas, G. 2006. Footings under seismic loading: Analysis and design issues with emphasis on bridge foundations. *Soil Dynamics and Earthquake Engineering*. 26(9):824–853.

Naeim, F., Tileylioglu, S., Alimoradi, A. & Stewart, J.P. 2008. Impact of foundation modeling on the accuracy of response history analysis of a tall building. *Proceedings, SMIP 2008 Seminar on Utilization of Strong Motion Data, Califonia Strong Motion Instrumentation Program, Sacramento, Califonia*. 19–56.

NEHRP Consultants Joint Venture. 2011. *Selecting and Scaling Earthquake Ground Motions for Performing Analyses, NIST GCR 11-917-15*.

NEHRP Consultants Joint Venture. 2012. *Soil-Structure Interaction for Building Structures, NIST GCR 12-917-21*. Prepared by NEHRP Consultants Joint Venture. A partnership of the Applied Technology Council and the Consortium of Universities for Research in Earthquake Engineering for U.S. Department of Commerce. National Institute of Standards and Technology. Enginee.

Newmark, N.M. & Hall, W.J. 1982. *Earthquake Spectra and Design*. Oakland, California.: Earthquake Engineering Research Institute.

Novak, M. & Sachs, K. 1973. Torsional and Coupled Vibrations of Embedded Footings. *Earthquake Engineering & Structural Dynamics*. 2(1):11–33.

Pais, A. & Kausel, E. 1988. Approximate formulas for dynamic stiffnesses of rigid foundations. *Soil Dynamics and Earthquake Engineering*. 7(4):213–227.

Parmelee, R.A. 1967. Building-Foundation Interaction Effects. *Engineering Mechanics Division*. 93(2):131–152.

Parmelee, R.A. & Wronkiewicz, J.H. 1971. Seismic Design of Soil Structure Interaction Systems. *Journal of the Structural Division*. 97(ST10):8437–2517.

Stellenbosch University https://scholar.sun.ac.za

PEER. 2010. *PEER Report No. 2010/05 Guidelines for Performance-Based Seismic Design of Tall Buildings*. University of California, Berkeley: Pacific Earthquake Engineering Research Center (PEER).

PEER. 2013. *Pacific Earthquake Engineering Research Center Ground Motion Database. [Online], available from URL:http://ngawest2.berkeley.edu*.

Priestley, M.J.N., Davidson, B.J., Honey, G.D., Hopkins, D.C., Martin, R.J., Ramsay, G., Vessey, J.. & Wood, J.H. 1986. *Seismic Design of Storage Tanks, Recommendations of a Study Group of the New Zealand National Society for Earthquake Engineering*.

Reissner, E. 1936. Stationäre, axialsymmetrische, durch eine schüttelnde Masse erregte Schwingung eines homogenen elastischen Halbraum. *Ingenieur Archiv*. VII(6):381–396.

Richart, F.E., Hall, J.R. & Woods, R.D. 1970. *Vibration of soils and foundations*. Englewood Cliffs, New Jersey: Prentice-Hall, Inc.

Riggs, H.R. & Waas, G. 1985. Influence of Foundation Flexibility On Soil-Structure Interaction. *Earthquake Engineering & Structural Dynamics*. 13(5):597–615.

Roesset, J.M. 1981. A Review of Soil-Structure Interaction. In *Soil-Structure Interaction: The Status of Current Analysis Methods and Research, Report No NUREG/CR-1780 and UCRL-53011*. J.J. Johnson, Ed. Livermore CA: Prepared by Lawrence Livermore Laboratory for Office of Nuclear Regulatory Research, Washington DC.

Roesset, J.M. 2013. Soil Structure Interaction the Early Stages. *Journal of Applied Science and Engineering*. 16(1):1–8.

SABS. 2011. *Basis of structural design and actions for buildings and industrial structures. Part 4: Seismic actions and general requirements for buildings (SANS 10160-4: 2011)*. 1.1 ed. South Africa Bureau of Standard (SABS).

SAISC. 2012. *Structural Steel Connections The Green Book*. Johannesburg: Southern African Institute of Steel Construction (SAISC).

Stellenbosch University https://scholar.sun.ac.za

SEiSMOSOFT. 2016. *SeismoSpect 2016 [Online].Available at: http://www.seismosoft.com/downloads [2016, April]*.

Shah, P.M. 1968. On The Dynamic Response of Foundation Systems. Rice University.

SIMULIA. 2012. *Abaqus Analysis User's Manual*. V. 4. SIMULIA.

Sonobe, Y. & Nishikawa, T. 1969. Study on the Earthquake Proof Design of Elevated Water tanks. *Proceedings of the 4th World Conference on Earthquake Engineering, 3(B-4), Santiago*. 11–24.

Steinbrugge, K. V. & Flores, A.R. 1963. The Chilean earthquakes of May, 1960: A structural engineering viewpoint. *Bulletin of the Seismological Society of America*. 53(2):225–307.

Stewart, J.P. 2004. *Overview of Soil-Structure Interaction Principles*. University of Califonia, Los Angels. [online]. Available:https://www.eeri.org/site/images/free_pubs/sem_Jon_Stewart.pdf [2015, April 6].

Stewart, J.P. & Tileylioglu, S. 2007. Input Ground Motions for Tall Buildings with Subterranean Levels. *Structural Design of Tall and Special Buildings*. 16(5):543–557.

Stewart, J.P., Fenves, G.L. & Seed, R.B. 1999. Seismic Soil-Structure Interaction in Buildings. I: Analytical Methods. *Journal of Geotechnical and Geoenvironmental Engineering*. 125(1):26–37.

Stewart, J.P., Seed, R.B. & Fenves, G.L. 1999. Seismic Soil-Structure Interaction in Buildings II: Empirical Findings. *Journal of Geotechnical and Geoenvironmental Engineering*. 125(1):38–48.

Stewart, J.P., Kim, S., Bielak, J., Dobry, R. & Power, M.S. 2003. Revisions to Soil-Structure Interaction Procedures in NEHRP Design Provisions. *Earthquake Spectra*. 19(3):677–696.

Sudhir, K.J. & Jaiswal, O.R. 2007. *Guidelines for Seismic Design of Liquid Storage Tanks, Report No. IITK-GSDMA-EQ08*. Kanpur: Indian Institute of Technology Kanpur.

Themelis, S. 2008. Pushover Analysis for Seismic Assessment and Design of Structures. Hariot-watt University.

Stellenbosch University https://scholar.sun.ac.za

Todorovska, M.I., Hayir, A. & Trifunac, M.D. 2001. Antiplane Response of a Dike On Flexible Embedded Foundation to Incident SH-Waves. *Soil Dynamics and Earthquake Engineering*. 21(7):593–601.

Veletsos, A.S. 1977. Dynamics Of Structure Foundation Systems. In *Structural and Geotechnical Mechanics*. W.J. Hall, Ed. Englewood Cliffs, New Jersey: Prentice-Hall, Inc. 333–361.

Veletsos, A.S. 1984. Seismic Response and Design of Liquid Storage Tanks. In *Guidelines for the Seismic Design of Oil and Gas Pipeline Systems*. New York: American Society of Civil Engineers. 255–370.

Veletsos, A.S. 1993. Design Concepts for Dynamics of Soil-Structure Interaction. In *Developments in Dynamic Soil-Structure Interaction*. P. Gülkan & R.W. Clough, Eds. The Netherlands: Springer Netherlands. 307–325.

Veletsos, A. & Meek, J. 1974. Dynamic Behaviour of Building-Foundation Systems. *Earthquake Engineering & Structural Dynamics*. 3(January):121–138.

Veletsos, A.S. & Nair, V.V.D. 1975. Seismic Interaction of Structures on Hysteretic Foundations. *Journal of the Structural Division*. 101(1):109–129.

Veletsos, A.S. & Prasad, A.M.. 1989. Seismic Interaction of Structures and Soils: Stochastic Approach. *Journal of Structural Engineering*. 115(4):935–956.

Veletsos, A.S. & Tang, Y. 1990. Soil-Structure Interaction Effects for Laterally Excited Liquid Storage Tanks. *Earthquake Engineering & Structural Dynamics*. 19(4):473–496.

Veletsos, A.S. & Vann, W.P. 1971. Response of Ground-Excited Elastoplastic Systems. *Journal of the Structural Division*. 97(4):1257–1281.

Veletsos, A.S. & Wei, Y.T. 1971. Lateral and Rocking Vibration of Footings. *ASCE Journal of Soil Mechanics and Foundations Division*. 97(SM9):1227–1248.

Veletsos, A.S. & Yang, J.Y. 1977. Earthquake Response of Liquid-Storage Tanks. In *Advances in Civil Engineering Through Engineering Mechanics*. 1–24.

Stellenbosch University https://scholar.sun.ac.za

Veletsos, a. S. & Verbic, B. 1973. Vibration of Viscoelastic Foundations. *Earthquake Engineering and Structural Dynamics*. 2(April):87–102.

Veletsos, A.S., Prasad, A.M. & Wu, W.H. 1997. Transfer Functions for Rigid Rectangular Foundations. *Earthquake Engineering and Structural Dynamics*. 26(1):5–17.

Verbic, B. & Veletsos, A. 1972. *Impulse Response Functions for Elastic Foundations. Issue 15 of Structural Research at Rice, Report, Rice University Dept. of Civil Engineering*. Houston, Texas.

Watson, G.N. 1995. *A Treatise on theTheory Of Bessel Functions*. Second Edi ed. Cambridge: Cambridge University Press.

Worku, A. 2014. Soil-structure- interaction provisions. A potential tool to consider for economical seismic design of buildings ? *Journal of South African Institution of Civil Engineering*. 56(1):54–62.

Wozniak, R.S. & Mitchell, W.W. 1978. Basis of Seismic Design Provisions for Welded Steel Oil Storage Tanks. *Advances in Storage Tank Design API, Refining 43rd Midyear Meeting*.

Stellenbosch University https://scholar.sun.ac.za

Appendices

Stellenbosch University https://scholar.sun.ac.za

Appendix A: Structural layout and dimensions of the water tower

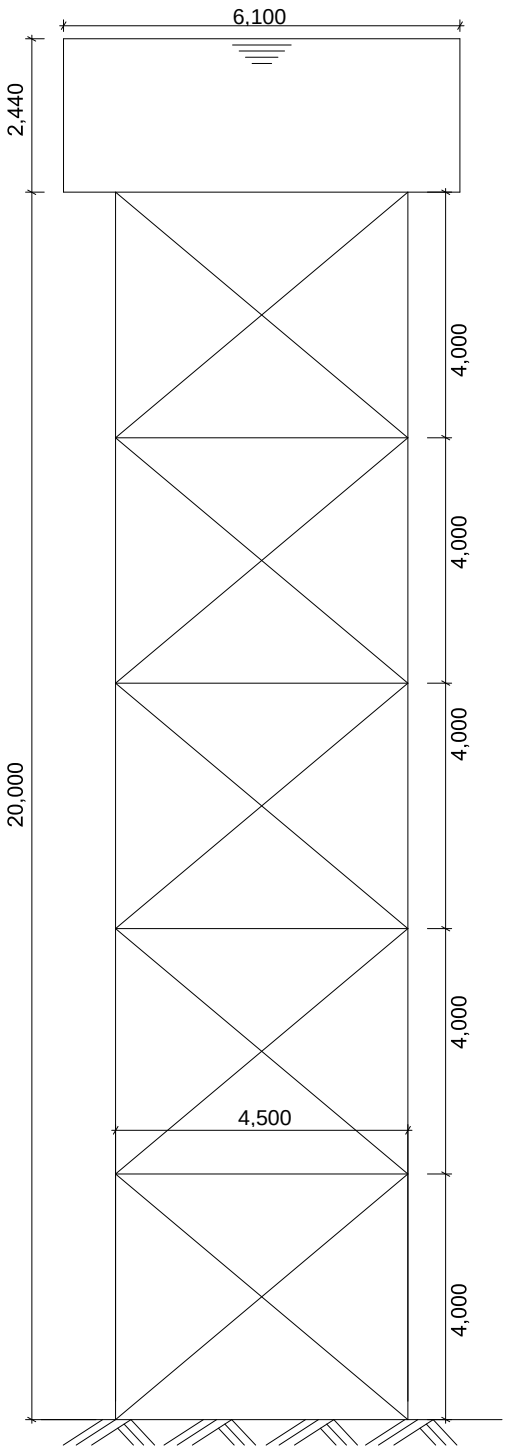

Cross section dimensions

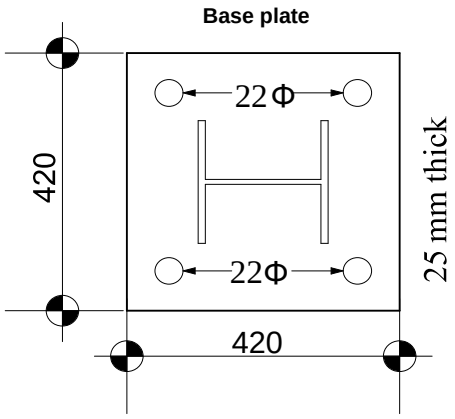

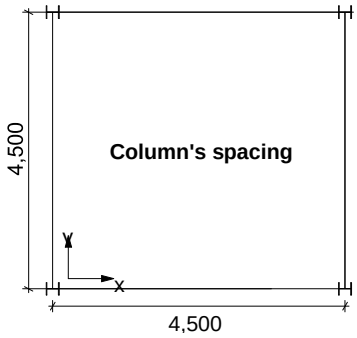

Stellenbosch University https://scholar.sun.ac.za

Appendix B: Development of the constant ductility response spectrum

1. Dynamic equation of a Single Degree of Freedom (SDOF)

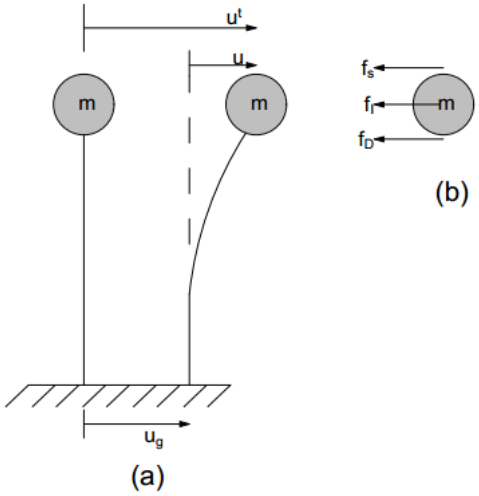

Figure B.1: (a) SDOF system excited by any given earthquake, (b) Generated forces at the mass of the system during the earthquake excitation

The forces acting on a SDOF system excited by any given earthquake are shown in Figure B.1(b). By application of Newton's second law of motion, the dynamic equation of the system is written as:

$$f_I + f_D + f_s = 0 \tag{B.1}$$

The inertia force f_I and damping force f_D are proportional to the total displacement u^t and the relative displacement u of the mass m. The total displacement u^t is the sum of the relative displacement u and ground displacement u_g induced by the earthquake at the base of the system (equation B.2). The force f_s is an elastic or inelastic resisting force depending on the applicable case.

$$u^t = u + u_g \tag{B.2}$$

For the system responding in an elastic range, the force f_s is proportional to the relative displacement of the mass m, whereas for the case of the system responding in an inelastic range it is proportional to the relative displacement u and velocity $\dot{u}$ of the mass m. Therefore, the equation B.1 is rewritten as follows:

Stellenbosch University https://scholar.sun.ac.za

$$m\ddot{u} + c\dot{u} + f_s(u,\dot{u}) = -m\ddot{u}_g \quad \text{for the inelastic response} \tag{B.3}$$

$$m\ddot{u} + c\dot{u} + ku = -m\ddot{u}_g \quad \text{for the elastic response} \tag{B.4}$$

Here c defines the viscous damping coefficient and k the static stiffness of the system.

2. Force-displacement relationship of an inelastic system

The force-displacement relationship of the elastoplastic system is shown in Figure B.2 in which f_y defines the yield force of the system.

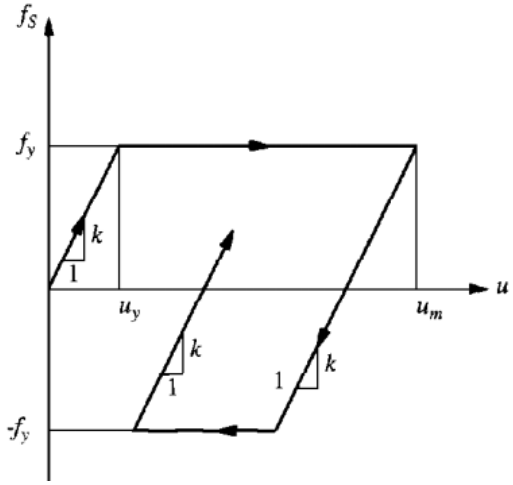

Figure B.2: Force-displacement relationship of the elastoplastic system (Chopra, 2007)

The maximum elastoplastic displacement of the system is associated to the maximum elastic displacement of the system as shown below.

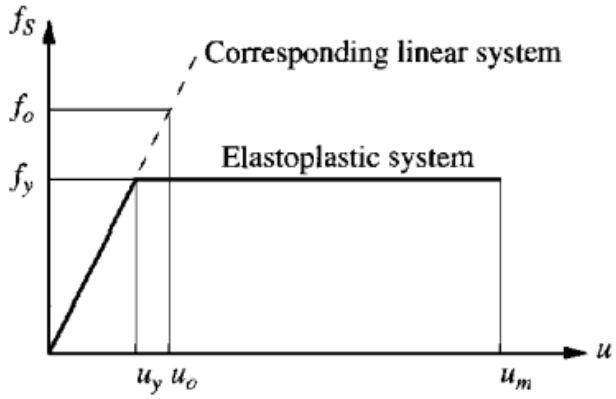

Figure B.3: Elastoplastic system and its equivalent elastic system (Chopra, 2007)

Stellenbosch University https://scholar.sun.ac.za

f_o and u_o are the maximum force and displacement induced by the earthquake on the system responding in its elastic range. In other words, f_o and u_o represent the required minimum capacity and deformation of the structure to respond elastically during a specified earthquake activity. Based on Figure B.3, two parameters can be defined i.e. the yield strength reduction factor R_y and the ductility factor μ. These parameters are as follows:

$$R_y = \frac{f_o}{f_y} = \frac{u_o}{u_y} \tag{B.5}$$

$$\mu = \frac{u_m}{u_y} \tag{B.6}$$

These factors are used to identify the region in which a given system is responding. Values of R_y and μ less than unity imply that the system is responding in its elastic range and the values of R_y and μ greater than unity define a system responding in its inelastic range. In other words, a value of R_y and μ less than unity implies that the yield capacity of the system is greater than the earthquake force induced on the system and a value of R_y and μ greater than unity shows that the earthquake induced force is greater than the yield capacity of the system.

The elastoplastic system can be expressed in terms of the elastic system by (Figure B.3):

$$f_o = f_y \tag{B.7}$$

$$u_o = u_m \frac{R_y}{\mu} \tag{B.8}$$

Equation B.8 was obtained by substituting equation B.6 into equation B.5. In addition, based on Figure B.3, the yield acceleration a_y is related to the yield displacement u_y as follows:

$$a_y = \omega^2 u_y \tag{B.9}$$

This equation was derived by relating the yield stiffness with the static stiffness.

Stellenbosch University https://scholar.sun.ac.za

3. The constant ductility response spectrum equation

Dividing equation B.3 by the mass *m* of the system, gives

$$\ddot{u} + 2\xi\omega_n\dot{u} + \omega_n^2 u_y \tilde{f}_s(u,\dot{u}) = -\ddot{u}_g \tag{B.10}$$

where

$$\omega_n = \sqrt{\frac{K}{m}} \qquad \xi = \frac{C}{2m\omega_n} \qquad \text{and} \qquad \tilde{f}_s(u,\dot{u}) = \frac{f_s(u,\dot{u})}{f_y} \tag{B.11}$$

For an instant of time t, the ductility factor (equation B.6) is equal to $\mu(t) = u(t)/u_y$. Therefore, $u(t) = u_y\mu(t)$, $\dot{u}(t) = u_y\dot{\mu}(t)$, and $\ddot{u}(t) = u_y\ddot{\mu}(t)$. By substituting these parameters into equation B.10 and dividing by u_y, it gives the constant ductility response spectrum equation (equation B.12).

$$\ddot{\mu} + 2\xi\omega_n\dot{\mu} + \omega_n^2 \tilde{f}_s(\mu,\dot{\mu}) = -\omega_n^2 \frac{\ddot{u}_g(t)}{a_y} \tag{B.12}$$

Here $a_y = f_y/m$ which represents the required acceleration to induce the yield force f_y. With reference to Mahin & Lin (1983), the equation B.12 is rewritten in terms of normalised yield strength η as follows:

$$\ddot{\mu} + 2\xi\omega_n\dot{\mu} + \omega_n^2 \tilde{f}_s(\mu,\dot{\mu}) = -\omega_n^2 \frac{\bar{\ddot{u}}_g(t)}{\eta} \tag{B.13}$$

Where

$$\eta = \frac{a_y}{PGA} \tag{B.14}$$

$$\bar{\ddot{u}}_g(t) = \frac{\ddot{u}_g(t)}{PGA} \tag{B.15}$$

Substitution of equation B.9 into equation B.14 gives

$$u_y = \eta\frac{PGA}{\omega^2} \tag{B.16}$$

Here PGA represents the peak ground acceleration.

Stellenbosch University https://scholar.sun.ac.za

4. Development of the constant ductility response spectra

The procedures for developing the constant ductility response spectra are defined as follows (Chopra, 2007; Mehani, 2012):

i. Identify the ground acceleration time history $\ddot{u}_g(t)$ of the earthquake of interest

ii. Identify and fix the damping ratio ξ of the system for which the response spectra are going to be plotted

iii. Identify a value for the normalised yield strength η;

iv. Determine the fundamental natural period T_n of the system;

v. Evaluate the ductility response $\mu(t)$ of the system associated to the selected values of the natural period T_n and damping ratio ξ of the system by numerical solution of equation B.13. From the results, determine $\mu_{\max}$, $u_{\max} = u_y \mu_{\max}$, $\dot{u}_{\max} = u_y \dot{\mu}_{\max}$, and $\ddot{u}_{\max} = u_y \ddot{\mu}_{\max}$. The yield displacement u_y is given by equation B.16;

vi. Repeat steps iv and v for a set of the natural frequency T_n. From the results, various plots can be obtained such as:

   (a) ductility demand response spectrum, $\mu_{\max}$ against T_n

   (b) acceleration-displacement response spectrum, $\ddot{u}_{\max}$ against $u_{\max}$;

vii. Repeat steps iii to vi for various values of η.